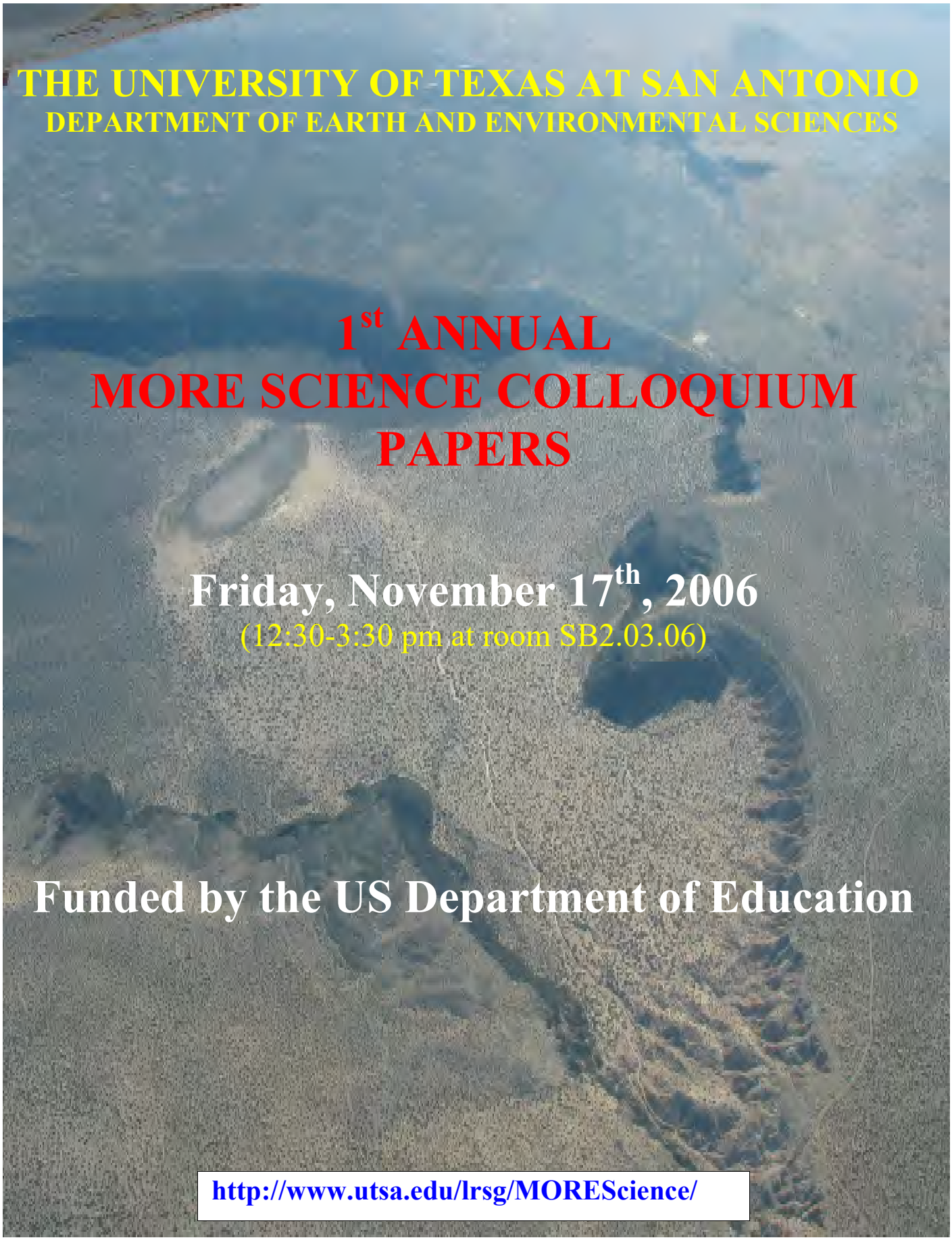

THE UNIVERSITY OF TEXAS AT SAN ANTONIO

DEPARTMENT OF EARTH AND ENVIRONMENTAL SCIENCES

1st ANNUAL MORE SCIENCE COLLOQUIUM PAPERS

Friday, November 17th, 2006

(12:30-3:30 pm at room SB2.03.06)

Funded by the US Department of Education

http://www.utsa.edu/lrsg/MOREScience/

TABLE OF CONTENTS

Small-Scale Performance of a Novel Arsenic Sorbent from Contaminated Groundwater

Undergraduate Student
Alexander S. Castillo

Advisors
Konstantinos C. Makris, Dibyendu Sarkar
Department of Earth and Environmental Sciences
University of Texas at San Antonio

Several arsenic (As) treatment technologies exist for arsenic-contaminated groundwater, but the majority of them are cost-prohibitive for rural communities and small municipalities around the world. Our proposed technology relies on a packed bed reactor (PBR) system, utilizing a novel, low-cost, As filter medium, i.e., the drinking-water treatment residuals (WTRs). The drinking-water treatment process generates a by-product, the WTRs, which are available, free of charge from the drinking water treatment facilities in the U.S. Earlier batch experiments have shown the tremendous affinity of WTRs for soluble As(V) and As(III). A small-scale (30 x 5 cm) PBR system containing the WTRs were tested for its effectiveness in treating As-contaminated, synthetic groundwater. Influent groundwater composition was 150 μgL^{-1} As added either as As(V) or As(III) mixed with 2 mg $^{Fe++}$ at a pH of 6.5. Influent solution was constantly purged with N_2 to simulate typical anaerobic conditions in groundwater, and it was delivered to the PBR filter medium consisted of either an Al-, or Fe-based WTRs (<1-mm). The total bed volumes processed varied between the WTR type (Fe-, or Al-based), and the As oxidation state (III vs. V). The Al-WTR was superior to the Fe-WTR effectiveness in treating both As(V) and As(III)-contaminated groundwater, processing > 18,000 bed volumes before exceeding the current MCL value for As in the U.S. and Europe (10 μgL^{-1}) for As in India and other developing countries that are being poisoned by their drinking water. Continuous monitoring of several metals (Al, Fe, Cr, Cu, Zn, Pb, and Mn) did not show that WTRs leached metals to the effluent solution to any measure of significance.

Introduction

Groundwater in many communities and regions around the world possess dangerously elevated concentrations of the trace heavy metal Arsenic (As). As is mainly encountered in nature as two forms: As(V) and As(III), available as arsenate and arsenite, respectively

(Smith et al, 1992). The carcinogenic properties compounded with chronic exposure of As creates degenerative and lasting effects to humans and animals. The intake amount of As has been attributed to an increase in the risk of various cancers, including skin, liver, lungs, bladder, and kidney (Smith et al, 1992). Many undeveloped and third world countries represent a large percentage whose water resources are affected by As infiltration of groundwater (Rahman et al, 2005). Contamination sites such as pesticide-treated soils (Murphy and Aucott, 1997), mining activity (Ng, 2005), treated lumber, and landfills, act as radiating reservoirs of both anthropogenic and naturally occurring arsenic, are the targets of environmental remediation (Chen et al, 1999). The World Health Organization (WHO) states a recommended level of arsenic in drinking-water at $10 \mu g\ l^{-1}$, which leaves approximately 3000 water systems in the United States, which supplies potable drinking-water to almost 11 million people, in need of new technologies to accommodate the new guidelines (Bang et al, 2004). In the international community, such as in West Bengal, India, 51% of the wells sampled had levels of soluble As above $50 \mu g\ l^{-1}$ (Rahman et al, 2004). Various remediation technologies have been implemented and tested, to counter As mobility, with degrees of success, such as: fungal biomass (Pokhrel and Viraraghavan, 2005), titanium dioxide, (Bang et al, 2004), Fe-oxyhydroxides (Morin and Calas, 2006), coagulation and filtration (Kapadia, 2000), granular ferric hydroxide, anion exchange, activated alumina, and reverse osmosis (Chen et al, 1999). Despite the varying effectiveness of each of the alternative treatments, rural and developing communities and municipalities are faced with the cost-prohibitive aspects of the As remediation. The granular ferric hydroxide method, for example, yields a cost of $350 per ton (Chen et al, 1999). Coagulation and filtration methods can require an infrastructure at a cost of $439,500 per 150 square feet of treated soils. Models show a wide range of costs for the different treatments, which can hinder progress for treating As contaminated groundwater (Kapadia, 2000). Previous published literature has reported an exceptional low-cost sorbent for both As(V) and As(III), found in a drinking-water waste by-product, known as water treatment residuals (WTRs). WTRs have shown to have a proven high affinity of sorption to both As(V) and As(III). The attractiveness of the use of the WTRs lies with, not only their effectiveness, but with the free of charge cost from water treatment plants in the United States (Makris, 2005). Our objective with this study is to test the effectiveness of the use of WTRs in a small-scale packed bed reactor (PBR) in order to determine the sorption capacities of soluble As(V) and As(III) in a synthetic groundwater.

Materials and methods

The varieties of WTRs were available in two forms for testing. The Al-based WTR, obtained from the Manatee County water treatment facilities in Bradenton, FL, and Fe-based WTR from the Hillsboro River water treatment facilities in Tampa, FL. The coagulants used for the WTRs are alum and a copolymer of sodium acrylate and acrylamide for the Al-based WTR, and $Fe_2(SO_4)_3$ for the Fe-based WTR (Makris, 2005). The water treatment plants provided the WTRs free of charge. The WTRs were granulated and passed through a mesh sieve providing a particle size of <250 μm. Various calculations were conducted on the WTRs to determine their specifications in order to utilize them effectively in this study. The water content (ω) was measured at 0.1722 and 0.1799, and bulk density (ρ_B) of 0.5497 g cm^{-3} and 0.9402 g cm^{-3} for the Al-based and Fe-based respectively.

The medium to be filtered through the WTRs was synthesized groundwater. The preparation for this groundwater was completed in three separate stock batches for As(V), As(III), and an As(V)+As(III) mixture. The As(V) and As(III) stock was prepared with sodium arsenate ($Na_2HAsO_4*7H_2O$) and sodium arsenite ($NaAsO_2$) respectively. The As stocks were prepared to a concentration of 100 ppm in dionized water. As(V) and As(III) were each weighed at 0.4165g and 0.1735g respectively into 150 ml to achieve the 100 ppm concentrations. The stocks were used to spike the synthesized groundwater. The groundwater was artificially created with 83.4 L of dionized water mixed with approximately 166.8 mg of ferrous (II) sulfate ($FeSO_4*H_2O$) to replicate the Fe (II) concentrations of 2ppm found in most groundwater. The batch was then spiked with the 125 ml of the respective As concentrations into the 83.4 L dionized water for a final 150 ppb As concentration. The As(V)+As(III) mixture required 62.5 ml of each As stock to obtain the 150 ppb concentration. The inert gas N_2 was continuously pumped into the synthesized groundwater to purge any available O_2 out of the batch to replicate the aerobic conditions of natural groundwater. A small scale water pump was utilized to pump the spiked synthesized groundwater influent into the PBR at a rate of 100 ml min^{-1}. Each influent batch was changed every 13 hours throughout the trials to ensure continuous flow into the PBR. The influent was sampled each time to monitor the pH and also collected for further analysis. The pH maintained was in a range

of 3.5-5.5 for As(V), 6.5-5.5 for As(III), and 6.5-5.5 for the As(V) + As(III) mixture. Each trial lasted approximately 2 weeks.

The small-scale packed bed reactor (PBR) was constructed out of commercial grade Polyvinyl Chloride (PVC) piping. The piping had an internal diameter of 5.08 cm and length of 30.0 cm and stood vertical. The bottom portion of the PBR was fitted with a mesh. The purpose of the mesh was to contain the granulated WTRs in the column. The ends of the PBR were fitted by coupling and adhered with generic pipe glue and cleaner. The lower coupling was permanently fastened with an intake nozzle fitted. The upper portion of the PBR was fitted with a threaded coupling for access and placement of the WTRs in the column. An outtake nozzle was fitted into this threaded coupling.

The batch trials had two specifications for each of the WTRs utilizing the above aforementioned WTR characteristics. For the Al-based WTR, 111.42 g of granulated WTR was placed into the PBR for a bedload height of 10cm. The Fe-based required 190.56 g of WTR for the same bedload height. Each new batch was calibrated for 24 to 48 hours at 10 ml min^{-1} with pure dionized water, prior to each trial to ensure even saturation of the WTRs. The effluent was pumped into a waste bin where it was sampled for the pH and collected for further analysis.

Results

In the case of the Al-based WTR, the sorption capacities exhibited similar results as previously published literature. The initial influent As concentration for As(V), As(III), and As(V)+As(III) mixture was maintained at 150 ppb. The effluent concentration for As(V) had initial measurements not exceeding 2 ppb for the first 41 hours or pore volume (τ) of 6407. An increase in soluble As(V) began, yet on average still remained below the WHO recommended levels of As concentrations of 10 ppb up to 154 hours or pore volume of 14881. The final duration of the As(V) trial showed a steady increase in the concentration of As(V). Similarly, in the case of As(III), the sorption capacity significantly dropped the concentration of soluble As(III) from the initial 150 ppb influent to not exceeding 17 ppb for the effluent. This trial was only carried out 247 hours or pore volume 23833. The increase in As(III) was not observed as it was in As(V). The case for the As(V)+As(III) mixture yielded concentration levels of As below

the 10 ppb limit in each sample. This trial duration only lasted 158 hours or pore volume 15261. The Fe-based batch trials were conducted only for As(V). The time duration did not exceed 200 hours or pore volume of 19173. In this time, the levels of As(V) never surpassed 10 ppb. For the Fe-based WTR, a micro-plate absorbance analysis was conducted to test if any concentration of Fe^{2+} may have precipitated out into the effluent. On average, concentration levels remained in the negative concentration levels.

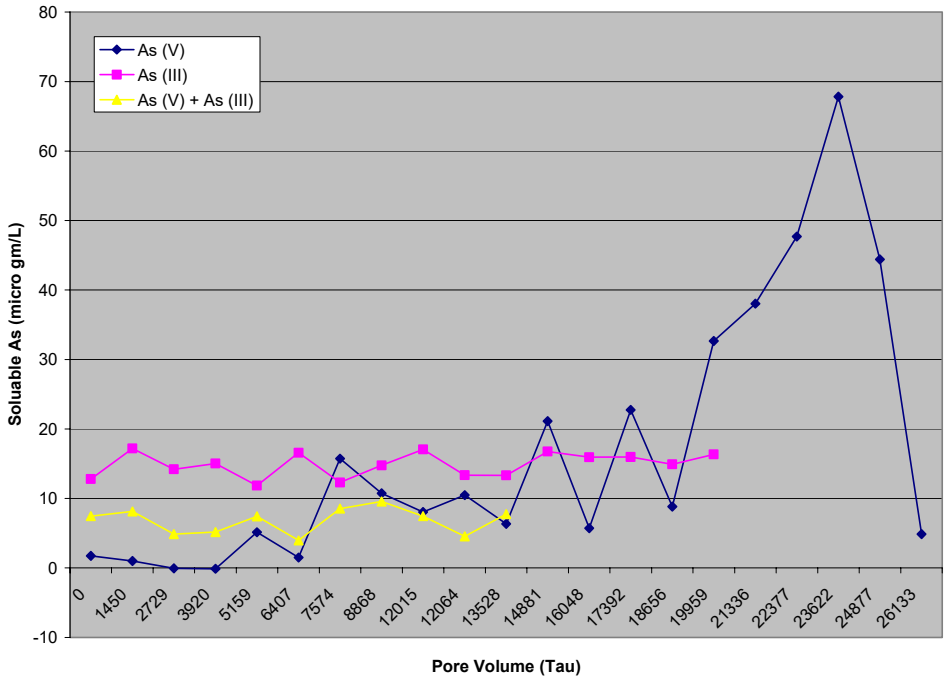

Figure 1. Concentration of As(V), As(III), and As(V)+As(III) mixture vs. PoreVolume in Al-basedWTR.

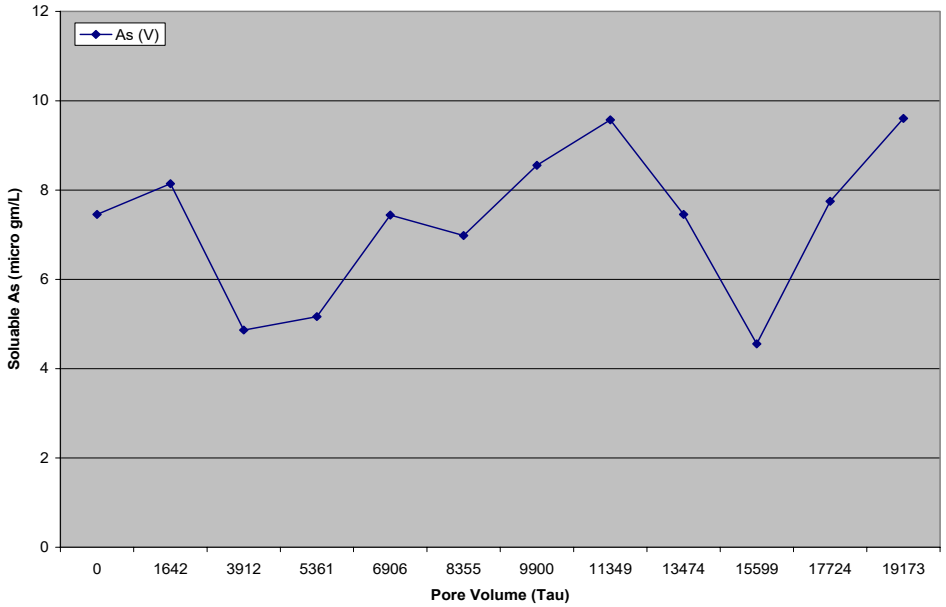

Figure 2. Concentration of As(V) vs. Pore Volume for Fe-based WTR.

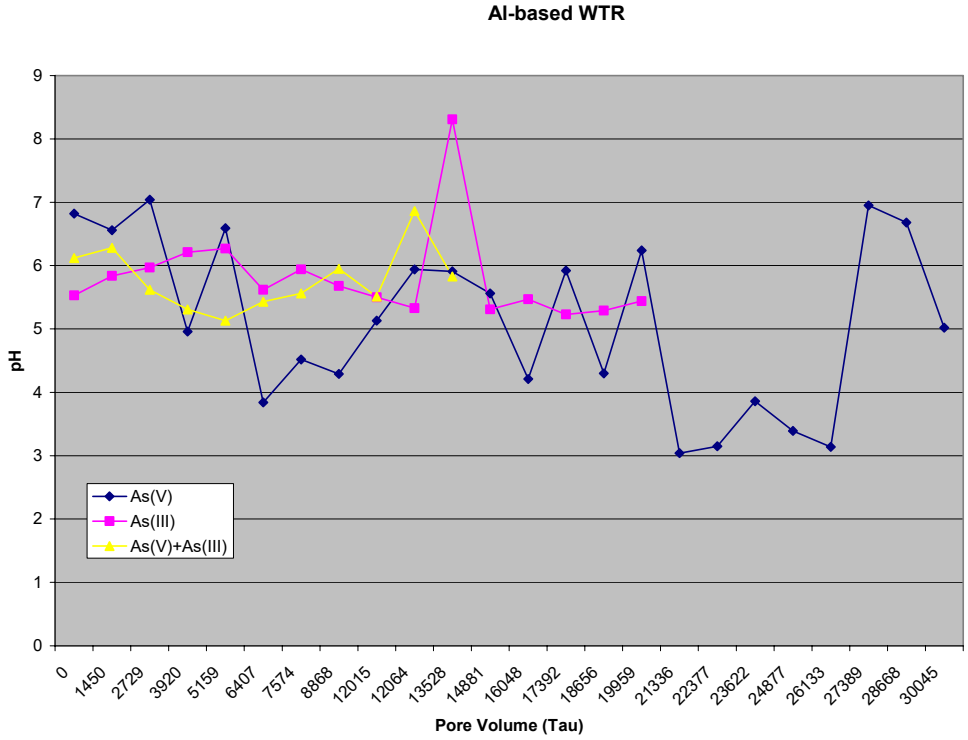

Figure 3. pH for As(V), As(III), and As(V)+As(III) in Al-based WTR for the effluent

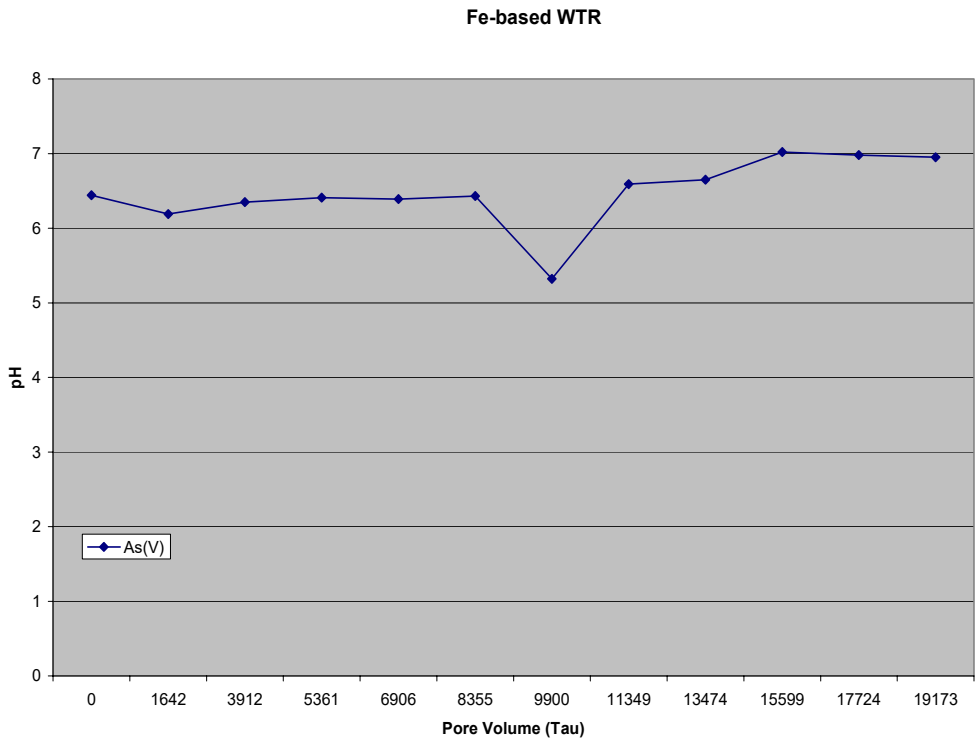

Figure 4. pH for As(V) in Fe-based WTR for the effluent

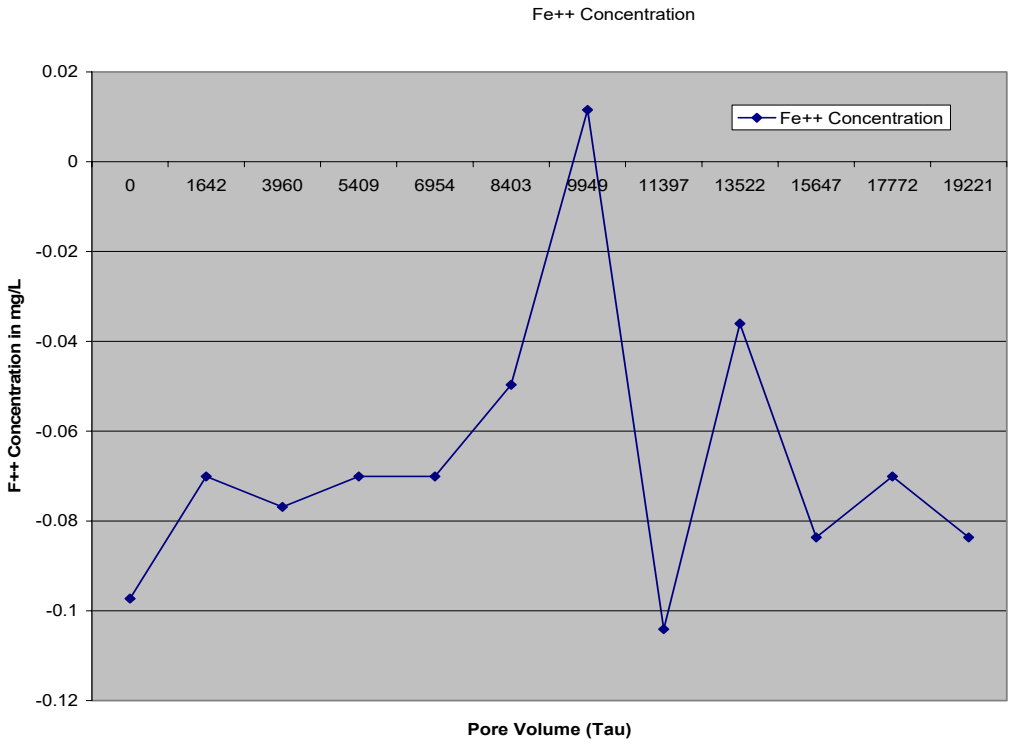

Figure 5. F++ Concentration vs. Pore Volume (Tau) for As(V) in Fe-based WTR

Discussion and conclusion

The trials exhibited varying, yet promising results. The WTRs exhibited high affinities for each form of soluble As. Time constraints and faulty measurements limited trials to be fully conducted for the Fe-based WTR on the different As species. Inaccurate measuring, sampling, or compromised stock solutions may have yielded the high error encountered with the Fe-based WTR trials. The Al-based WTR's effectiveness exhibited trends similar to previous studies. The Fe-based WTR showed varying results which does not fit previous models (Makris, 2005). This may be an indication that Al-based is superior to that of Fe-based with respect to sorption capacities. In the usage of Fe-based WTRs, through the absorbance analysis, Fe^{2+} did not precipitate out into the effluent. The Fe-based WTR exhibited exceptional stability in the aqueous solution. Overall, the WTRs showed great promise as an effective, both cost and performance, method to countering As mobility in groundwater, when utilized in a small-scale PBR system. With very little overhead, WTRs can be made available to rural communities and developing countries which possess highly elevated concentrations of soluble As in ground and drinking-water sources. The sheer simplicity of the small-scale PBR system allows usage for virtually any income. Developing technologies can assist implementing WTRs as a filtering medium on a large scale for not only As, but other heavy metal cations.

Acknowledgments

The author would like to thank Dr. Alyson Ponomarenko for the opportunity provided by the MORE Science internship. The assistance of Dr. Konstantinos Makris, Dr. Dibyendu Sarkar, Dr. Rupali Datta, and the diligent staff of the Environmental and Geochemistry Lab at UTSA with the lab education and utilities training and equipment usage. Financial support was provided by the MORE Science internship program.

References

[1] Bang S, Patel M, Lippincott L, Meng X, 2005. "Removal of Arsenic from Groundwater by Granular Titanium Dioxide Adsorbent", *Chemosphere*, pp.389-397.

[2] Charlet L, Polya DA, 2006. "Arsenic in Shallow, Reducing Groundwater in Southern Asia: An Environmental Health Disaster", *Elements, pp.91-96.*

[3] Chen H, Frey MM, Clifford D, McNeill LS, Edwards M, 1999. "Arsenic Treatment Considerations", *American Water Works Association*, pp.74-85.

[4] Ghosh A, Saez AE, Ela W, 2006. "Effect of pH, Competitive Anions and NOM on the Leaching of Arsenic from Solid Residuals", *Science of the Total Environment*, pp46-59.

[5] Kapadia A, 2000. "Technologies and Costs for Removal of Arsenic from Drinking Water", *Environmental Protection Agency,* EPA 815-R-00-028.

[6] Makris KC, Sarkar D, Datta R, 2005. "Evaluating A Drinking-water by-product as a Novel Sorbent for Arsenic", *Chemosphere*, pp.1-12.

[7] Morin G, Calas G, 2006. "Arsenic in Soils, Mine Tailings, and Former Industrial Sites", *Elements*, pp.97-101.

[8] Murphy EA, Aucott M, 1998. "An Assessment of the Amounts of Arsenical Pesticide Used in a Geographical Area", *The Science of the Total Environment*, pp. 89-101.

[9] Ng JC, 2005. "Environmental Contamination of Arsenic and its Toxicological Impact on Humans", *Environmental Chemistry*, pp.146-160.

[10] Pokhrel D, Viraraghavan T, 2005. "Arsenic Removal from Aqueous Solution By Iron Oxide-Coated Fungal Biomass: A Factorial Design Analysis", *Water, Air, and Soil Pollution*, pp.195-208.

[11] Rahman MM, Sengupta MK, Ahamed S, Chowdhury UK, Hossain A, Das B, Lodh D, Saha KC, Pati S, Kaies I, Barrua AK, Chakraborti D, 2005. "The Magnitude of Arsenic Contamination in Groundwater and its Health Effects to the Inhabitants of the Jalangi-One of the 85 Arsenic Affected Blocks in West Bengal, India", *Science of the Total Environment*, pp.189-200.

[12] Smith AH, Hopenhayn-Rich C, Bates MN, Goeden HM, Hertz-Picciotto I, Duggan HM, Wood R, Kosnett MJ, Smith MT, 1992. "Cancer Risks from Arsenic in Drinking Water", *Environmental Health Perspective*, pp.259-267.

Statistical analysis and prediction of mean temperature on West Texas based on El Niño Southern Oscillation Index

Undergraduate Student
Melissa Quiñones

Advisor
Huade Guan
Department of Earth and Environmental Sciences
University of Texas at San Antonio

This research explores the possibility of predicting monthly temperatures in stations located in the Trans Pecos division (NOAA Climatic division number 5: Alpine, Brewster, El Paso and Winkler counties) based on a correlation with El Niño Southern Oscillation (ENSO) index, using the NOAA mean monthly temperature from 1954 to 2004 in NOAA climatic stations spanning the geographical region of the Trans Pecos division. Through statistical analysis of temperature data and correlation with the ENSO index the predictability of monthly temperature is determined for each station. Results found that predictability of temperature varied greatly depending on the conditions of the ENSO index. The best chance of prediction occurs in the winter months of years with an active El Niño phenomenon. Conversely, the lowest chance of prediction corresponds to neutral years, when no El Niño or La Niña phenomena are occurring. Ability to predict temperature also varied spatially, as evidenced by different predictability results in different stations. This suggests that prediction can be achieved to some degree locally but may not be possible in a regional effort. Therefore, it is recommended that future studies focus on smaller geographic regions in order to increase the chance of successful prediction.

Introduction

The state of Texas is located in a geographic region characterized by extreme weather conditions. Constant variations of weather conditions have a big effect on urban areas. For example, West Texas has been historically subject to severe droughts, placing

additional stress on a limited water supply. Previous investigations suggest different methods to manage water resources in an efficient way. Through this study we hope to provide the framework for new and more efficient water management modeling strategies.

Climatic conditions are affected daily by different parameters. The most significant of these parameters is the effect of El Niño Southern Oscillation (ENSO) phenomenon. During El Niño phenomenon abnormally warm sea surface temperatures (SST) often signal the beginnings of positive SST anomalies on the eastern half of the equatorial Pacific. During the periods of "La Niña", which is the opposite phenomenon, abnormally cold SST in the eastern half of the equatorial Pacific occurs. The "Southern Oscillation", consists of an east-west atmospheric pressure that has a direct effect on tropical weather at a global scale. "El Niño/La Niña" and swings of the "Southern Oscillation" typically occur in conjunction. These events last from several months up to one year and are called "ENSO events", their influence has a global impact.

This research focus on the Statistical analysis and prediction of mean temperature based on El Niño Southern Oscillation Index in Brewster county, El Paso county and Winkler county; which are located in the West of Texas. The objective of this research is to find if it is possible to predict mean surface temperature based on analysis of the ENSO index. The data used to for this investigation was provided by The NOAA Climatic Center. The NOAA National Climatic Center has divided the state of Texas into ten climate divisions (name divisions). Each division is subdivided into climate stations. Because of time limitation the project focuses on one of the ten divisions: division five known as the Trans Pecos division.

Study Area

The principal study area is NOAA climatic division five. Division number five is located in the state Texas, particularly in the west area. Division five is known as the Trans Pecos division. The specific names and locations that correspond to the climatic stations used for this investigation are the following: Alpine (Brewster county), Chisos Basin (Brewster county), Marathon (Brewster county) Hereford (Brewster county) La Tuna 1s (El Paso county) and Wink Winkler (Winkler county). In the beginning of the investigation data from two other stations was used for comparison of variability in each

area with respect to the others. The other divisions used where NOAA climatic divisions one and six. Division one is known as the High Plains division and division six is known as the Edwards Plateau division.

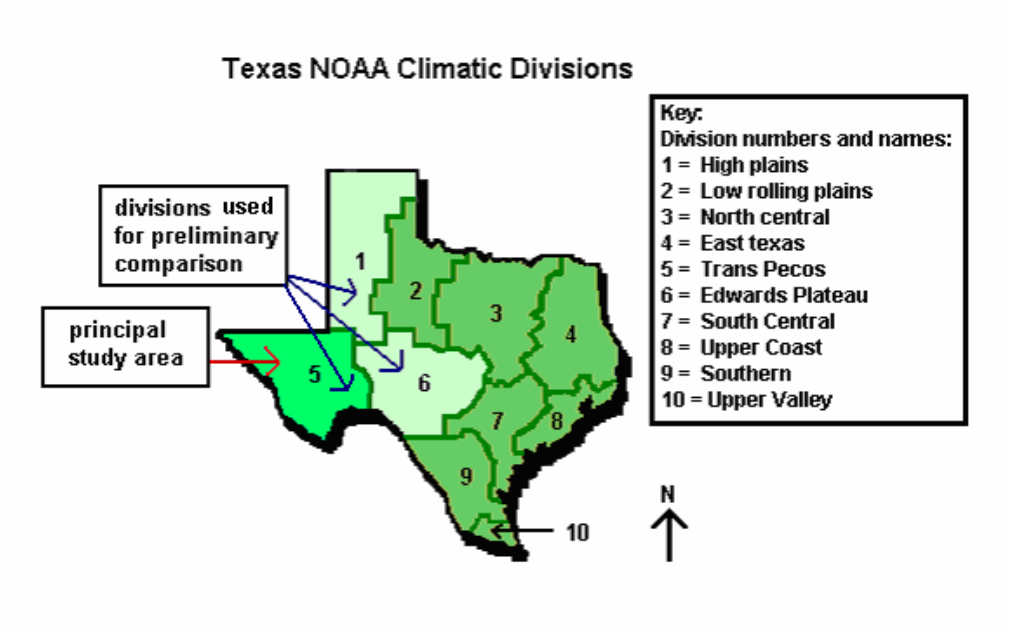

Figure 1: Map of NOAA Climatic Divisions in the state of Texas

(Modified from: **http://cdo.ncdc.noaa.gov/pls/plclimprod/somdmain.subquery1**)

Methodology

Criteria to select stations

This research focuses on the general comparison of the mean temperature variability from 1947 until 2004 on three of the ten divisions: division one (High Plains), five (Trans Pecos and division six (Edwards Plateau). Data analysis from divisions one, five and six were conducted and the Trans Pecos division (five) was selected for a detailed analysis. In order to have accurate results, the data selected for this research comes from climatic stations that have a continuous record of at least fifty years of collected data.

Obtaining the data

The data used in this project was surface monthly mean maximum and minimum temperature data downloaded from the NOAA National Climatic Data Center (**http://hurricane.ncdc.noaa.gov/CDO/cdo**) and was processed and analyzed with Mat lab and Microsoft Excel.

Processing the data

Data downloaded were monthly surface temperature data (mean temperature, maximum temperature and minimum temperature). The time range was from 1947 to 2004. The temperature data was changed from Fahrenheit to degrees Celsius and was then organized into different worksheets. To create uniform data; the gaps in the data were replaced by the average of the temperature in the previous year and the following year in the same station.

Temperature Anomaly

The temperature anomaly, defined as a deviation from the mean temperature, was calculated for each month in each station. The anomaly was calculated by subtracting the specific mean temperature for each station (1947 to 2004) from the monthly temperature. The result of this calculation is then compared with the ENSO Index (El Niño Southern Oscillation), which is also an anomaly calculation.

ENSO Index

El Niño and La Niña are defined as warming or cooling, respectively, phenomena occurring in a particular region of the equatorial Pacific Ocean over a three-month period. These variations in the Sea Surface Temperature (SST) affect the climatic conditions. ENSO Index is a three month average of the sea surface anomalies in the Niño 3.4 region. A strong ENSO event lasts for more than three months and shows an increase in Sea Surface Temperature (SST).

Correlation and correlation coefficient

The anomaly in each station was correlated with the ENSO Index. There are three different patterns of correlation: positively correlated, negatively correlated, or uncorrelated. A positive correlation between the monthly anomaly and ENSO Index means that the values of both variables have a similar behavior (increase or decrease at the same time). A negative correlation between anomaly and ENSO Index means that as one of the variables increase the other variable decreases. If the variables are uncorrelated this means that an increase or decrease on one variable has no effect on the other variable.

The statistic function used to express the relationship between two variables is called the correlation coefficient. To calculate the correlation coefficient between the ENSO Index and the temperature anomaly between divisions one, five and six, we used the following equation:

$$p = \frac{\frac{1}{n}\sum_{i=1}^{n}(x_i - m_x)(y_i - m_y)}{\sigma_x \sigma_y}$$

Where p= the linear relationship between the ENSO Index and the anomaly of each station, the number of data is *n,* $x_1 \ldots, x_n$ are the ENSO Index monthly values from 1931 to 2004, m_x is their mean values, and σ_x is their standard deviation; $y_1,\ldots,y_n$ are the monthly anomaly values from 1931 to 2004, m_y is their mean, and σ_y is their standard deviation. If p= +1, then the scatter plot is going to have a positive 45° slope; if p= -1, then the scatter plot is going to have a 45° negative slope.

Linear Regression

After calculating the correlation between the ENSO Index and the anomaly of the stations in divisions one, five and six; we try to predict future temperature anomalies based on the current ENSO Index data and anomaly data. In order to calculate these predictions we made a linear regression assuming the dependence of a future anomaly based on a known ENSO Index.

Probability or Confidence Test

A Probability Test was performed on the final result (predictions); the result of the test is represented as percentage. The probability % value is the relative frequency of times that the confidence interval actually does contain the temperature parameter, assuming that the estimation process is repeated a large number of times.

Discussion of results

The anomalies of the mean temperature vary from station to station and from month to month. Figures number two to number four are graphical representations of anomaly calculations of La Niña (figure 2), El Niño (figure 3) and the Neutral years (figure 4) for the monthly mean temperature of each station based on the ENSO index (correlation).

For La Niña years (figure 2) in the months of January and February the anomaly is always positive; while during the months of July, August and September is always negative. For El Niño years (figure 3) from October to June the anomaly is always negative and from August to September is always positive.

For the Neutral years (figure 4) during the month of January the anomaly is always negative and the values are significantly smaller than during La Niña and El Niño years. In the cases that the value is negative the current mean temperature value correlates negatively to the actual ENSO index anomaly value, so the temperature is cooler than usual. A positive value indicates that current monthly mean temperature is positively correlated to the ENSO index anomaly, which means that current mean temperature in this area is warmer than usual.

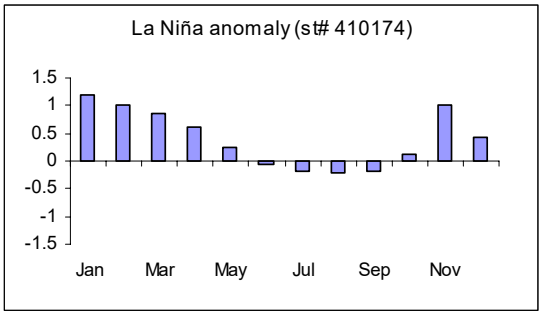

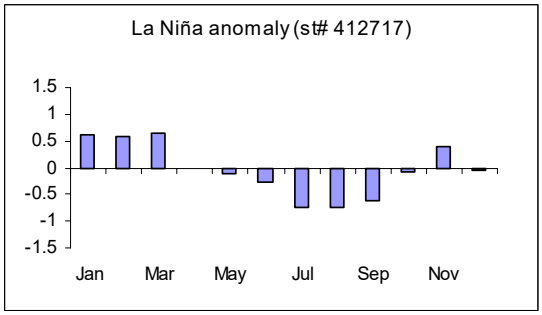

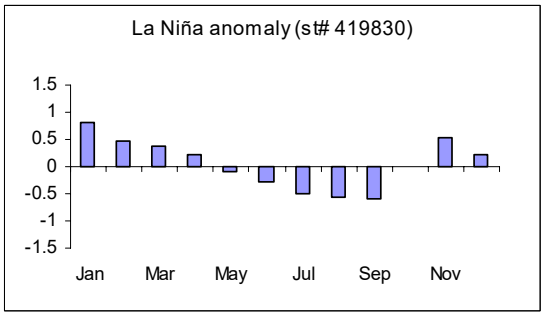

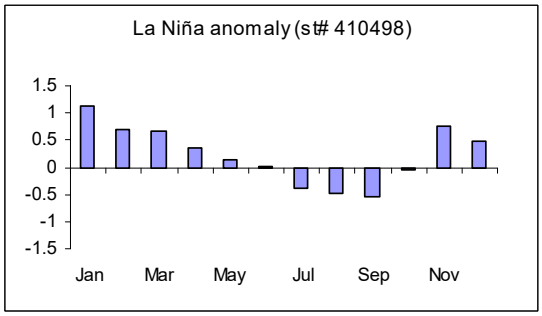

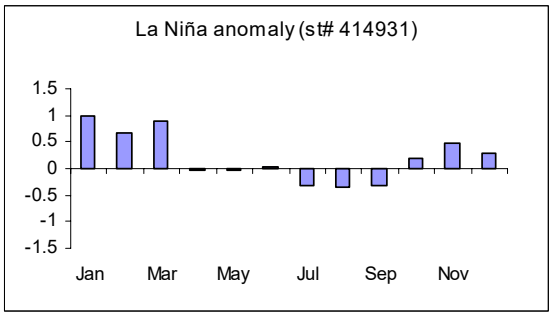

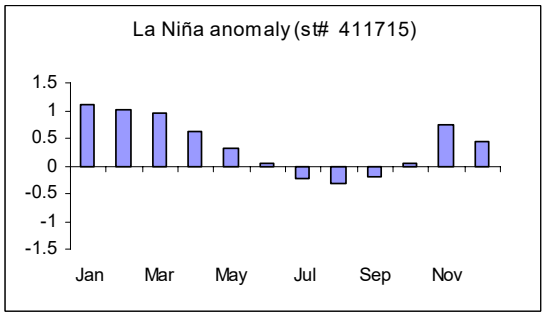

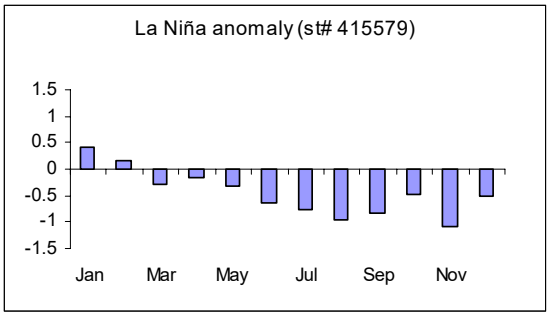

Figure 2: **Anomaly of monthly mean temperature of studied stations based on the ENSO index for La Niña years**

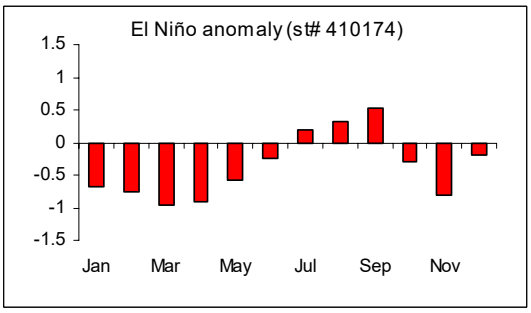

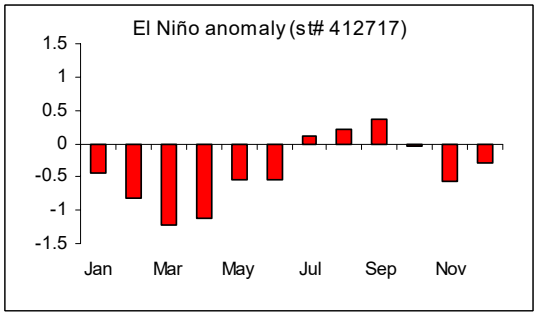

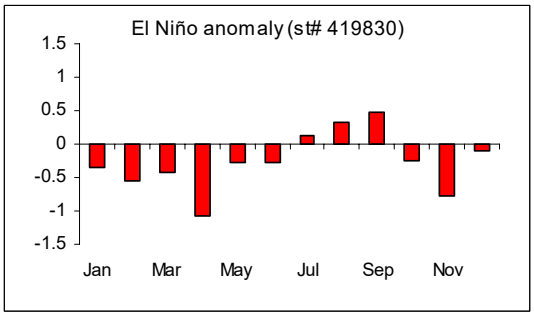

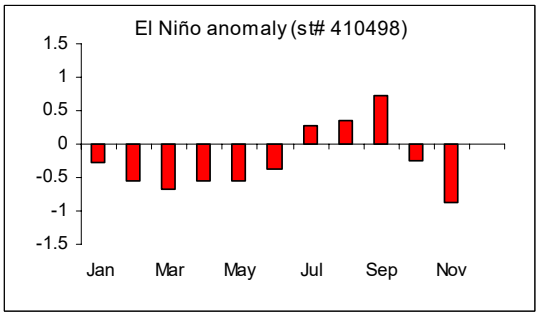

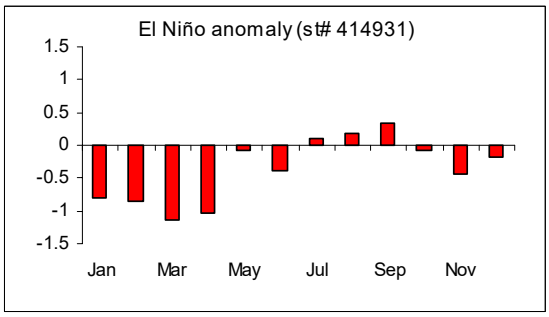

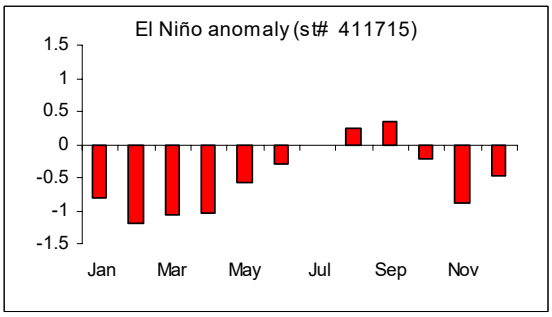

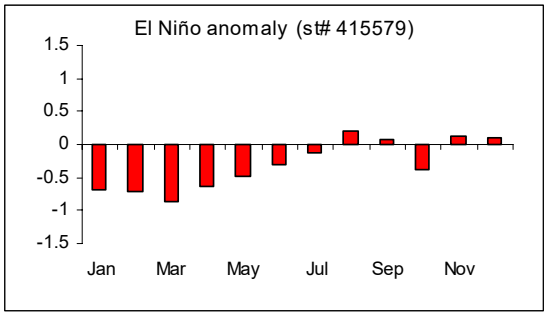

Figure 3: **Anomaly of monthly mean temperature of studied stations based on the ENSO index for El Niño years**

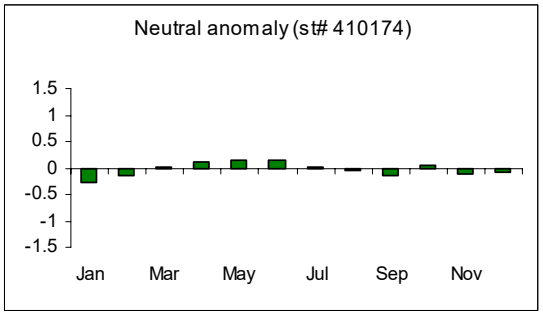

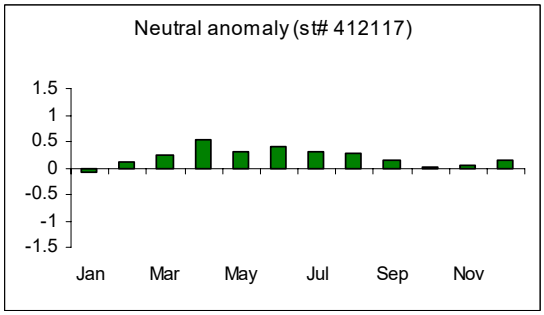

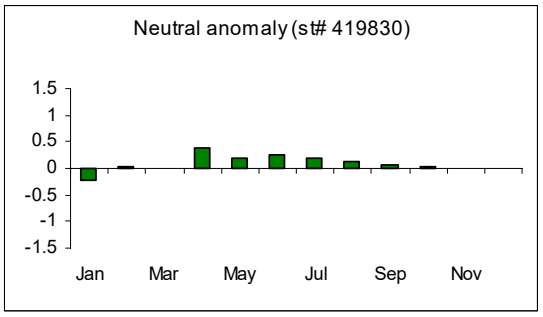

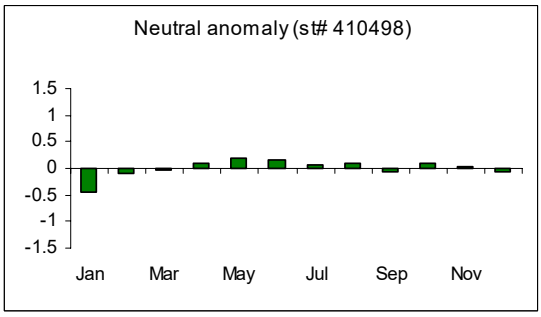

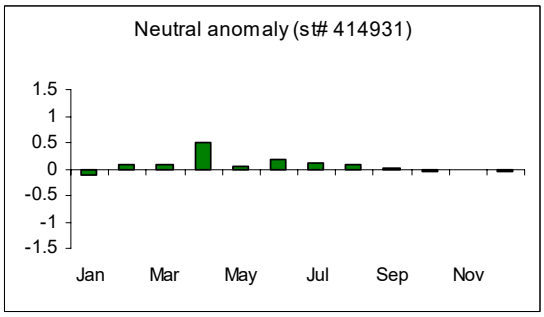

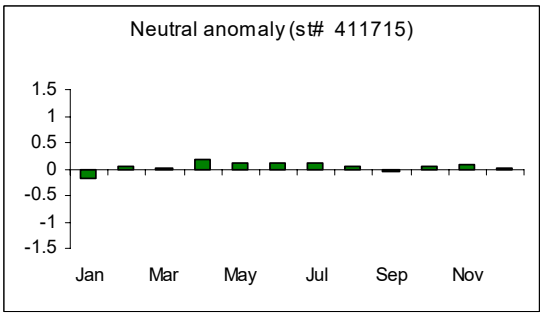

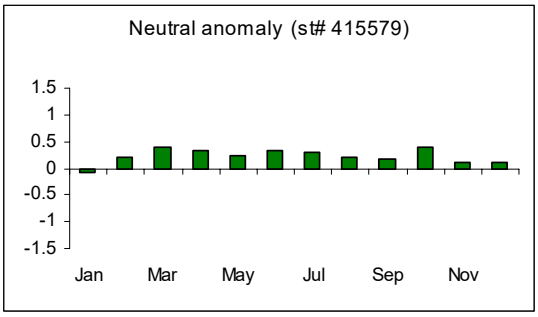

Figure 4: **Anomaly of monthly mean temperature of studied stations based on the ENSO index for Neutral years**

The anomaly calculations were also compared with the standard deviation of the monthly mean temperature. The standard deviation is represented in figure 5 by dashed lines in the graphs. The standard deviation for the observed monthly mean temperature is larger than the standard deviation of the Predicted temperature.

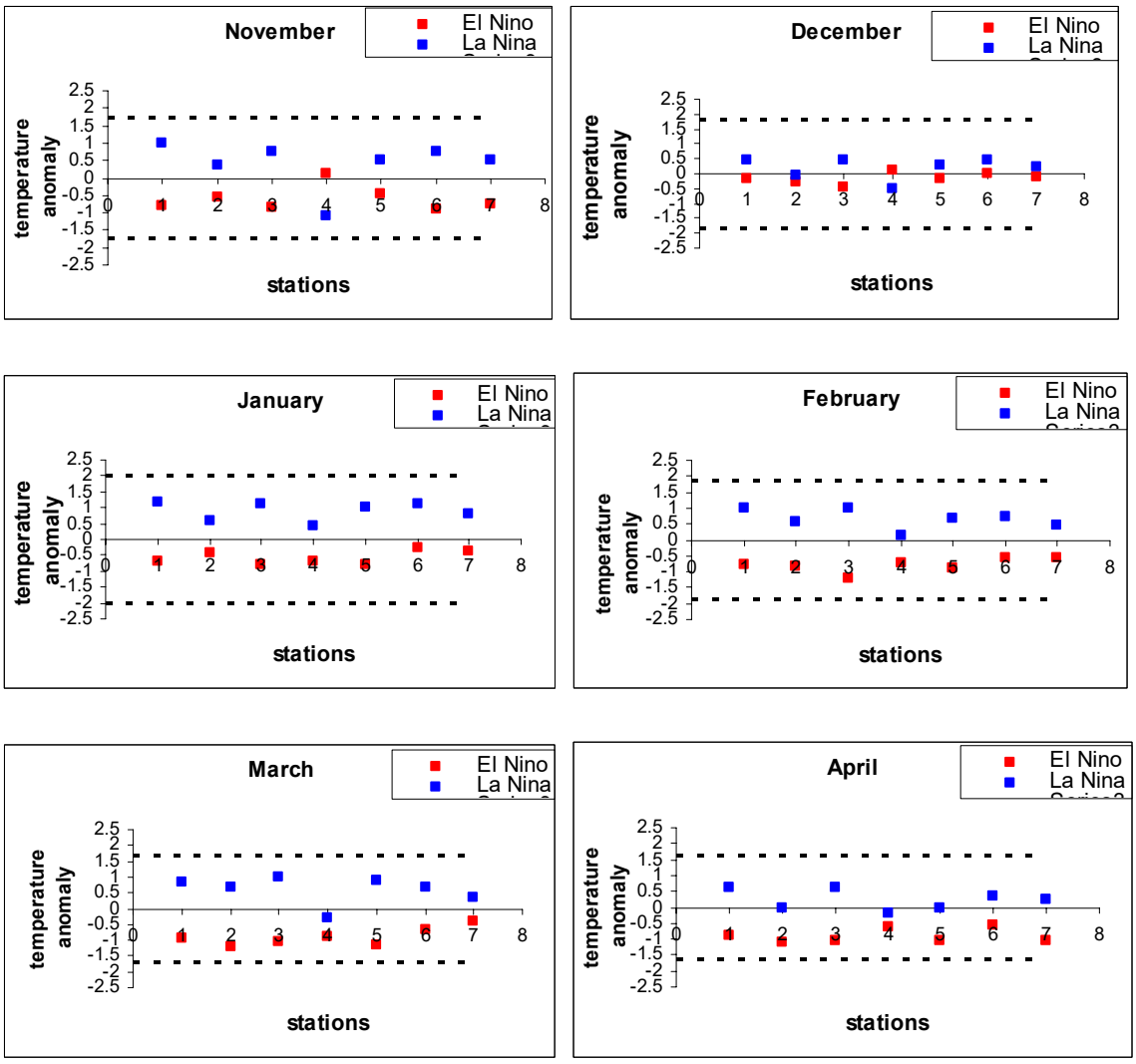

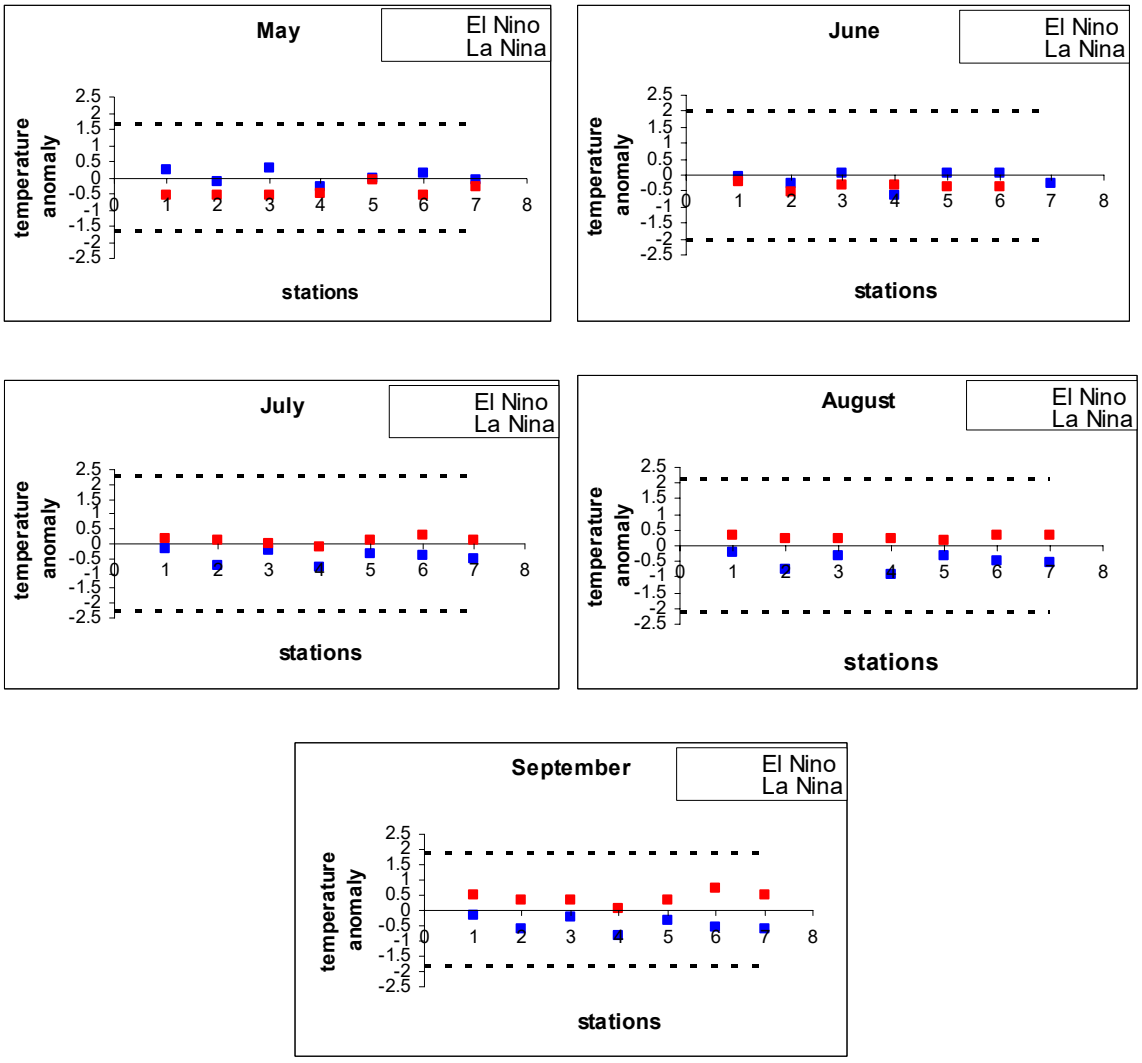

Figure 5: **Anomaly of monthly mean temperature of studied stations based on the ENSO index for El Niño and La Niña years compared with the standard deviation of the monthly mean temperature**

A Probability or Confidence Test was performed to determine the accuracy of the results obtained. The percentage values of the significance vary from month to month through each one of the categories (El Niño, La Niña and Neutral years). The temperature predicted for the neutral years have about 60-70% significance; while the highest significant percentage corresponds to the months of January (93%), February (84%), March (90%), May (89%), August (91%) and November (92%) for La Niña years and February (92%), March (95%), April (97%) and November (91%) for El Niño years.

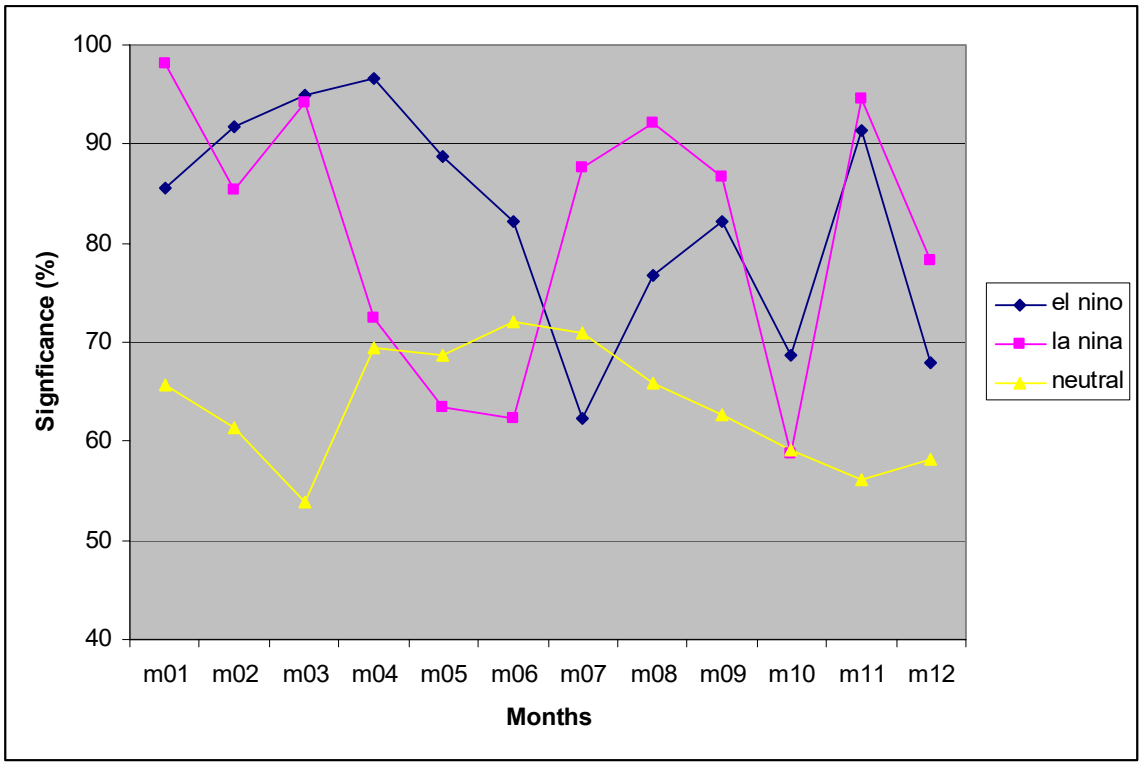

Figure 6: **Probability Test representation**

Conclusion

The analysis of the monthly mean temperature over the years of 1947-2004 demonstrates that although we don't expect to see significant difference between ENSO index and the long term mean in Neutral years, the Neutral category has about 60-70% significance. This difference apparently is due to the non-ENSO-related signal or noise (random variability); which demonstrates that ENSO phase (either La Niña or El Niño) does not affect monthly mean temperature in the studied area. The results found for the months of May, June and October of La Niña years are examples of this.

The above observations also demonstrate that the monthly mean temperature during the winter months (Nov-Mar) is significantly related to ENSO phase. Summer temperature is significantly related to La Niña phase. Finally, the prediction of future monthly mean temperature can be achieve for winter months using the ENSO index, and the temperature for summer months can only be predicted for La Niña years.

References

A. Klein, S. Lee and T. Over, "Effects of El Niño/Southern Oscillation on Temperature, Pecipitation, Snow Water Equivalent and Resulting Stream flow in the Upper Rio Grande River Basin," *Hydrological Processes.* Vol. 18, pp 1053-1071, 2004.

J. Bartholy and R. Pongrácz, "Regional effects of ENSO in Central/Eastern Europe," *Advances in Geosciences*. *European Geosciences Union*. vol. 6, pp. 133-137, January 2006.

M.F. Triola, *Elementary Statistics,* 8th edition. Chapter 6. Addison – Wesley Longman, 2001.

P. I. Good, *Introduction to statistics through re-sampling methods and Microsoft Office Excel***,** New Jersey: Wiley-Interscience/ John Wiley, 2005

R. J. Harris, *A Primer of Multivariate Statistics*, 3rd edition, Lawrence Erlbaum Associates, Mahwah, New Jersey, 2001, 609p.

http://cdo.ncdc.noaa

lynx http://hurricane.ncdc.noaa.gov/CDO/cdo

http://www.allmeasures.com

http://home.clara.net/sisa/signhlp.htm

http://www.onlineconversion.com/temperature.htm

http://www.cdc.noaa.gov/ENSO/enso.mei_index.html, August 13, 2006.

http://www.cdc.noaa.gov/ENSO/enso.glossary.html, August 13, 2006.

http://www.jigsao.washington.edu/data/globalsstenso/, August 13, 2006.

Measurement of the benthic loading from an aquaculture operation in Culebra, Puerto Rico

Undergraduate Student
Melissa Quiñones

Advisor
Wilson R. Ramírez
Department of Geology
University of Puerto Rico

The following study is part of a multidisciplinary long term project to determine the environmental impact caused by fish farms on the west coast of Culebra, P.R. It is believed that such fish farms may produce environmental changes including the action of the sedimentation, affecting grain size distribution and composition. A change in sedimentary processes may affect organisms that live on the ocean floor, adding a pronounced environmental effect. Four stations were set up along a transect on the study area. Each station contains 2 sediment traps (replicates). Samples of sediment traps were complemented by core samples. X-Ray diffraction analysis, grain size and distribution, and composition analysis were done in the sediments. Traps and cores have similar mineralogical composition in all the samples. The cumulative curves show that there is not a significant change in grain size as we move along the transect away from the cage. The exception was the station located under the cage, were the grains are finer. The organic matter was always lowering the sediment the traps compared with the cores measured. There were also more terrigenous sediment in the traps that in the cores. The most abundant component in traps and cores were carbonates. There were more carbonates in the cores that in the traps. The information obtained in the study suggests that the organic loading from the cage (traps) is not impacting the bottom significatively because the organic material is not being deposited on the bottom (cores).

Introduction

A company named Snapperfarm has installed an aquaculture project two miles of the west coast of Culebra, P.R. The demonstration project consists of a fish farm compose of two cages located twenty meters from each other. Each one of the cages produces about one hundred tons of fish.

This investigation is part of a long term multidisciplinary project to determine the environmental impact of the demonstration project in the benthic areas in the area surrounding the two cages. The research problem addressed in this proposal was the measurement of the sea floor sediments texture and composition (cores) and the benthic loading caused by the cages (sediment traps and composition analyses).

This project that has a focus toward the environmental sciences includes geological and biological aspects. The Grain size analysis, the composition analysis and the mineralogy of the cores and trapped sediment samples are important geological aspects in the development of this environmental impact study.

Study Area

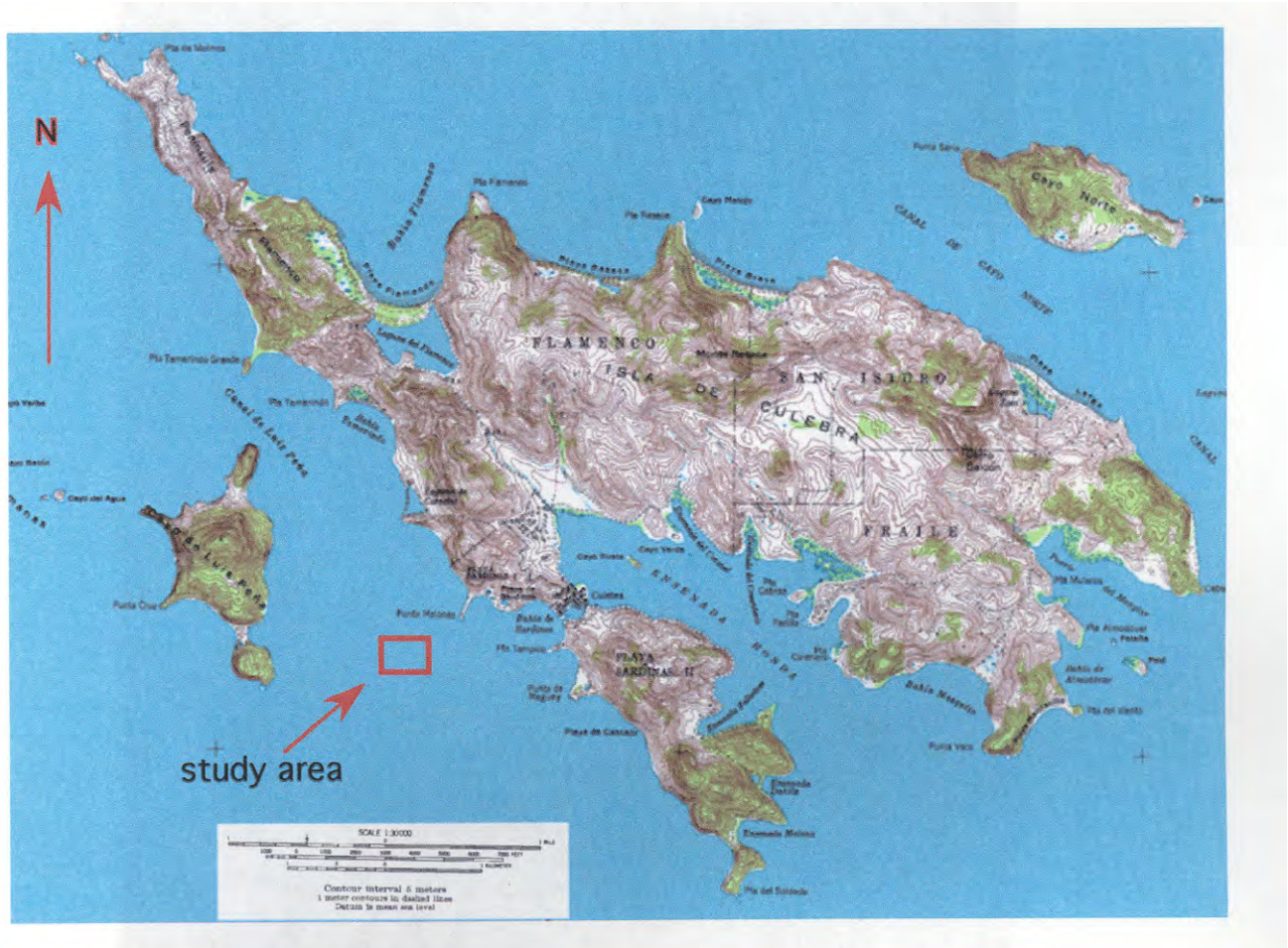

Fig. 1: **Study location in Culebra, PR**

Modified from: USGS Topographic Map of Culebra and adjacent Islands, PR, 1948

The study area is composed of the in wish the fish farm cages are located and their surrounding areas. This fish area is located at 18 16.418 N, 65 19.764 W and at a depth of ninety (90) feet. The ocean floor in situ is composed of non consolidated calcareous sediment material. No high relieve geomorphological structures like corral reefs are present. On the ocean floor a large quantity of pebbles and cobbles composed of parts of organisms (bioclasts) are present. No corals (seleractinium and octocorals) have been observed in the area. The ocean currents in study area are predominantly from the north-east although there are known changes to the south- west. Water column visibility varies from twenty to fifty feet. During normal conditions waves are predominantly from one to three feet height, except during the occurrence of a storm or other atmospheric events.

Methodology

Field work

There are two kinds of fish farm designs: Square pen and circular designs. The average dimension of a typical square pen are 10 meters on a side by 4 meters deep, but, circular designs can be up to 30 meters in diameter and 30 meters deep (Massachusetts Office of Coastal Zone Management).

The fish farm is composing of two cages (circular design cages).

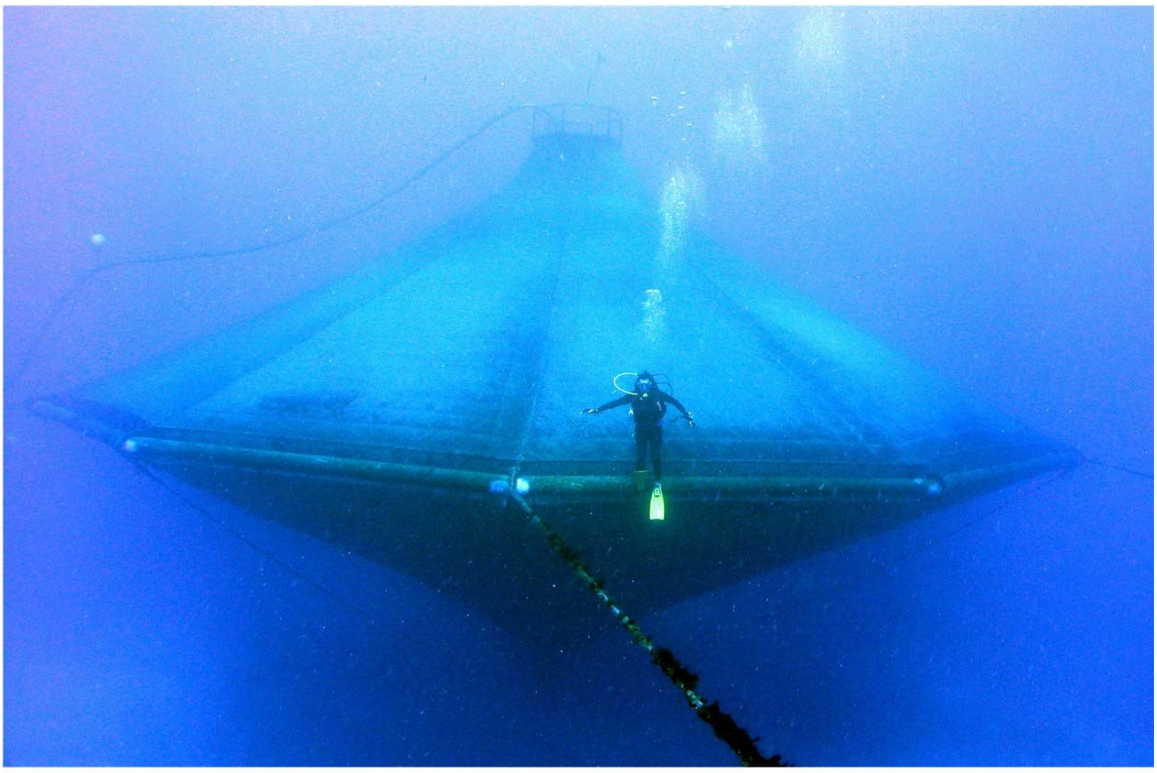

Fig. 2: **One of the cages, Culebra PR.**

To study the load produced from the cages stations were set up at a distance of eight, twenty five, sixty and ninety meters, forming a transect running southwest of the cage, as illustrated on figure 3).

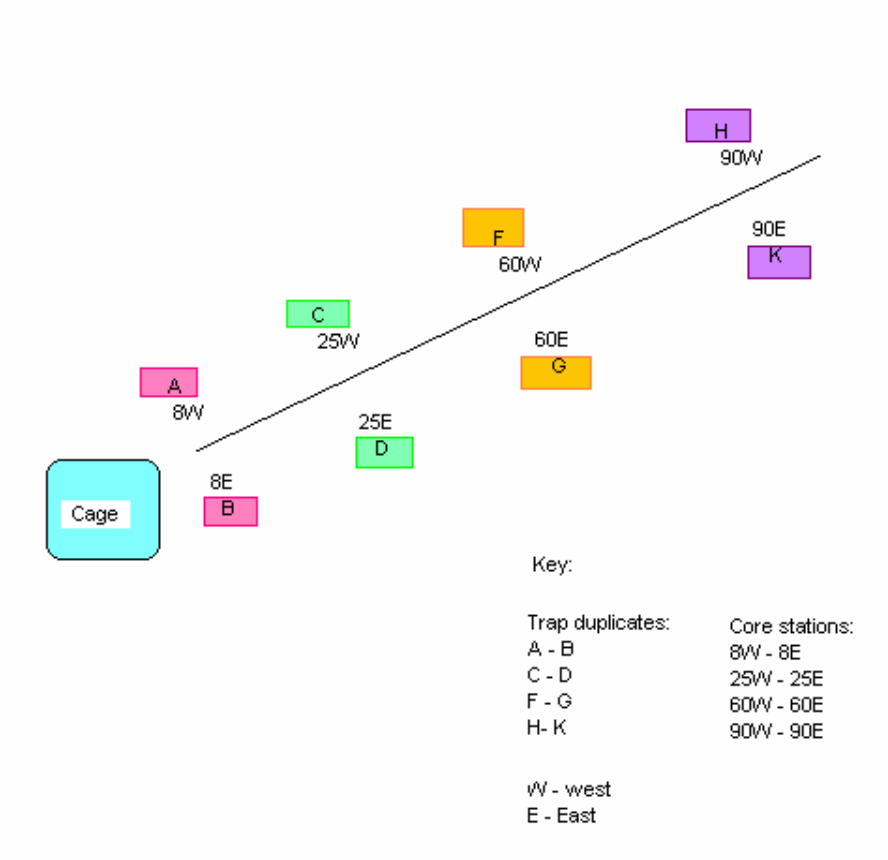

Fig. 3: **Diagram (not a scale) of the localization of the stations**

(Traps and cores)

Two Sediment traps were located in each one of the stations (8 meters, 25 meters, 60 meters and 90 meters). The estimated work time for a diver is about twenty minutes at 90 feet and only experienced divers are allow collecting the samples. Water conditions at the site (wave actions and strong currents) prohibit diving on some days. Sometimes is necessary to extend the field work for several days. Sharks are abundant in the place (dead fish on the cages) making the collection of the samples even more difficult.

Fig. 4: **Diver installing the trap**

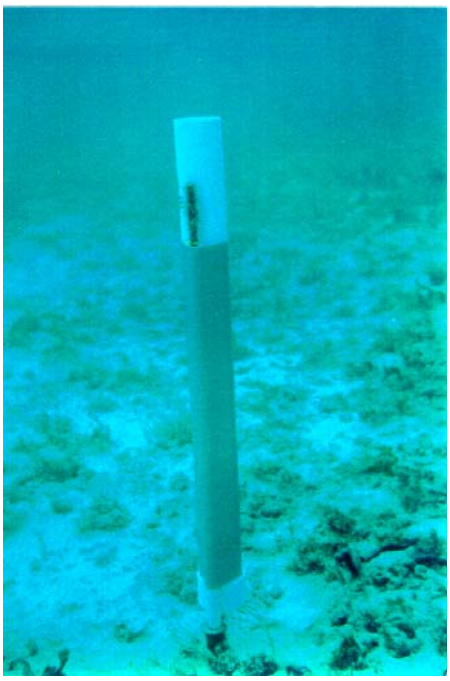

Fig. 5: **Sediment trap fixed to the ocean floor by a permanent reebar**

Fig.6: **Sediment traps**

Fig. 7: **Model holding a sediment trap**

The sediment traps are made of PVC pipes. The length of each one of the traps is 97.5 cm. and has a diameter of 8.5 cm. The traps are nested to the bottom. The trap dimensions are set to prevent any disruption in sediment deposition. In addition to the

traps the divers are collect cores at the same stations (8, 25, 60, and 90) every time they extract the traps. The sampling cores have length of 11.5cm. and a diameter of 5.72 cm (Rapp and Ramirez, 2002).

Fig. 8: **Core and holder**

Fig. 9: **Core filled with sample**

Fig. 10: **Core and core holder**

To create a hyper saline environment in the trap two pounds of salt are place at the base of the trap. The hyper saline environment reduces the amount of biological alterations to the organic sediments collected in the trap because the salt reduces the colonization of bacteria in addition. Thirty sixth inch cores were taken to identify possible changes in bacteria. Grain size and composition bellow a depth of 15 cm to avoid the heavily

bioturbated zone in the near surface. Formalin was used to treat all samples (traps and cores) immediately after collection to reduce any decay and change in the original organic matter collected.

Fig. 11: **Salt that was in one of the traps**

Laboratory work

After the divers extract the traps and the cores and add formalin, they are bringing to the laboratory of the geology department. The total number of samples per trip is about twenty two. Three analytical tests were made to each one of the samples; sediment composition, X-Ray diffraction (XRD) and grain size analysis. The objective of the composition analysis is to determine the amount of organic, carbonates and terrigenous materials and how it varies with distance from the cage (up to 90 meters). The analyses on grain size of the sediment under and around the cages help determine variations in grain size as we move from under the cage into the surrounding environment.

Discussion of results

This project includes three sets of samples that were collected and processed during a period of three months. The divers collect the traps and the cores during the first week of each month. The first set of samples was taken from July 30 to August 1, 2004. The second set was extracted from September 3 to September 5, 2004 and the third set of the samples was extracted from October 1 to October 3, 2004.

X- Ray diffraction

A total of 44 XRD analyses were made to the samples (7 sediment trap samples and 37 core samples). The purpose of the XRD analysis was identifying the mineralogical composition of the samples. Minerals found on the samples indicate that the mineralogy of ocean floor in the study area is composing predominantly of calcareous material. The calcareous material present in the study area (calcite, aragonite and magnesian calcite) is probably produced by organisms.

Two different types of Halite were distinguished: Halite (NaCl) the mineral and Halite Syn (rock salt). The Halite Syn forms as a result of evaporation of saline water in the process of drying the samples.

	Minerals present on the samples					
Sample name	***Calcite magnesian***	***Halite, syn***	***Aragonite***	***Kaolinite***	***Halite***	***Calcite***
25 B aug	x		x			
23 aug	x		x	x		
8 B aug	x		x	x		
J 60 aug	x	x	x	x		
J 90 aug	x		x	x	x	
T 90 aug	x		x	x	x	
60 aug	x	x	x	x		
W 60 aug	x	x	x	x		
8 aug	x		x		x	
Core debajo de jaula	x	x	x	x		
Core transecto	x		x		x	
GP 2 aug	x		x		x	
GP 1 aug	x		x		x	
P	x		x		x	x
S	x	x	x			x
X	x		x		x	x
Q	x		x		x	x
Z	x		x		x	x
W	x		x		x	x
T	x		x		x	x

E 60 E sept	x	x	x			
90 W sept	x	x	x			
60 W sept	x	x	x			
25 W sept	x	x	x	x		
8 W sept	x	x	x	x		
E 25 E sept	x	x	x			
E 8 E sept	x	x	x			
E 90 E sept	x	x	x			
Sept 3 90 bellow 2	x	x	x			
Sept 3 90 upper 2	x	x	x			
Sept 3 60 bellow 2	x	x	x			
Sept 3 60 upper 2	x	x	x			
Sept 3 0 bloque upper 2	x	x	x			
Sept 3 0 bloque bellow 2	x	x	x			
60 W	x	x	x			
90 w	x	x	x			
E 25 E	x	x	x			
E 60 E	x	x	x			
E 8 E	x	x	x			
E 90 E	x	x	x			
25 W	x	x	x			
8 W	x	x	x			
GP 2	x	x	x			
GP 1	x	x	x			

Fig. 12: **Minerals present on the samples**

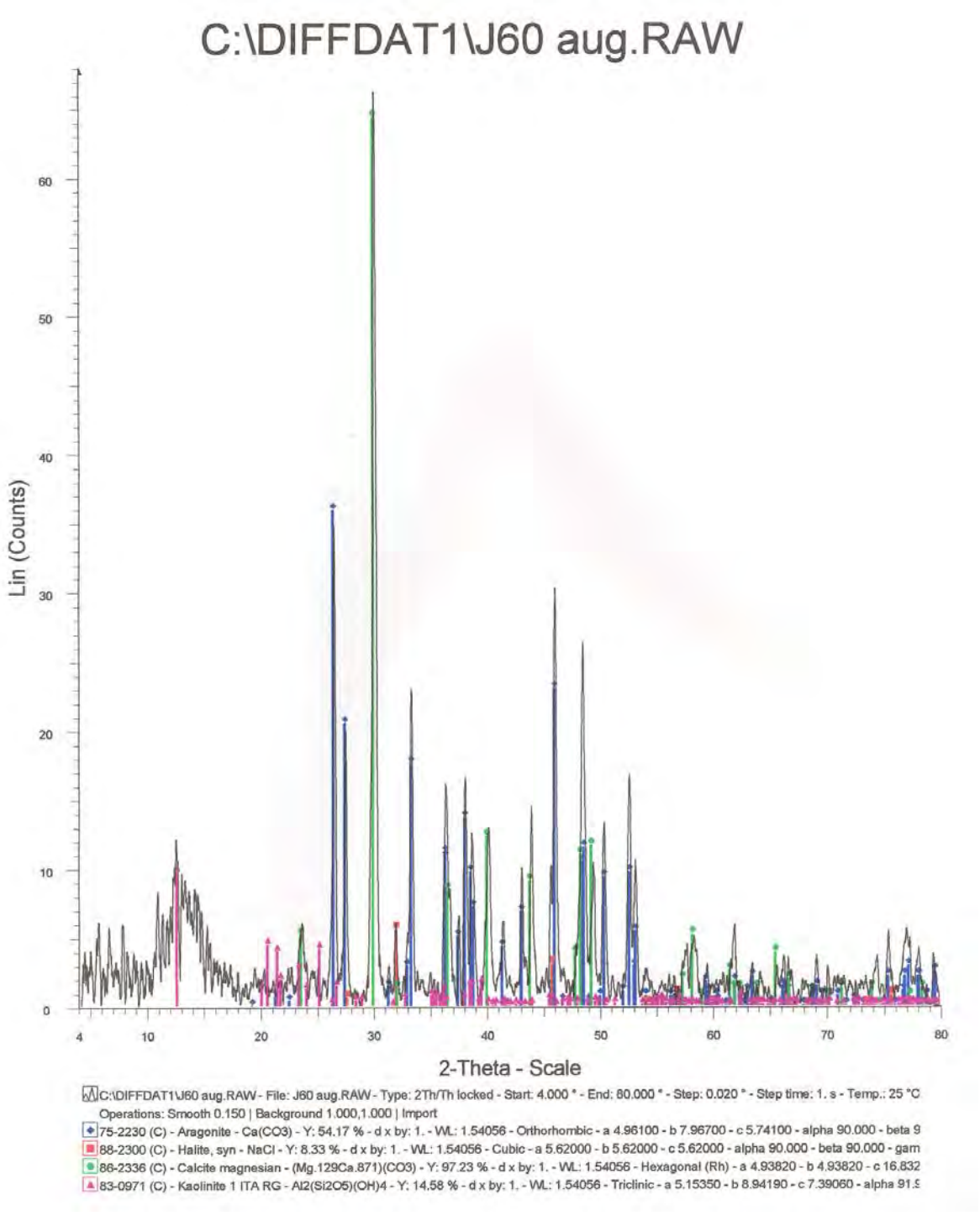

Fig. 13: **Example of a graph obtained from the XRD analysis of a core sample from the station at 60 meters**

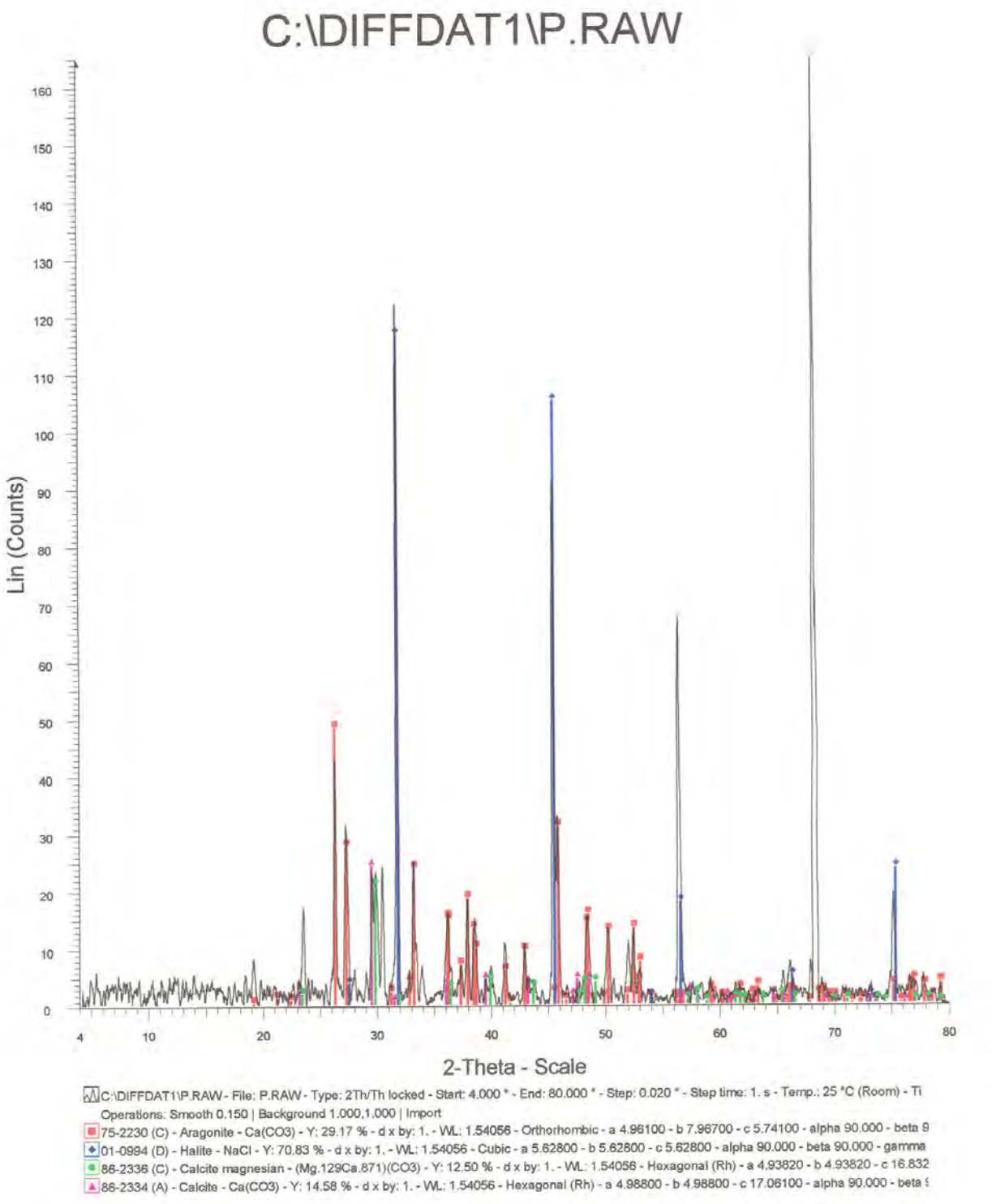

Fig. 14: **Example of a graph obtained from the XRD analysis of a trap sample from the 25 meter station**

Grain size analysis

A total of 36 Grain size analyses were done in the core samples. The purpose of the grain size analysis was identifying how the size of the grains varies in with distance from the

cage. The samples were screened for –3 phi to >4 phi sizes. Histograms and Cumulative curves were developed to characterized the bottom conditions and to determine if there were changes in grain sizes along the lineal distance along the transect.

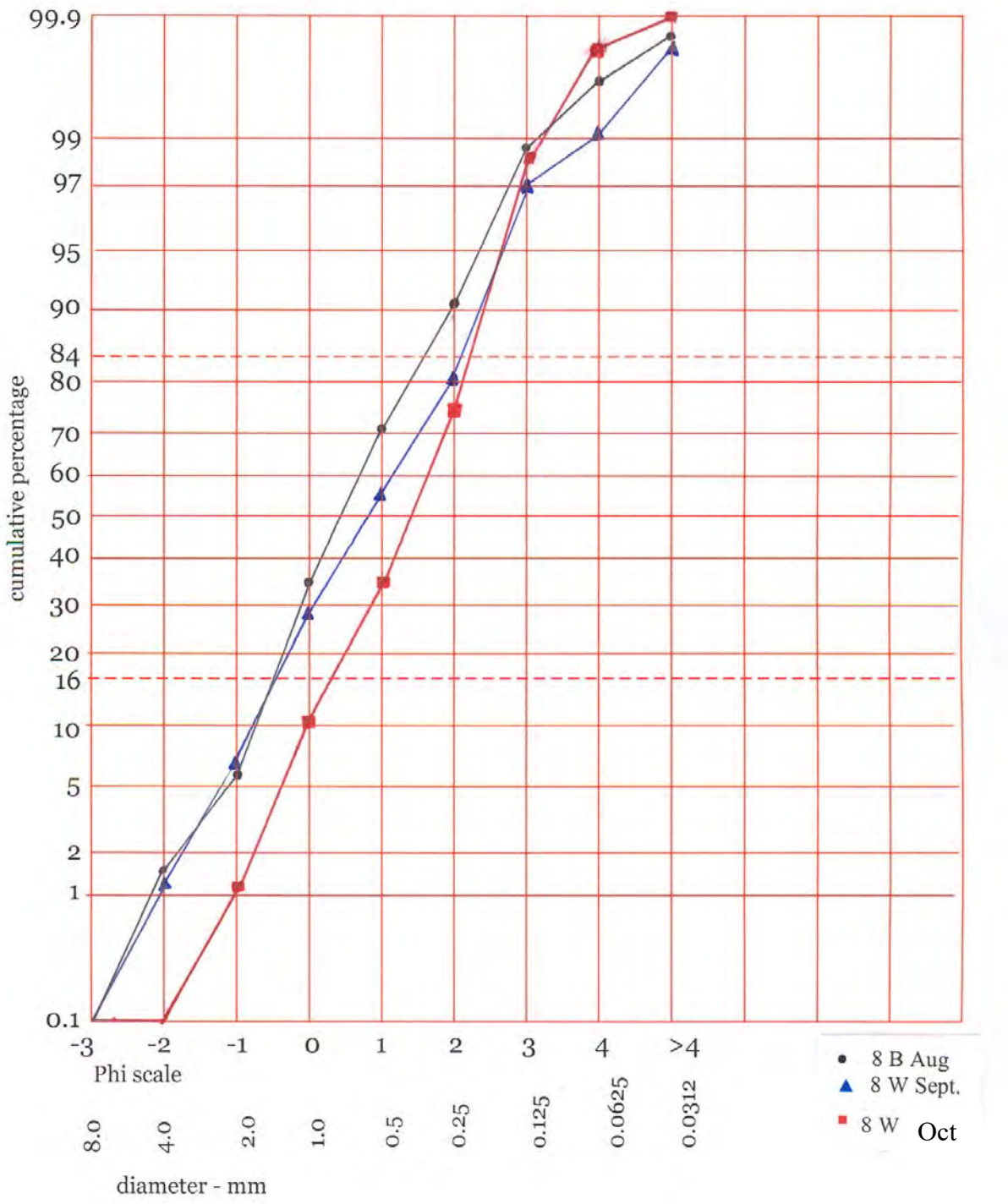

Fig. 15: **Cumulative curves showing the grain size variations at the 8m (8 meters distance from the cage) during the months of August, September and October**.

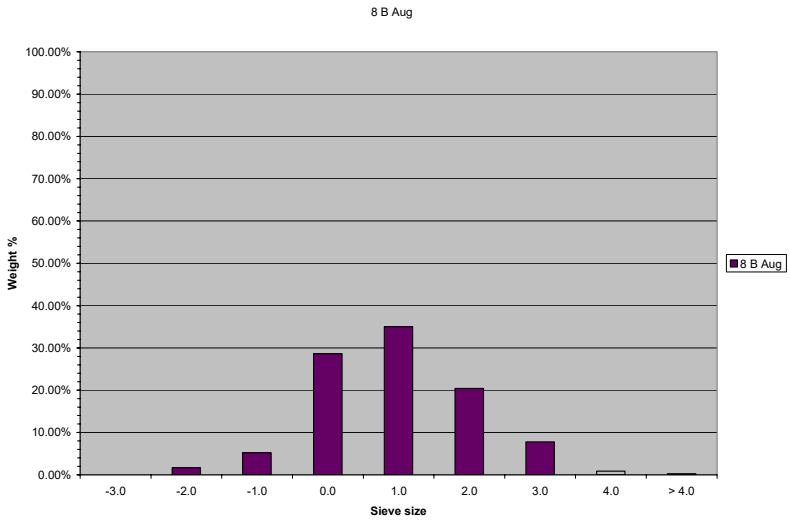

A.

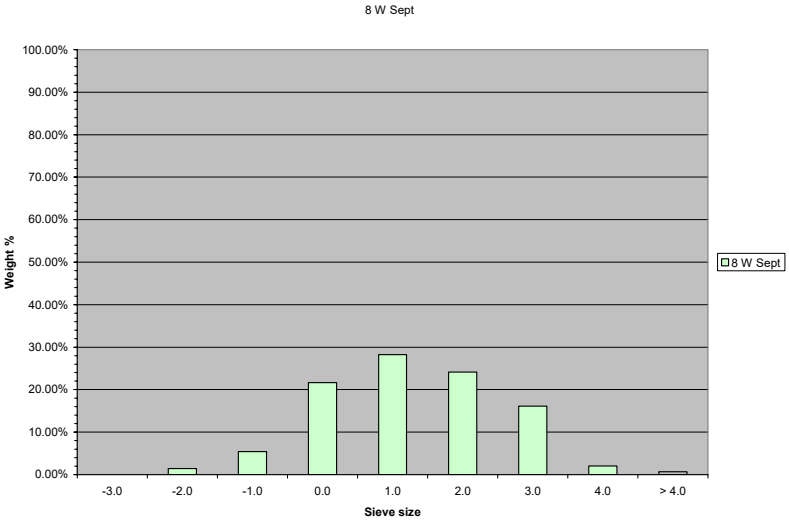

B

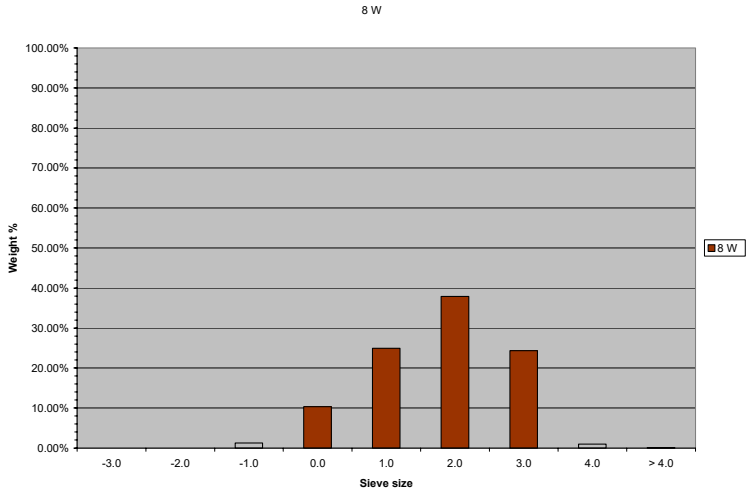

C.

Fig. 16: **Histograms with the grain size variation at the 8m west station for the months of August (A), September (B) and October(C) of 2004.**

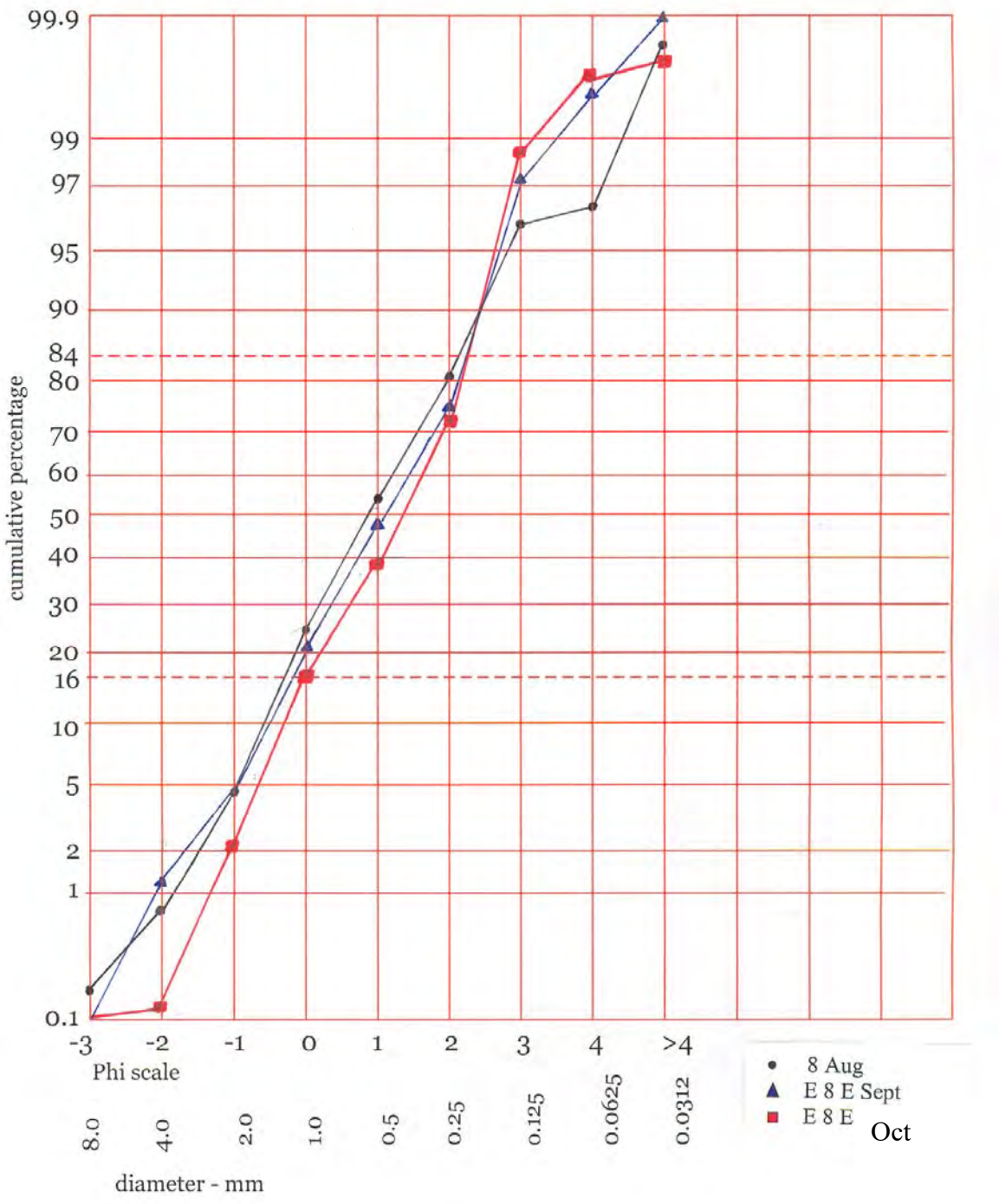

Fig. 17: **Cumulative curves showing the grain size variations at the 8m east (8 meters distance from the cage) during the months of august, September and October**

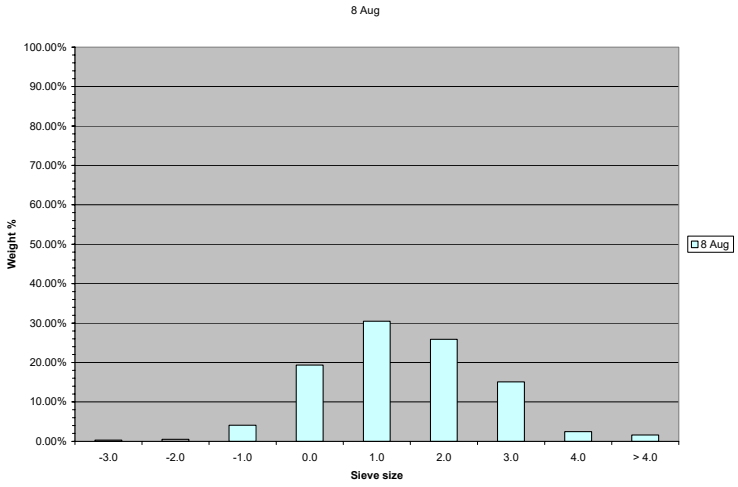

A.

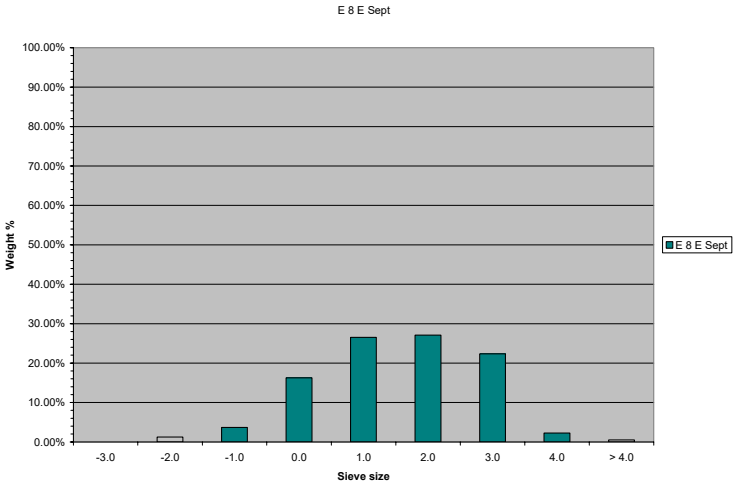

B.

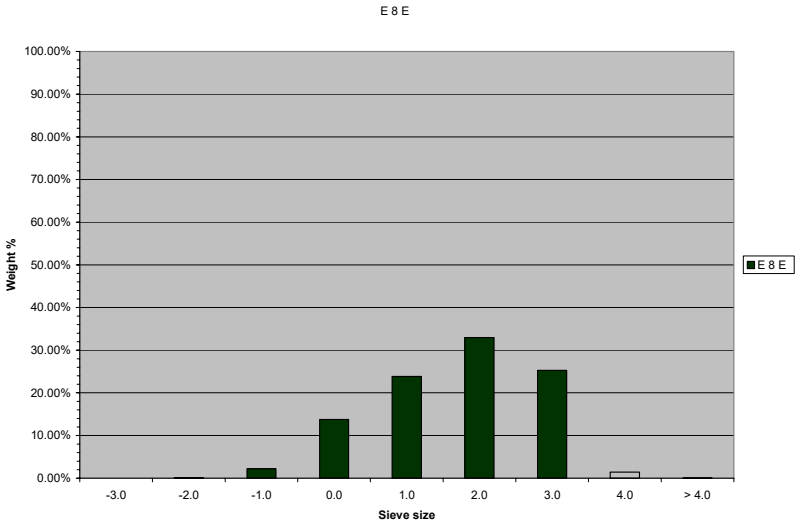

C.

Fig. 18: **Histograms with the grain size variation at the 8m east station for the months of August (A), September (B) and October(C) of 2004.**

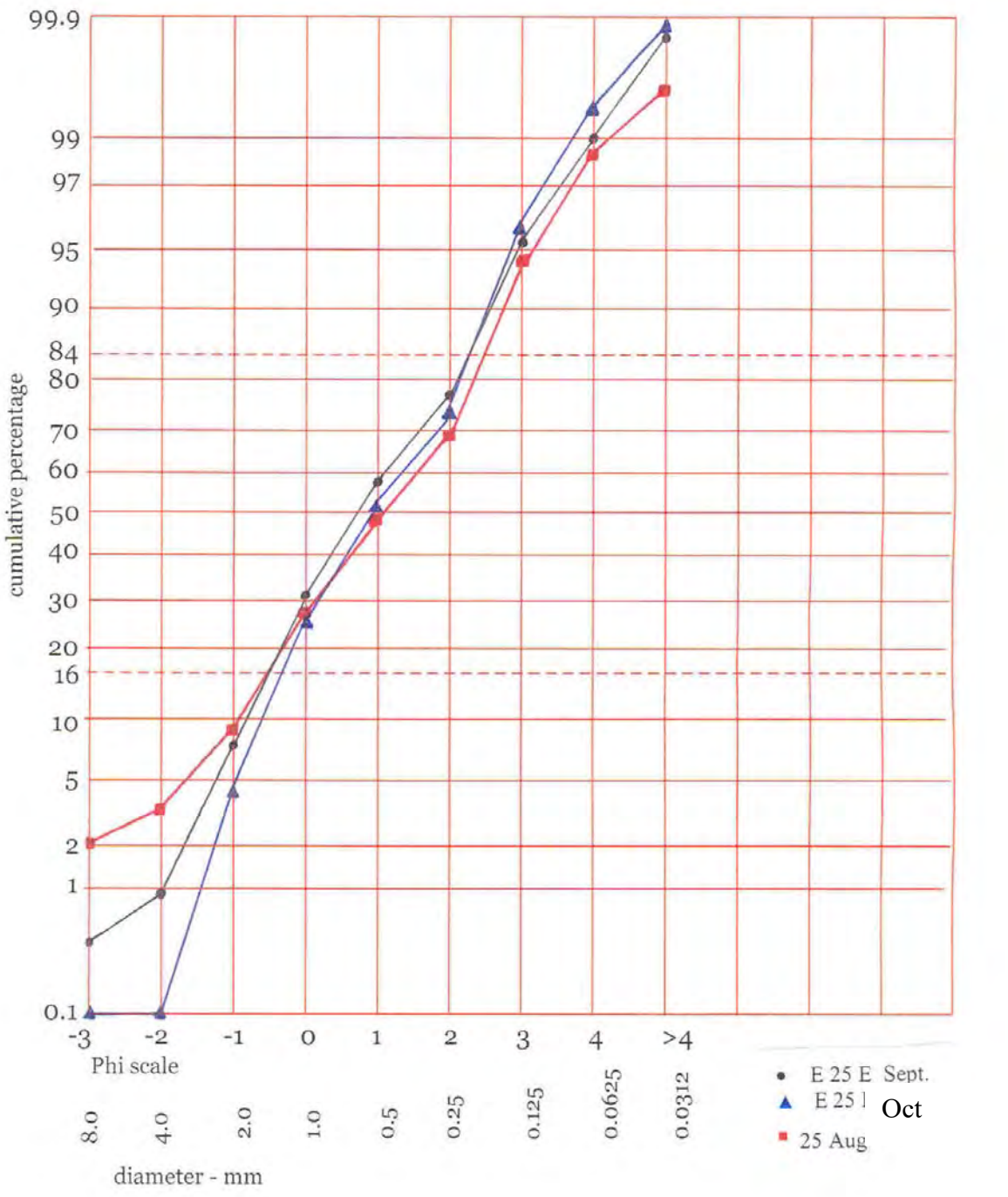

Fig. 19: **Cumulative curves showing the grain size variations at the 25m east station (25 meters distance from the cage) during the months of August, September and October.**

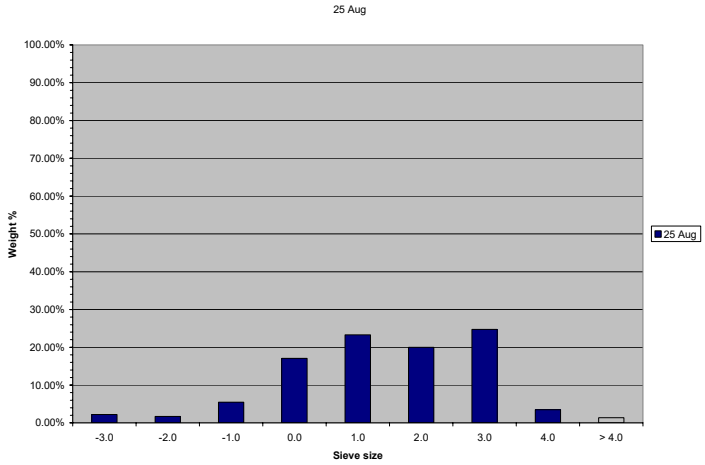

A.

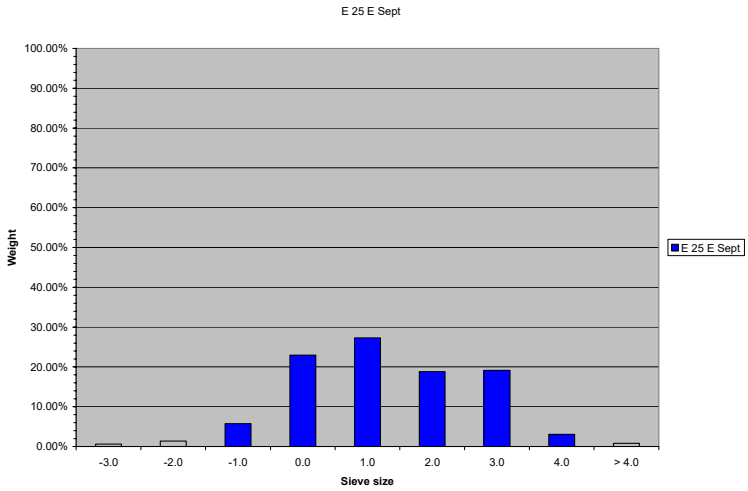

B.

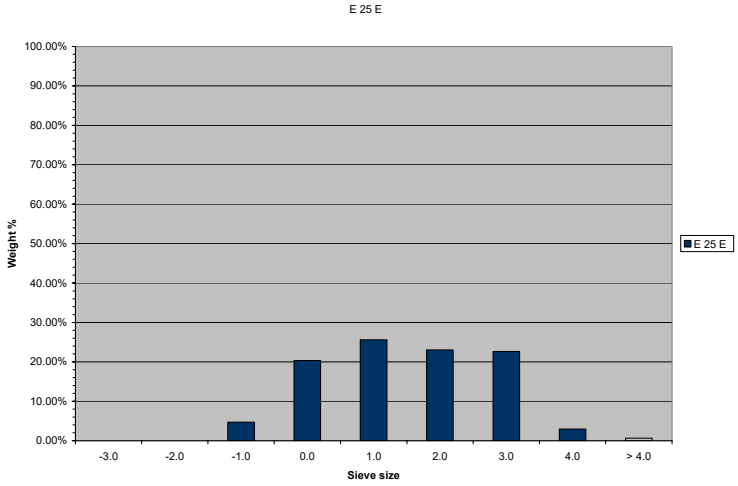

C.

Fig. 20: **Histograms with the grain size variation at the 25m east station for the months of August (A), September (B) and October(C) of 2004.**

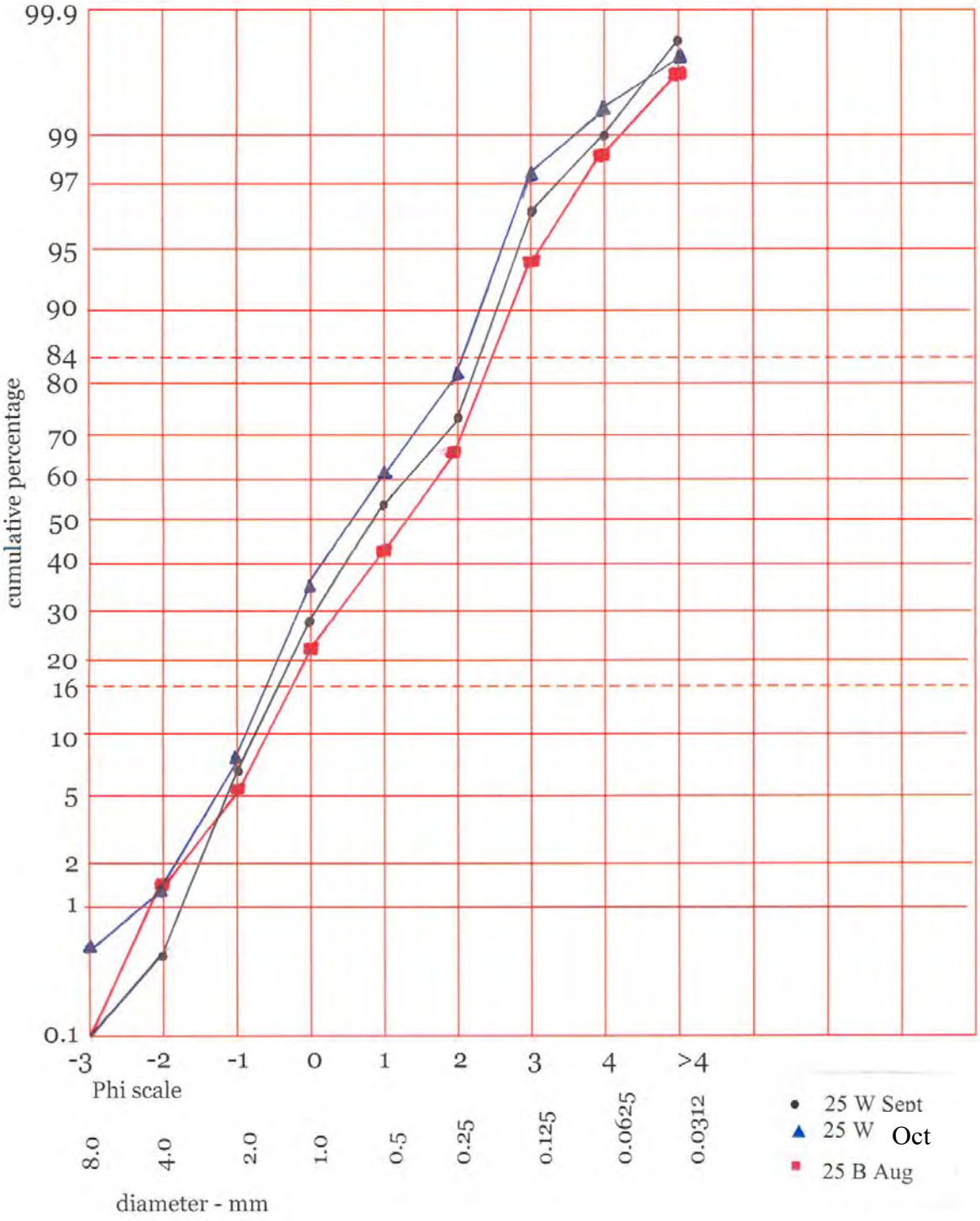

Fig. 21: **Cumulative curves showing the grain size variations at the 25m west station (25 meters distance from the cage) during the months of August, September and October.**

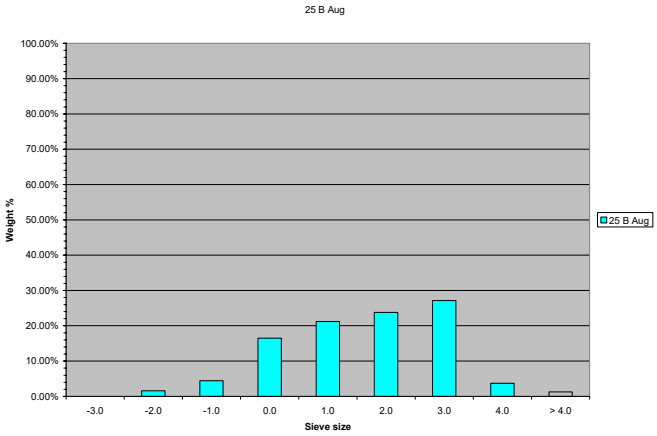

A.

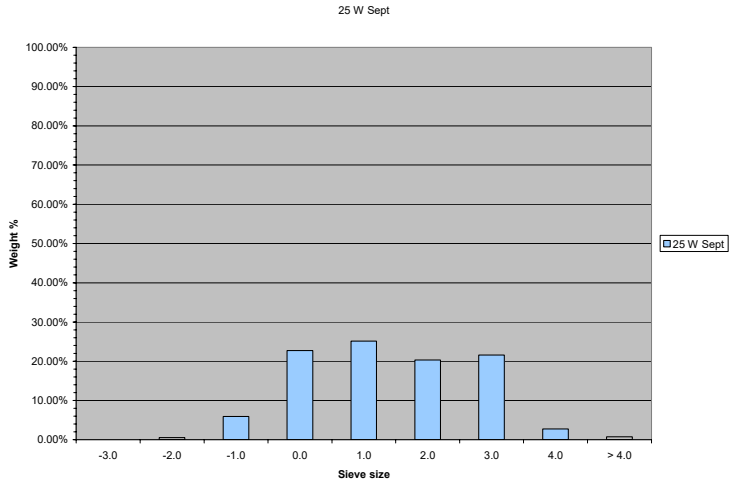

B.

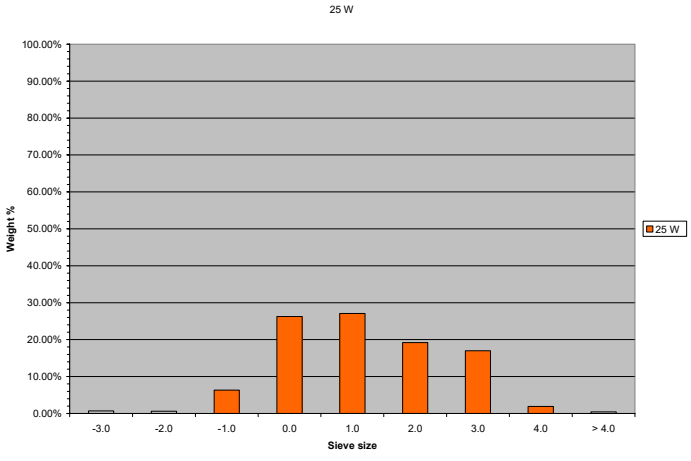

C.

Fig. 22: **Histograms with the grain size variation at the 25m west station for the months of August (A), September (B) and October(C) of 2004.**

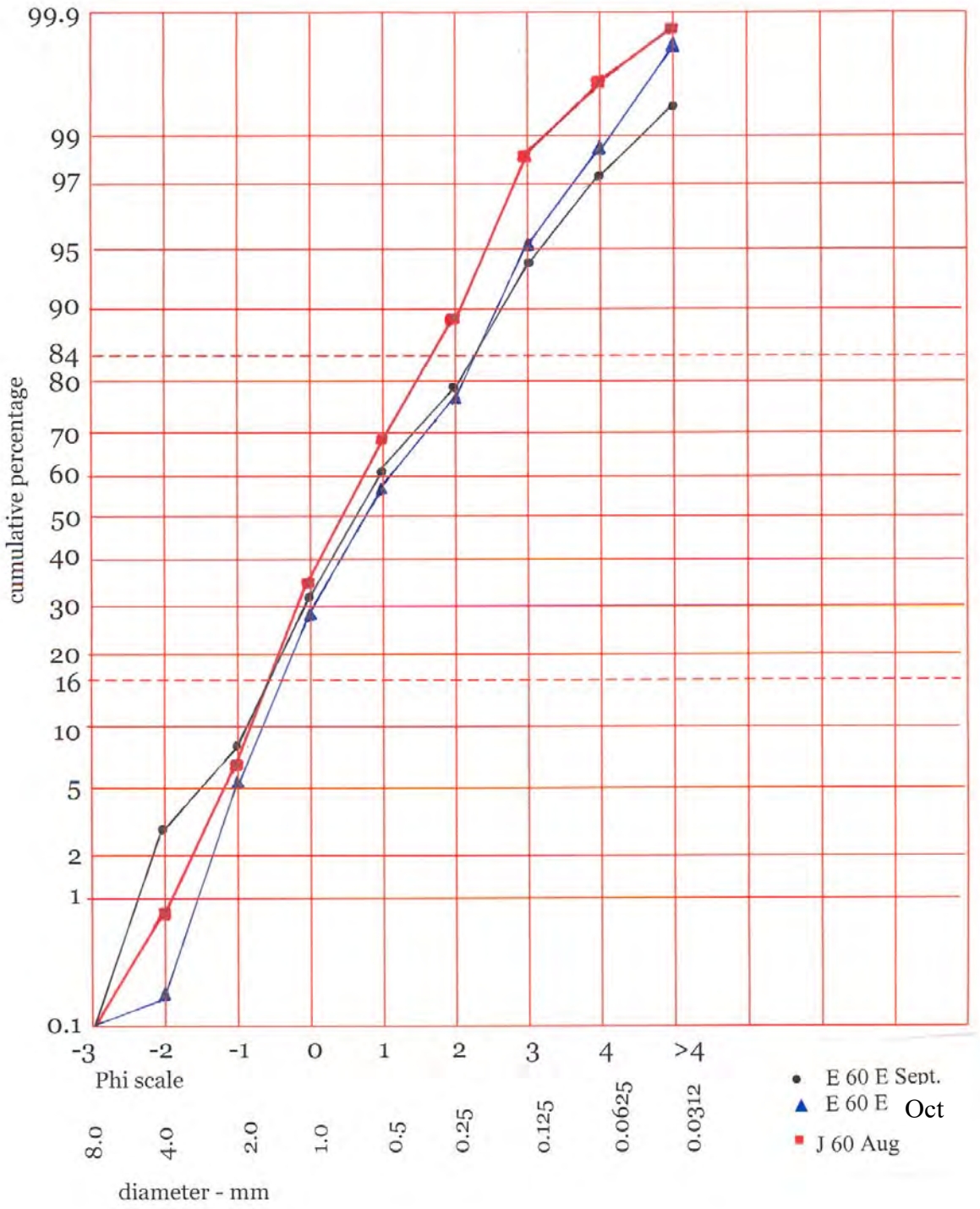

Fig. 23: **Cumulative curves showing the grain size variations at the 60m east station (60 meters distance from the cage) during the months of August, September and October.**

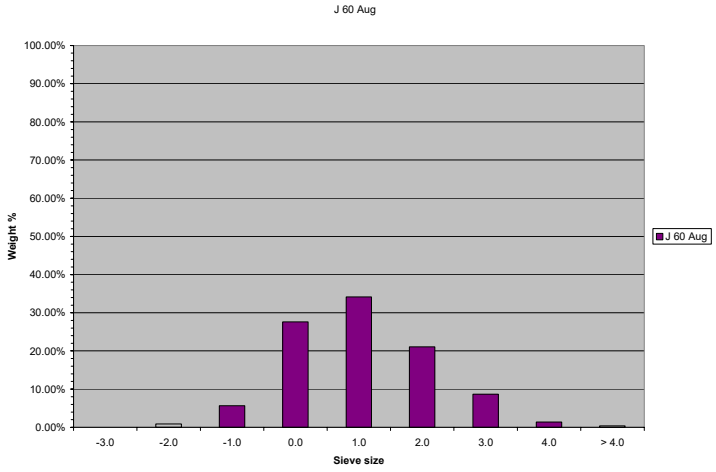

A.

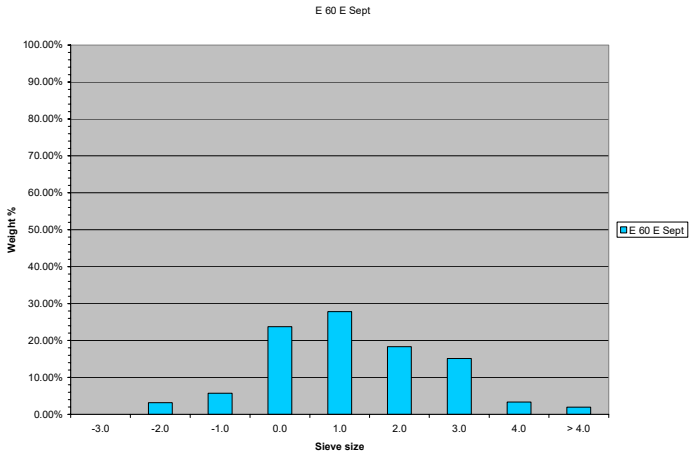

B.

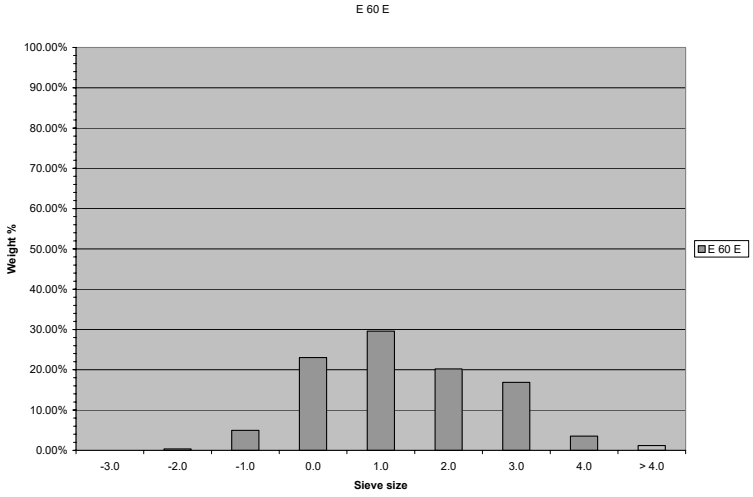

C.

Fig. 24: **Histograms with the grain size variation at the 60m east station for the months of August (A), September (B) and October(C) of 2004.**

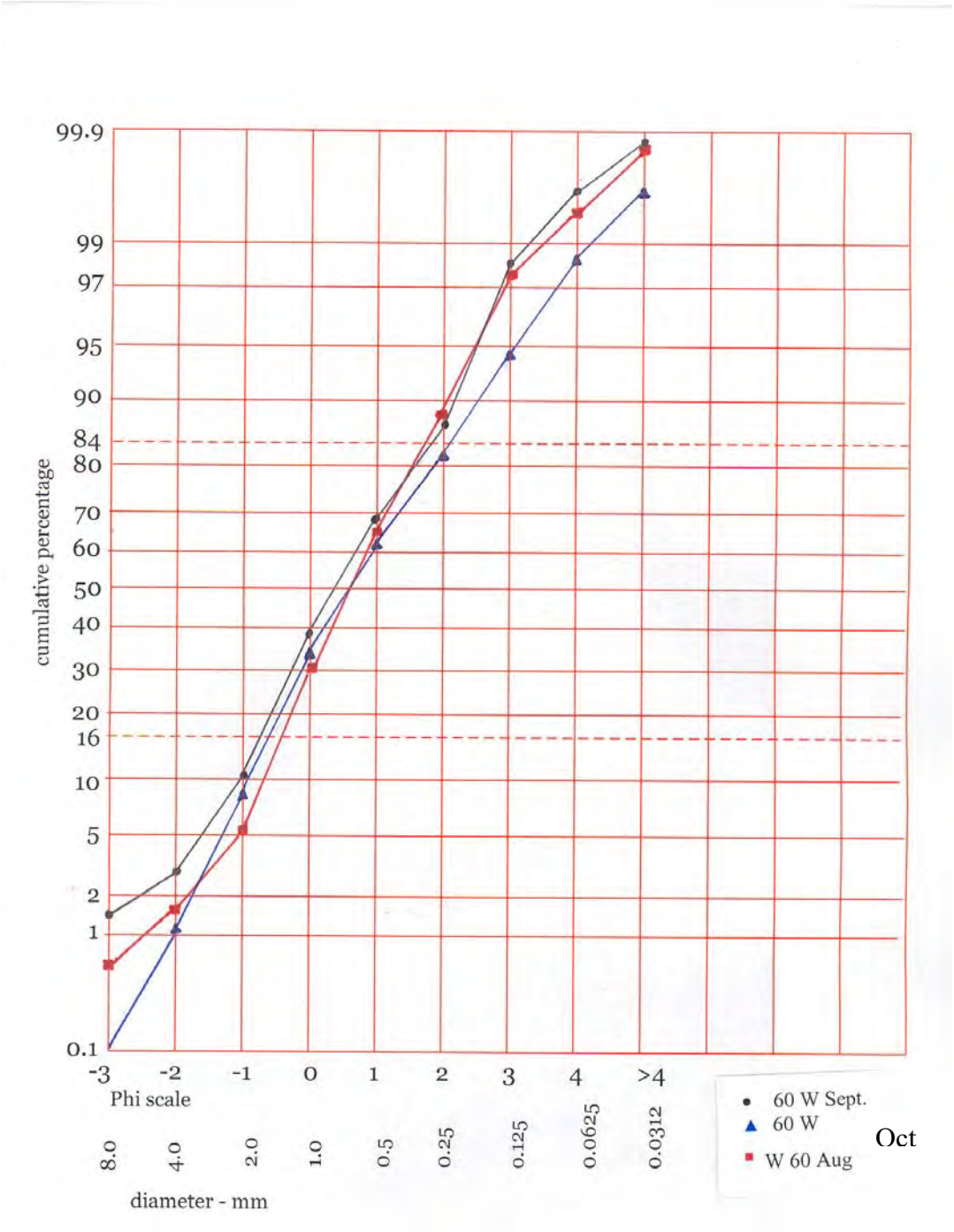

Fig. 25: **Cumulative curves showing the grain size variations at the 60m west station (60 meters distance from the cage) during the months of August, September and October.**

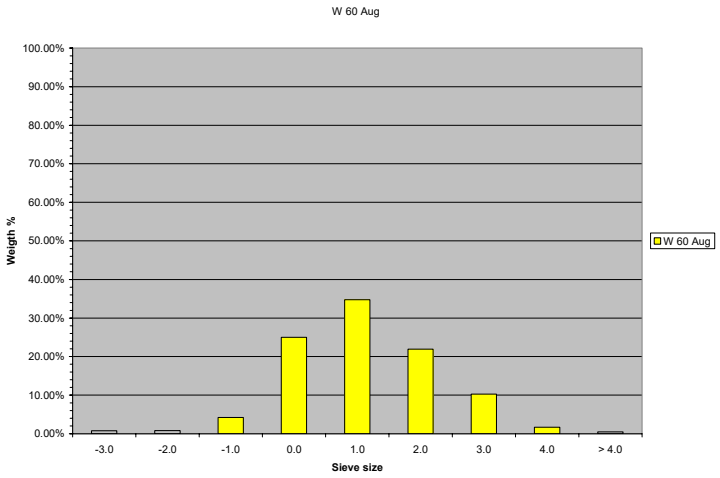

A

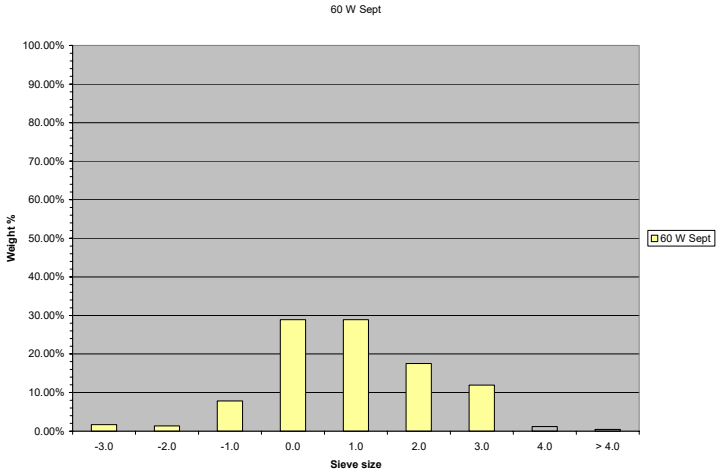

B.

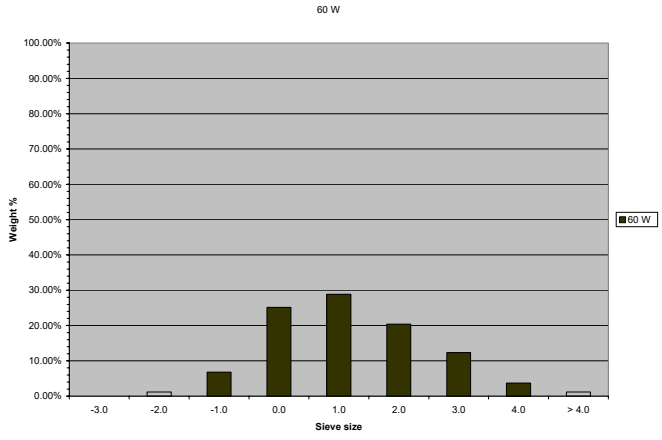

C.

Fig. 26: **Histograms with the grain size variation at the 60m west station for the months of August (A), September (B) and October(C) of 2004.**

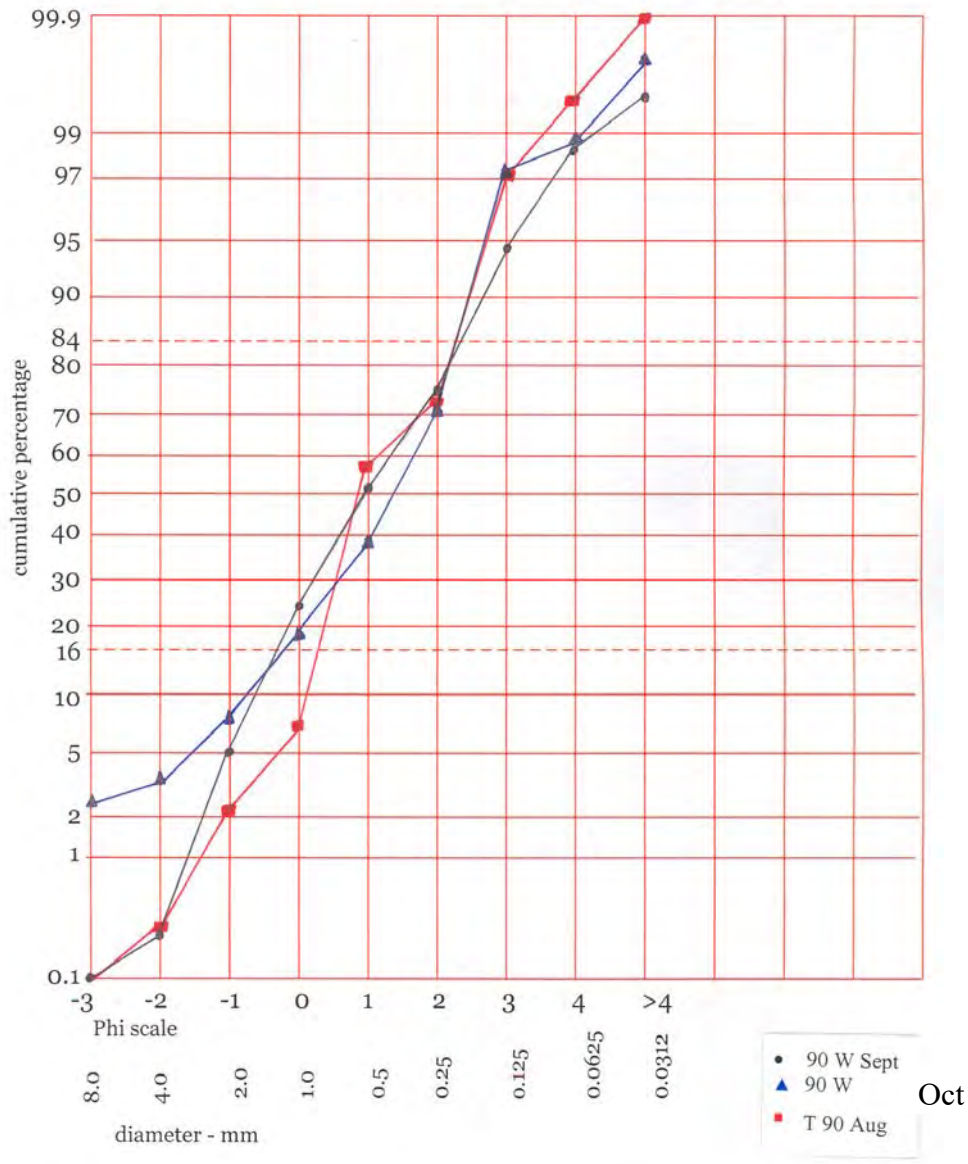

Fig. 27: **Cumulative curves showing the grain size variations at the 90m west station (90 meters distance from the cage) during the months of August, September and October.**

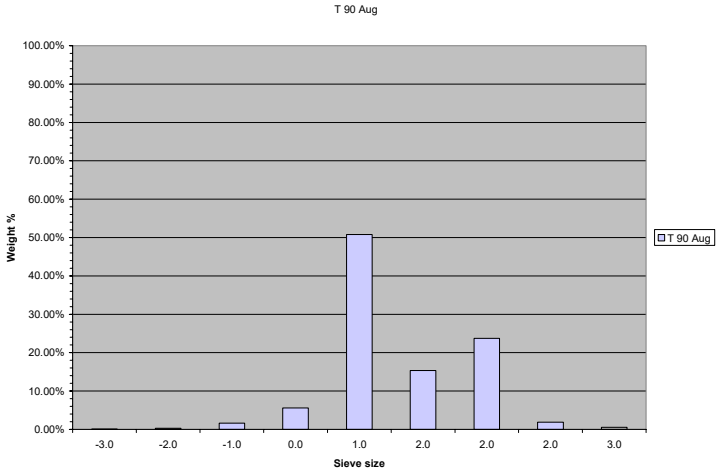

A.

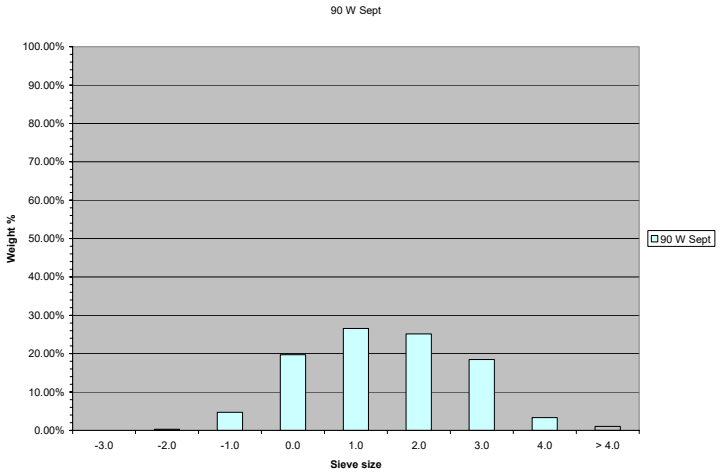

B.

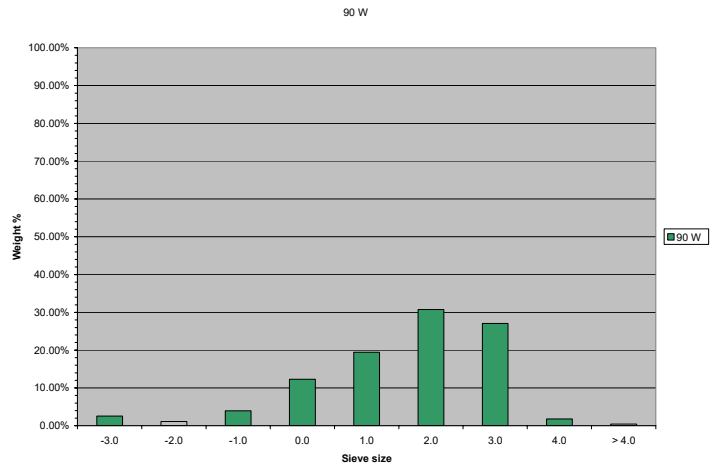

C.

Fig. 28: **Histograms with the grain size variation at the 90m west station for the months of August (A), September (B) and October(C) of 2004.**

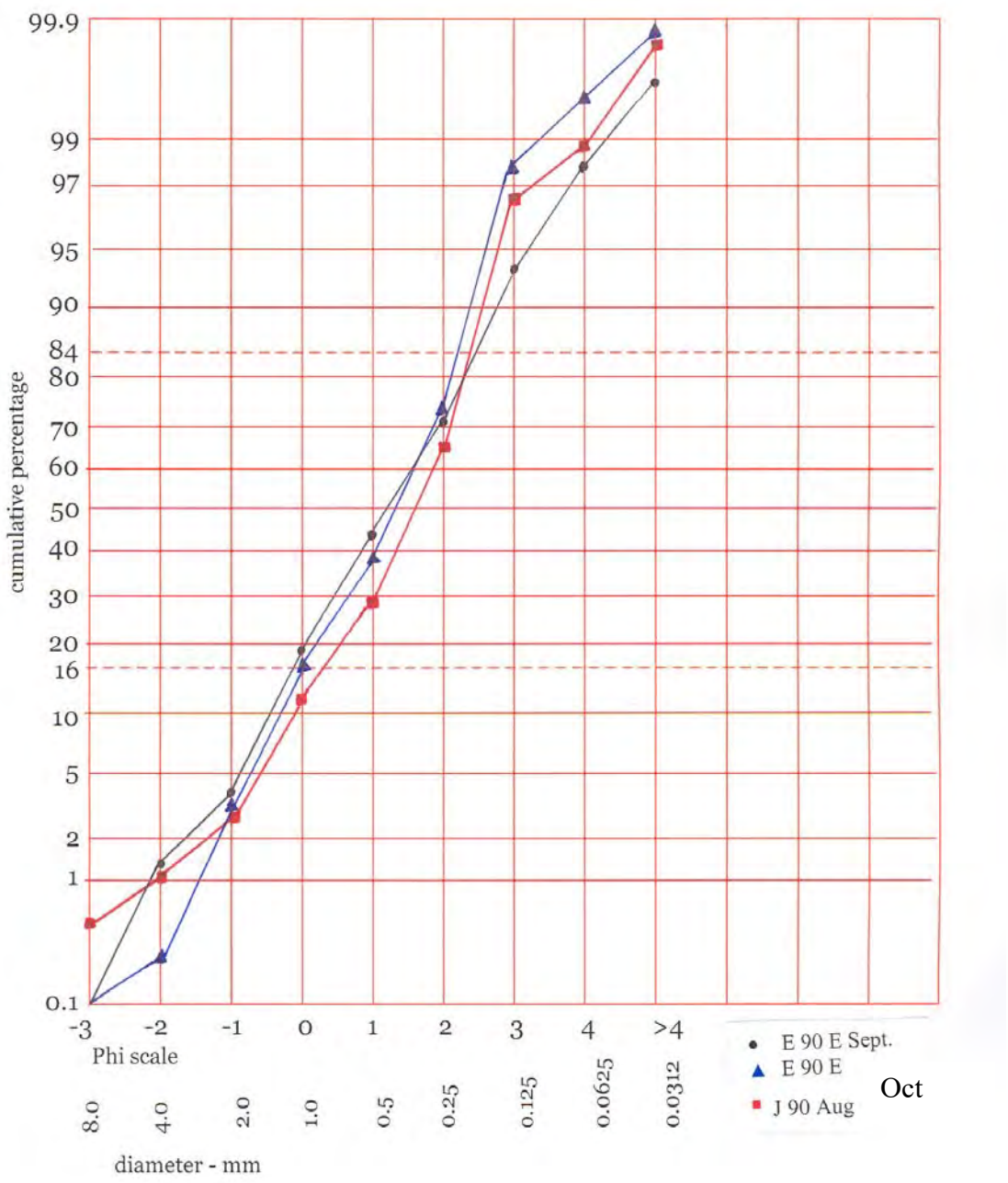

Fig. 29: **Cumulative curves showing the grain size variations at the 90m east station (90 meters distance from the cage) during the months of August, September and October.**

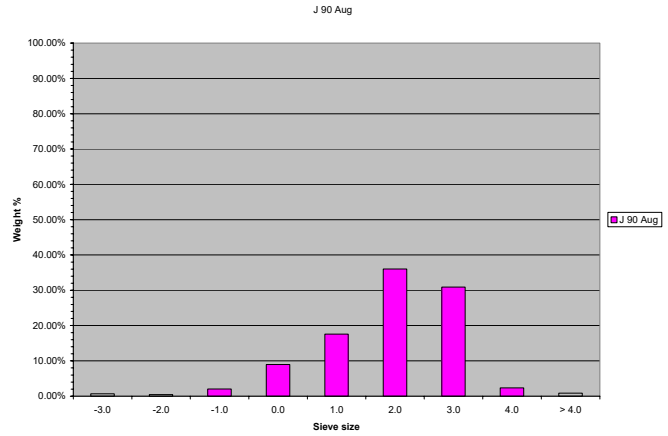

A.

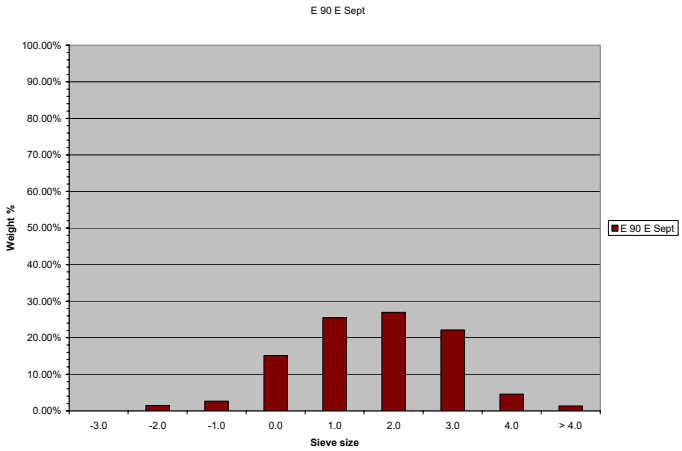

B.

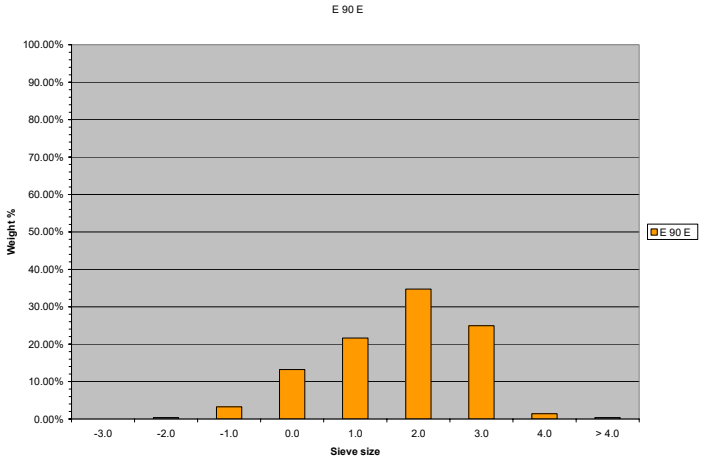

C.

Fig. 30: **Histograms with the grain size variation at the 90m east station for the months of August (A), September (B) and October(C) of 2004.**

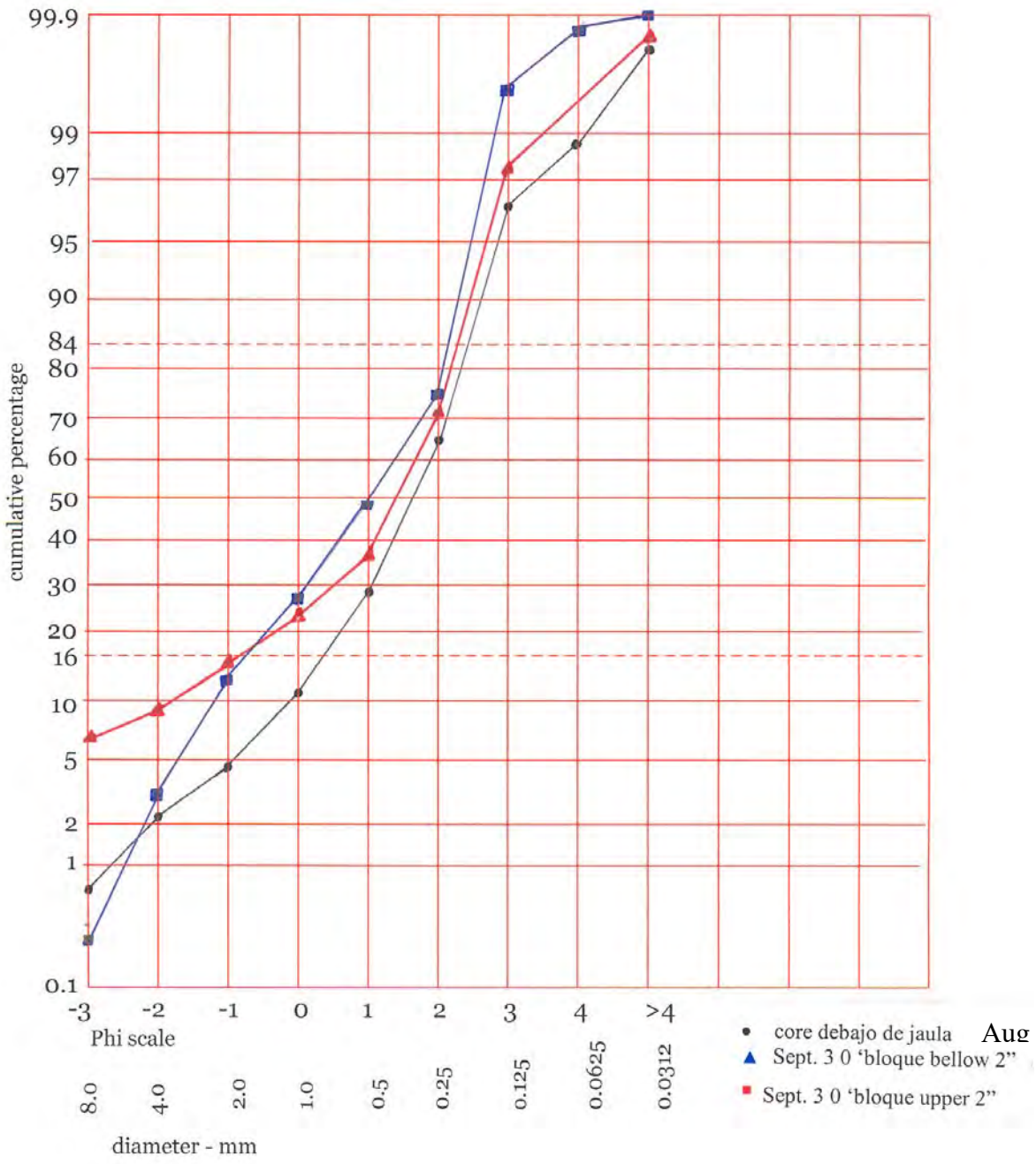

Fig. 31: **Cumulative curves showing the grain size variations at the core debajo de la jaula (under the cage), during the months of August and September.**

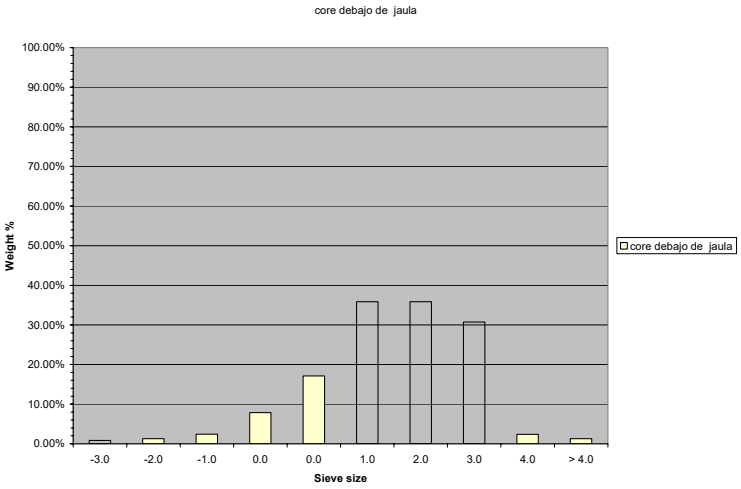

A.

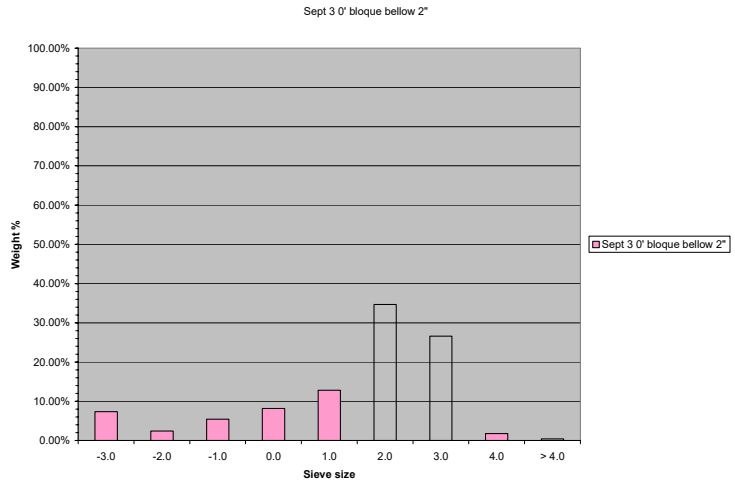

B.

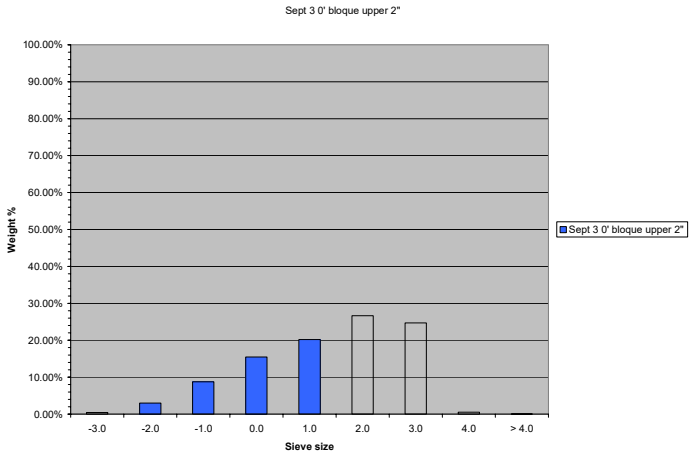

C.

Fig. 32: **Histograms with the grain size variation of the core debajo de la jaula station for the months of August (A) and September (B and C) of 2004.**

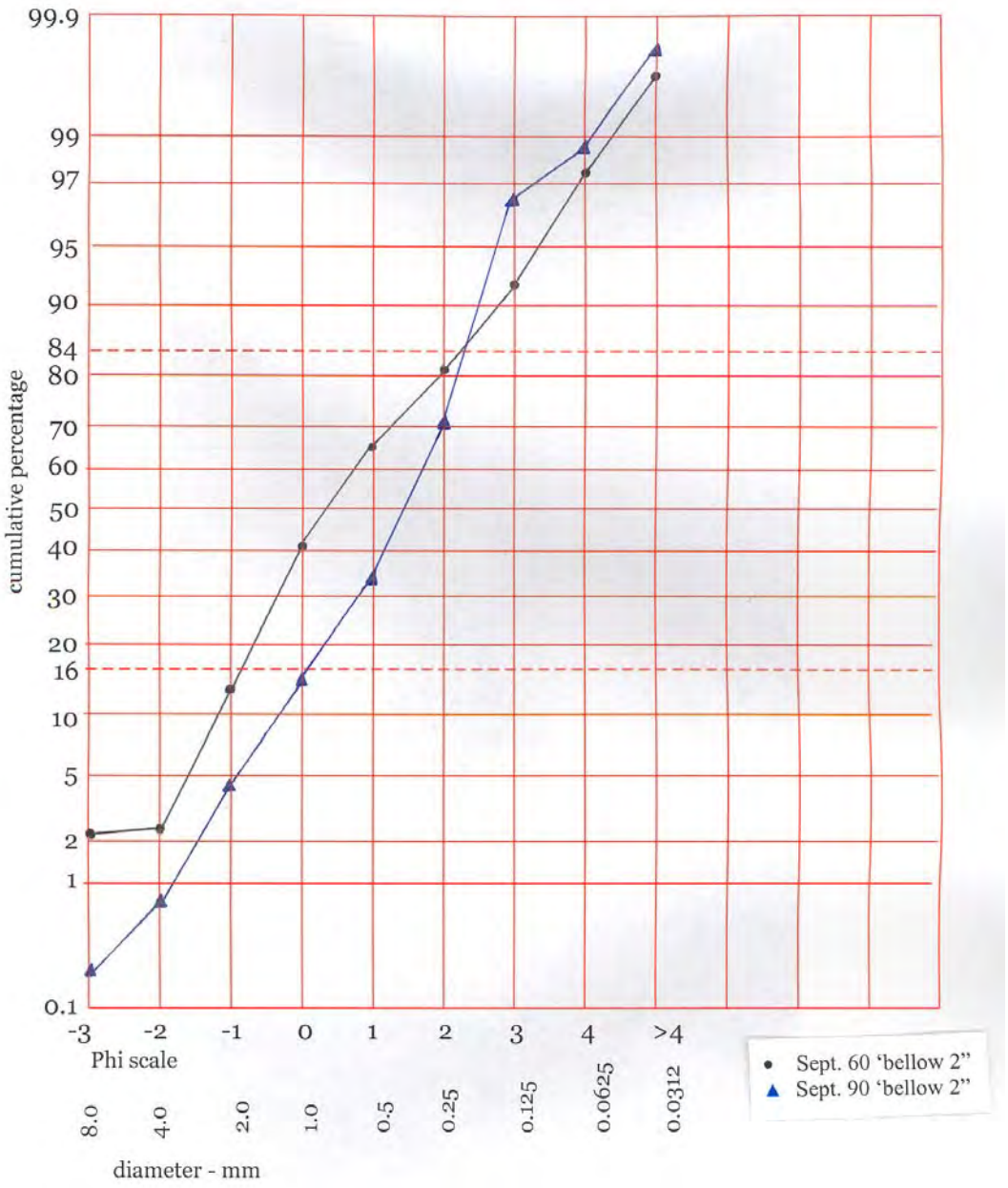

Fig. 33: **Cumulative curves showing the grain size variations at cores taken from the 60m and 90m stations (60 and 90 meters distance from the cage) during the month of September.**

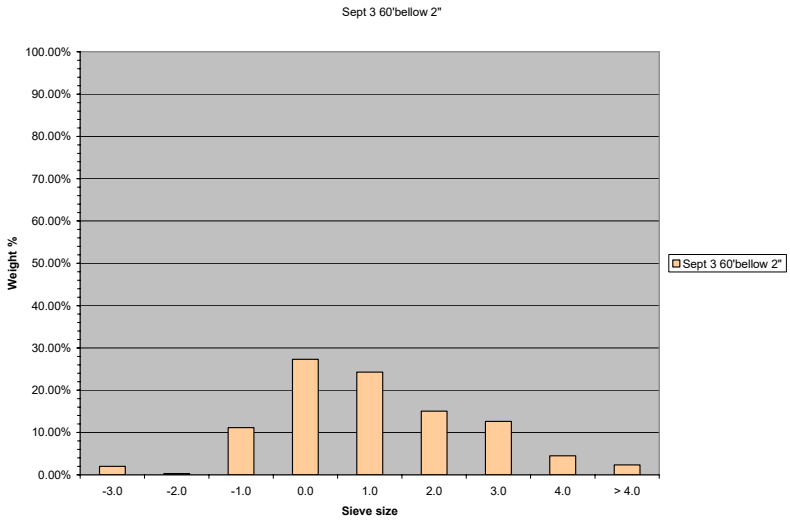

A.

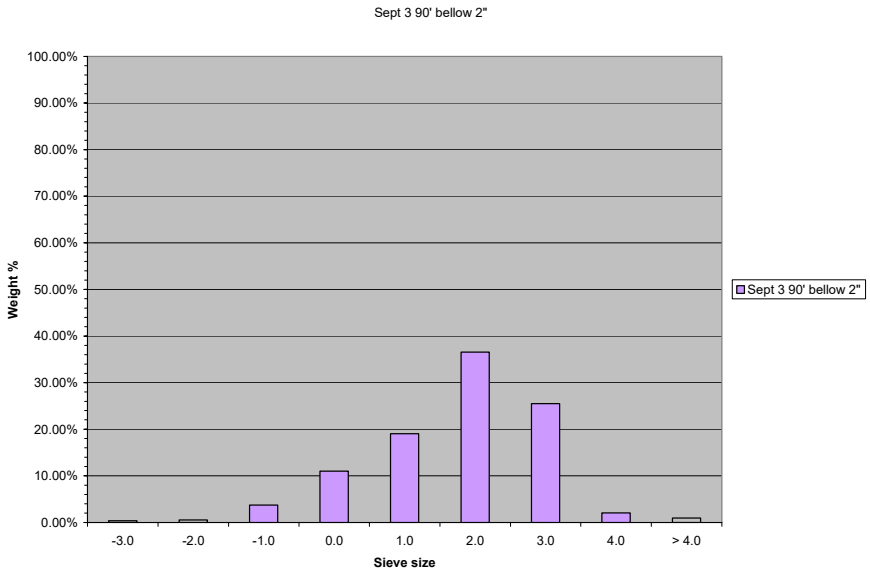

B.

Fig. 34: **Histograms with the grain size variation from cores taken at 60m and 90m stations for the months of September (A and B) of 2004.**

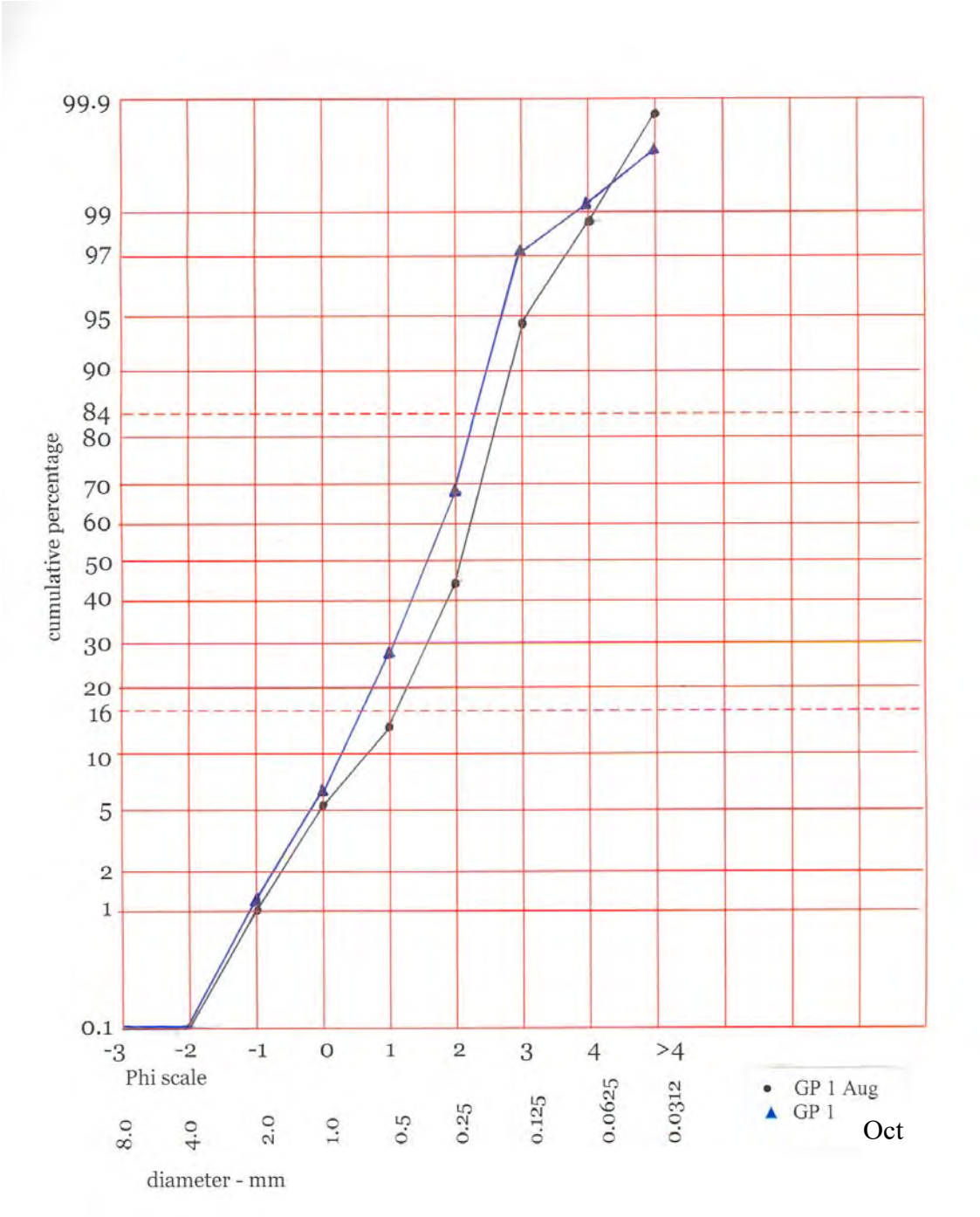

Fig. 35: **Cumulative curves showing the grain size variations at the GP (Garden Plot 1 placed in the area around the cage) during the months of August and October.**

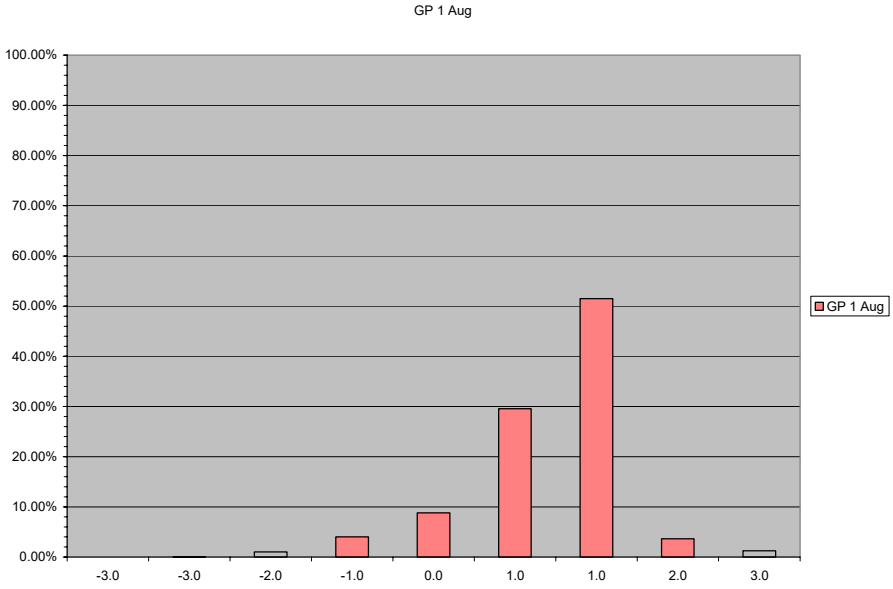

A.

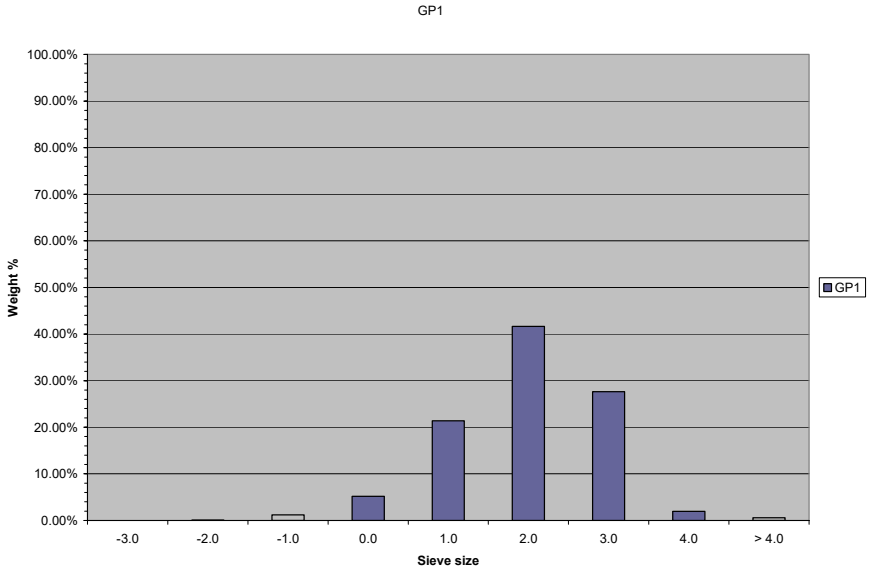

B.

Fig. 36: **Histograms with the grain size variation at the GP 1 (Garden Plot) station for the months of August (A) and October (B) of 2004.**

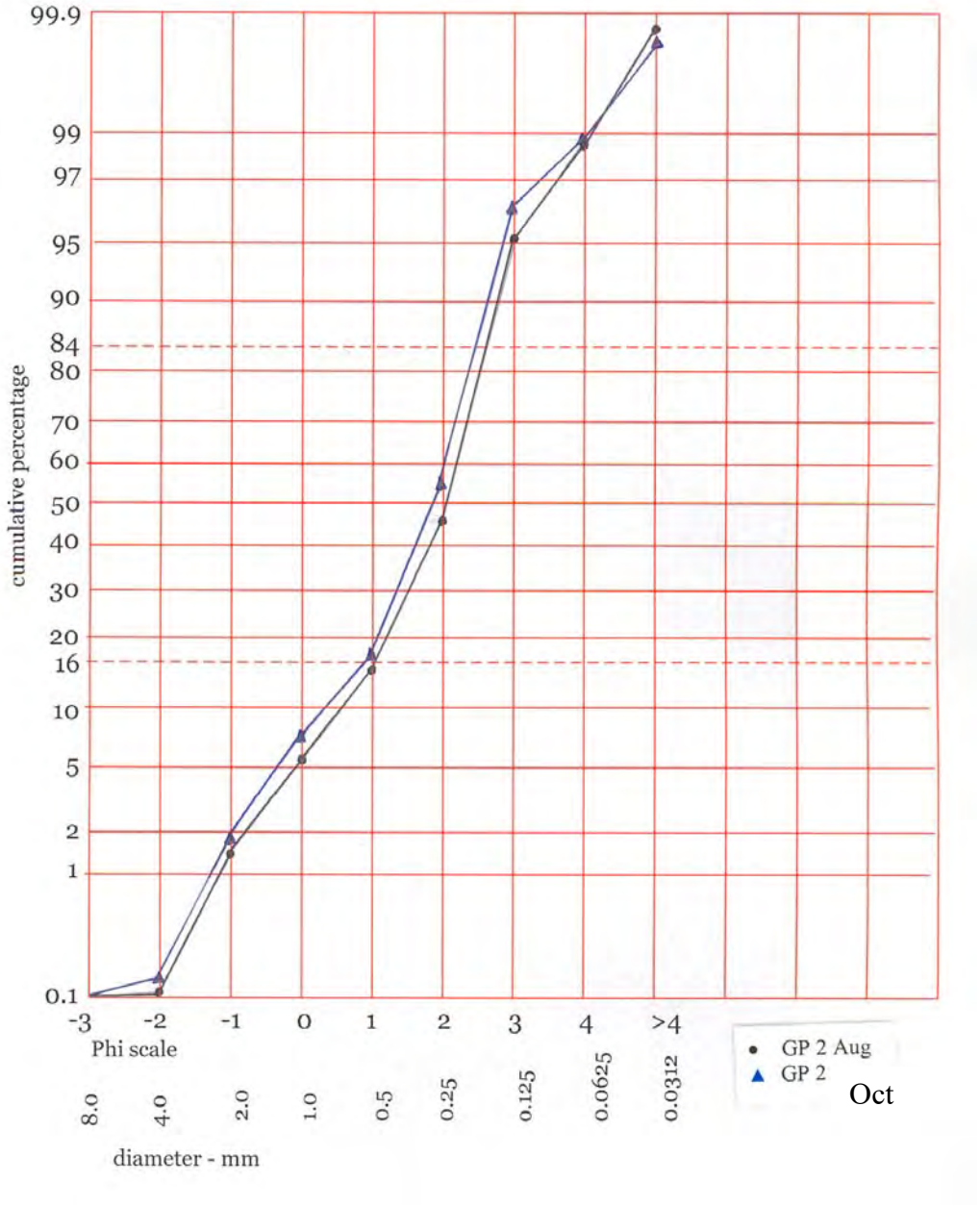

Fig. 37: **Cumulative curves showing the grain size variations at the GP 2 (Garden Plot 2 placed on the area around the cage) during the months of august and October.**

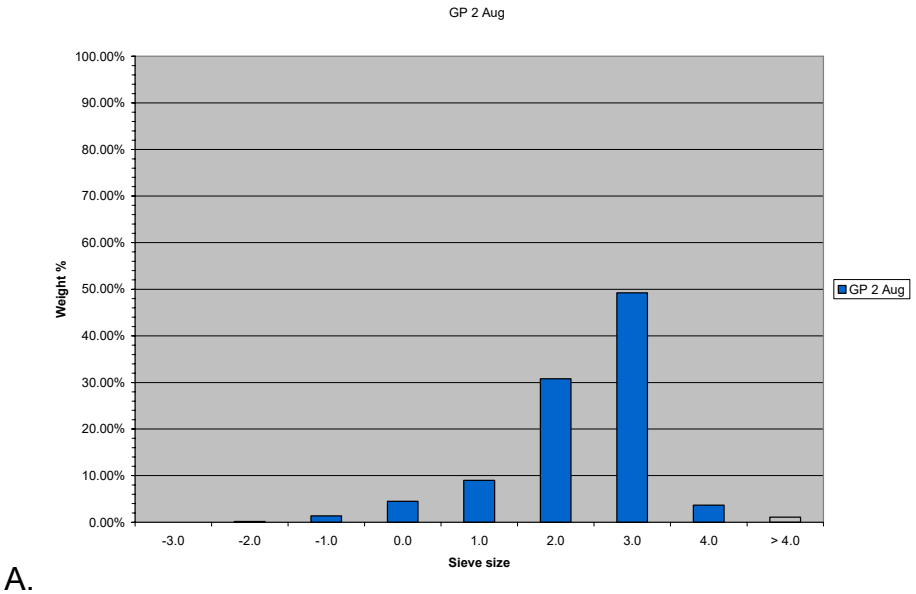

A.

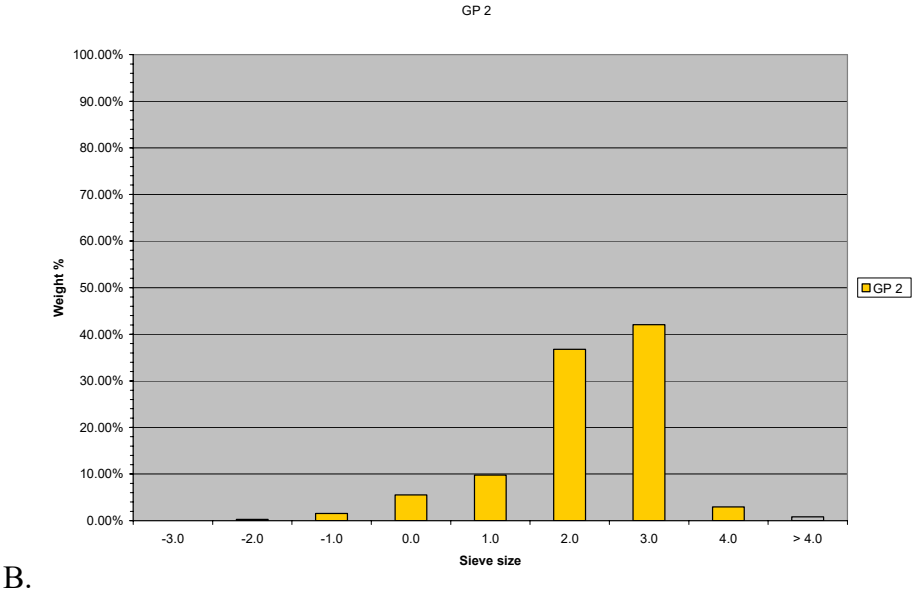

B.

Fig. 38: **Histograms with the grain size variation at the GP 2 station for the months of August (A) and October (b) of 2004.**

Most of the cumulative curves show that there is not a significant change in grain size as we move along the transect away from the cage. The exception was the station located under the cage, were the grains are finer. The differences can be appreciated by looking the positions of the points on the curve and the slope of the graph. A big loose block under the cage is responsible at maintaining the balance of the cage and seems to be causing this difference in grain size it grinds the bottom bouncing on it. This indicates a definitive impact of the cage operation on the sea floor.

Composition

Composition analyses were made to determine the amount of organic material, carbonates and terrigenous material and how it varies with distance from the cage.

A.

.

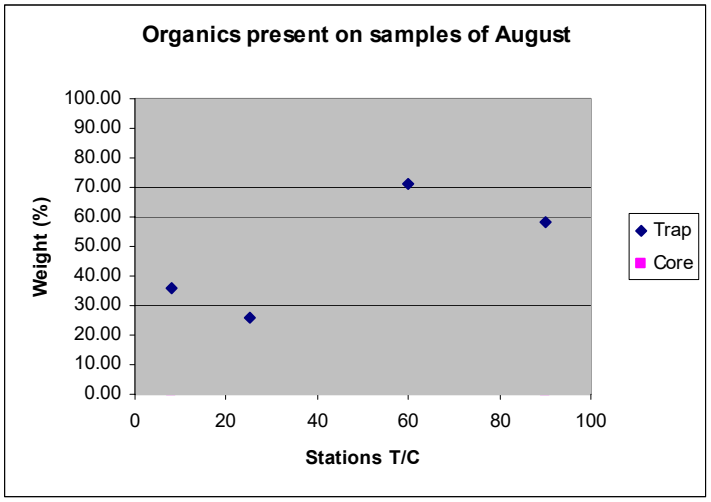

B.

Station T/C	Average on organics on August
8 mT	35.82
25 mT	25.76
60 mT	71.09
90 mT	57.98
8 mC	1.46
25 mC	2.62
60 mC	2.01
90 mC	1.16

C.

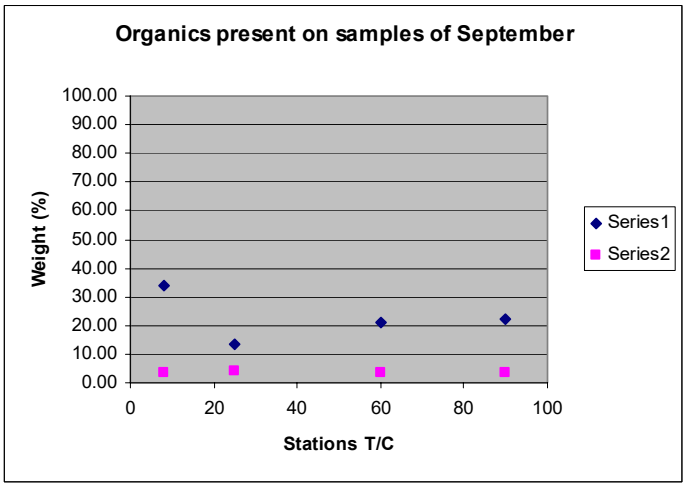

D.

Station T/C	Average on organics on September
8 mT	34.06
25 mT	13.38
60 mT	21.11
90 mT	22.04
8 mC	3.55
25 mC	4.18
60 mC	3.77
90 mC	3.71

E.

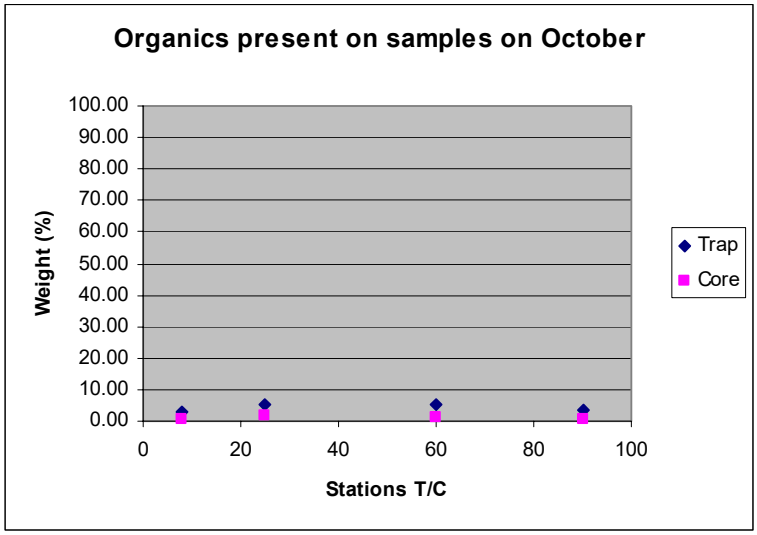

F.

Station T/C	Average on organics on October
8 mT	3.05
25 mT	5.26
60 mT	5.39
90 mT	3.46
8 mC	0.76
25 mC	1.58
60 mC	1.01
90 mC	0.56

Fig. 39: **Graphs and tables showing variations on the amount of organic composition on the samples of August (A and B), September(C and D) and October (E and F).**

A.

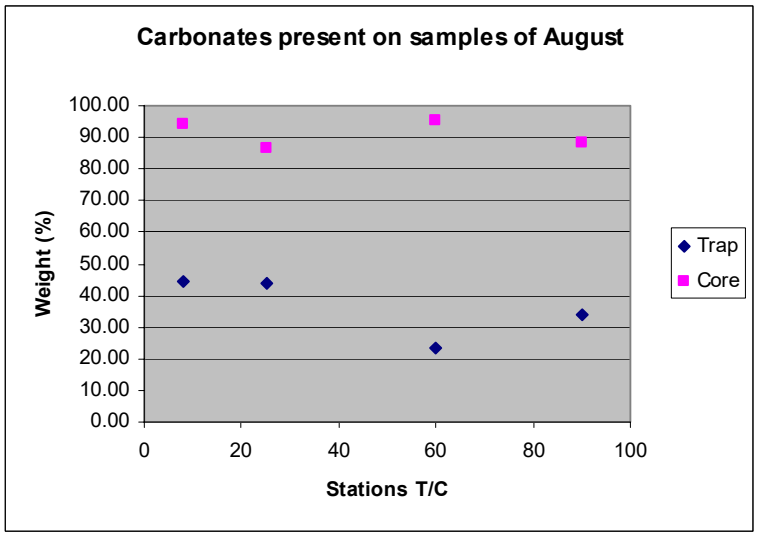

B.

Station T/C	Average on carbonates on August
8 mT	44.18
25 mT	43.72
60 mT	23.36
90 mT	33.91
8 mC	93.99
25 mC	86.35
60 mC	95.56
90 mC	88.03

C.

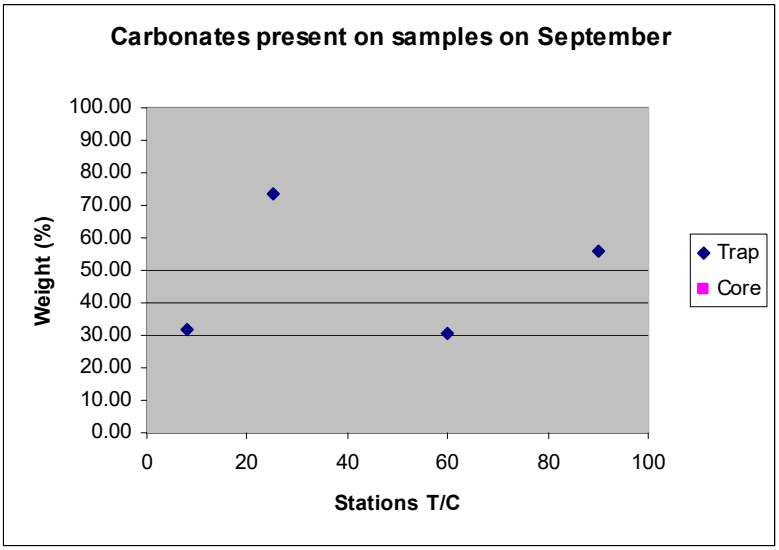

D.

Station T/C	Average on carbonates on September
8 mT	31.88
25 mT	73.24
60 mT	30.46
90 mT	55.92
8 mC	88.01
25 mC	90.66
60 mC	85.99
90 mC	88.32

E.

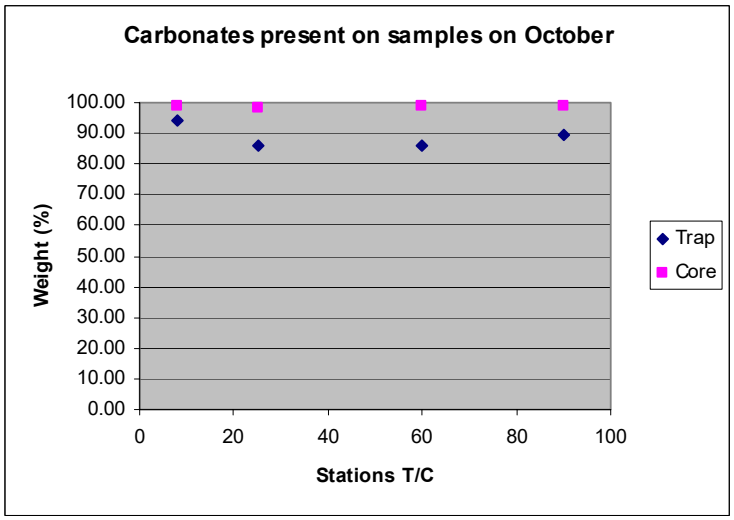

F.

Station T/C	Average on carbonates on October
8 mT	93.87
25 mT	85.95
60 mT	85.90
90 mT	89.53
8 mC	99.00
25 mC	98.37
60 mC	98.72
90 mC	98.92

Fig. 40: **Graphs and tables showing variations on the amount of carbonate composition on the samples of August (A and B), September (C and D) and October (E and F).**

A.

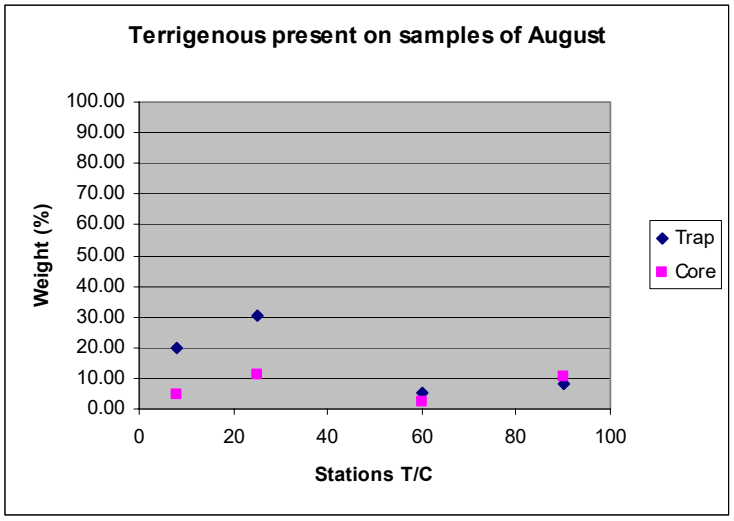

B.

Station T/C	Average on terrigenous on Augusr
8 mT	20.01
25 mT	30.52
60 mT	5.55
90 mT	8.12
8 mC	4.55
25 mC	11.04
60 mC	2.43
90 mC	10.81

C.

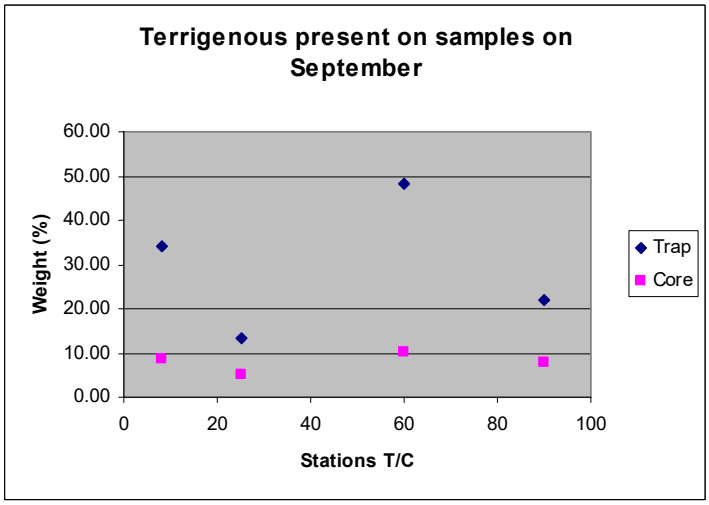

D.

Station T/C	Average on terrigenous on September
8 mT	34.06
25 mT	13.38
60 mT	48.43
90 mT	22.04
8 mC	8.44
25 mC	5.16
60 mC	10.24
90 mC	7.97

E.

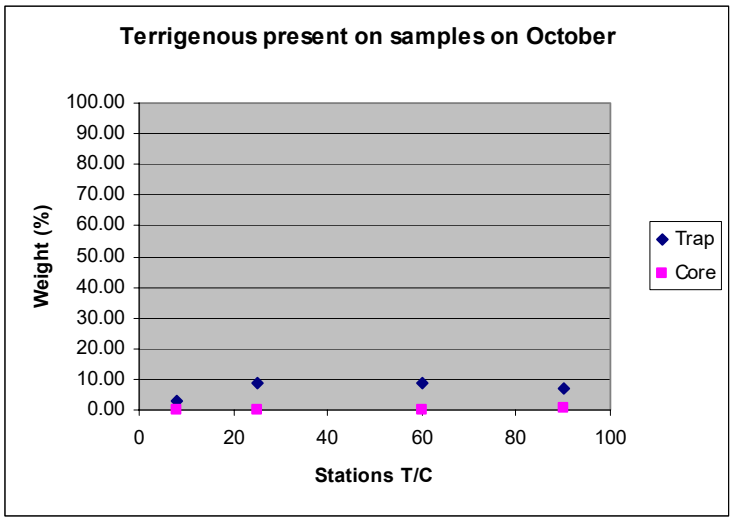

F.

Station T/C	Average on terrigenous on October
8 mT	3.08
25 mT	8.79
60 mT	8.71
90 mT	7.01
8 mC	0.24
25 mC	0.05
60 mC	0.27
90 mC	0.52

Fig. 41: **Graphs and tables showing variations on the amount of terrigenous composition on the samples of August (A and B), September (C and D) and October (E and F).**

Organics

In all of the trapped sediments the organic matter in the trap sediments has decreased from august to October. The probable reasons for this was that there were bigger fish (more food) were collected and sale at the end of august and smaller fish were added to the cage on September (less food).

The relevant information obtained from the trap vs core comparison is that none of these variations in organic matter measured in the traps are detected in the cores. As a matter of fact the organic matter were always small in all of the cores measures, this indicates that the organic loading from the cages is not having a direct impact on the study area.

Terrigenous

In all cases there is more terrigenous sediment in the traps that in the cores. This is probably because of these sediments are composed of clays that are trapped and stored in the trap. The rest of the terrigenous sediments are carried and not deposited at the ocean floor. The highest concentrations of terrigenous sediment were found on September. This coincides with the tropical storm Jeannie.

Carbonates

Carbonates are the most abundant composition in both cases (Traps and Cores). In this case there are more carbonates in the cores that in the traps. This is probably caused because there is a much higher production of calcium carbonate on the bottom of the ocean floor than on the water column. The highest concentrations of this were not determined.

Conclusion

Traps are designed to capture the effluent that drops from the cage and from the water. Cores trap the material that stays on the ocean floor and is not carried away by currents or waves.

Minerals found in the samples indicate that the mineralogy of the ocean floor on the study area is composed predominantly of calcareous material (calcite, aragonite and magnesian calcite). Terrigenous and organic sediments are present but in small quantities.

Cumulative curves show that there is not significant change in grain size along the transect. The exception was the station located under the cage was the grains were finer. Visual information of divers confirms the difference in grain size; of the transect vs. the area under the cage. The appearance of the ocean floor under the cage is different from the surroundings.

The organic matter in the trap sediments has decreased from August to October. These responses to the change in operation because bigger fish was present in August but were harvested and newer smaller fish were introduced in September. The organic matter was always smaller that the trapped on all of the cores measured. In all cases there is more terrigenous sediment in the traps that in the cores both instance response to the ability of the trap to collect material that do not remain at the bottom. Carbonates are the most abundant component in both traps and cores. In this case of the carbonates there were more carbonates in the cores that in the traps in all cases.

We determined the material that is falling from the water column which includes the organic loading from the cages and the material that stays on the bottom. This information is important to determine the real impact of the loading of the bottom. The

information suggests that the organic loading from the cage is not impacting the bottom significatively because the organic material is not being deposited on the bottom.

References

Massachusetts Office of Coastal Zone Management. No date given. Massachusets Aquaculture White Paper – Fish Farms & Other Types of Aquaculture. **http://www.mass.gov/czm/WPFISHOS.HTM. August 19**, 2004.

P. D. Rapp, W.R. Ramírez, 2002. Afield study of cylindrical sediment traps in energetic water: relating trap geometry to maximum current speed and ambient mass density. Sea Grant Program. University of Puerto Rico at Mayagüez.

Bibliography

Bale, A.J., 1998. Sediment trap performance in tidal waters: comparison of cylindrical and conical collectors. *Continental Shelf Research*, 18, 1401 – 1418.

Elizabeth Querna. Fixing Fish Farms: Aquaculture has a bad rep, but innovators are finding healthy ways to return it to the U.S. waters. **http://www.usnews.com/usnews/issue/040816/misc/16aquaculture.htm. August** 19, 2004.

Hargrave, B.T., Burns,N.M., 1979. Assesment of sediment trap efficiency. *Limnology and Oceanography*, 24(6), 1124 – 1136.

Lau, Y.L., 1979. Laboratory study of cylindrical sedimentation traps. *J. Fish. Res. Board Can*., 1288 – 1291.

Texas and the Edward's Aquifer

Undergraduate Student
Robert R. Ramirez

Advisor
Kyle Murray
Department of Earth and Environmental Sciences
University of Texas at San Antonio

For my More Sciences project, Dr. Kyle Murray and I got together to produce the idea of creating GIS maps of both Shavano Park and the counties that overlay the Edwards Aquifer. We chose this idea because we both have experience in this field. Since I have already taken the class in GIS mapping and Dr. Murray specializes in it, it only seem an elementary idea. The area in the first map which is of Shavano Park is special because we wanted to show where the fluorescent tracing dyes where being found and help find contaminated runoff into the aquifer. The second was simply a map displaying the aquifer with the counties and showing the importance of the preservation of the Edwards Aquifer. The tools we used were simply Arc map and Arc catalog. We also got some gis data from several other state agency websites. Dr. Murray did actually use on of the maps for a paper he composed about using fluorescent dyes and OBs (optical brighteners) to locate contaminated water runoff from the Shavano Park streets and sewers and into the aquifer below.

Time Series Resistivity Surveys of Water Content in Edwards Fissures

Undergraduate Student
Beverly Saunders

Advisor
Alan Dutton
Department of Earth and Environmental Sciences
University of Texas at San Antonio

The purpose of this project was to test current theories which state that recharge and pollution of the Edwards Aquifer tend only to happen rapidly at sites of low and level elevations. Water content variations in fissures and porous media were measured, in a time series, at a high elevation site near Headquarters cave, Camp Bullis, Bexar County, Texas. The water content measurements were taken by setting up a fixed resistivity sampling line at the site and collecting data, every two weeks, to determine where water accumulated and moved in the ground after precipitation had fallen. Variations in these water content numbers and their placement in relation to the fissures should allow determination of preferential flow pathways of water at that site. One of two alternative flow pathways is expected to dominate after further investigation. The first of these two is that the precipitation will run down the slope of the land towards levels of lower elevation (which would show if the water content stayed and moved along the surface). The second includes the possibility that the water will run directly through the fissures present and go straight to the subsurface karst features (the water content would accumulate in fractures and not percolate through high amounts of soil). The study is still being conducted and the results are pending but through preliminary investigations the suspected results will be a lean towards the latter of the two scenarios aforementioned. The conclusions of this study will indicate whether the fissures play a large factor in preferential flow pathways of water and precipitation. Further studies could allow a look at the aquifer recharge in high elevation areas and could find more rapid aquifer recharge and contamination potential in areas of high elevation then originally believed were true.

Introduction

The Edwards is a karst aquifer with part of its recharge zone located within San Antonio. In recent years the clearing and construction of buildings and residential areas near the recharge area has caused a great deal of concern to both environmental activist and

citizens about the effects of the modifications on the rates of recharge and the potential for the aquifer to become polluted.[1]

Two major flow pathways are possible when referring to the recharge of an aquifer and both often work simultaneously. The first is uniform path flow where the source of the water percolates through the sediments at a uniform rate. The second involves preferential flow pathways where the water source travels in a specific direction according to sediment type, elevation, fractures and many other factors.[2] It is important to understand the different pathways of potential recharge sources as to accurately predict recharge rates and pollution risks.

The purpose of this project was to find the preferential flow pathways of water that falls on high elevation land, by using resistivity tests taken over a time series to analyse the variations in water content at the site. By finding this pathway it will allow for a better understanding of potential recharge and pollution rates in areas of high elevations within the Edwards recharge zone.

Camp Bullis

The site chosen for this experiment is found on the southwest end of Camp Bullis, Bexar County, Texas on a site over the karst formation Headquarters Cave.[3] This site was chosen for various reasons pertaining to this experiment.

The first reason the site was chosen was due to the visible karst formations, fractures and fissures that were located at the site. The second was due to the high elevation of the site and the fact that it was located on a slope (allowing for ideal conditions for the flow pathway to go down in elevation). The third was the fact that no stream recharge was present within this site, ensuring us that the water content that got measured was completely through precipitation. The site was also ideal due to the fact that it was a secure site. This was because the resistivity setup was permanent and could not be removed in between each study.

The final and most important reason that this experiment was done, on this site in particular, was the fact that there was and is another experiment being done on the site

simultaneously involving the measuring of precipitation that falls on the area and correlating that data with the amount of water that gets through to the karst formations below. This study is crucial to our project and a largely explains why the site indicated was chosen. By taking advantage of the precipitation data it will be possible to compare the preferential flow pathways that are found through our surveys to the amount of water (precipitation) present in the time preceding when the survey was taken. This allows for a more complete analysis of the destination of the water sources in that area.

Methods

Resistivity surveys were used to find these flow pathways because of their sensitivity to water content in soil environments. Forty eight electrodes were placed on a line perpendicular to the slope of the hill. Each electrode was spaced 1 meter apart and hammered securely into the ground. This line remained constant and was not removed at any point during the experiment as to ensure securing data that was not affected by location, this also allowed for fewer variables and will make it easier when the data is analyzed. A visual of the line once it is set up is located in Appendix A Figure 1a.

When a survey was conducted the same procedure was followed every time. The electrodes were joined by a conductive cable and connection clips and then hooked to a resistivity meter and a battery. The readings were taken through dipole-dipole methods, a process that sends electric current through the electrodes in specific orders and sequences and finds the resistivity measurements of the media below.

One test has been done every two weeks for the past eight months and tests are still being conducted in the same fashion and along the same time line (every two weeks). By doing the test in a time series it allows for comparison of resistivity measurements and for conclusions to be formed on where fallen water accumulates.

All of the materials used for this study (other than electrodes) are indicated in Appendix A Figure 1b.

Results

The measured, calculated and inverse model resistivity pseudo-sections obtained from readings collected on April 17th, June 26th and July 22nd are shown in appendix A Figure 2a, 2b and 2c. High resistivity (or low water content) are represented by blue while the high resistivity areas, like the cave system located at the bottom of all three cross sections, are represented by reds. Differences in the near surface resistivity values are evident.

Discussion

Results are still pending for various aspects of this report. In order to analyze the data both the resistivity pseudo-sections and the precipitation reports must be obtained, calculated, grouped and compared. At this point some of the pseudo-sections have been calculated but the precipitation data is not yet available. This data is needed in order to proceed with the analysis.

All that, at this point, can be concluded, from the comparison and the analysis of the pseudo sections, is that there were differences in the resistivity measurements; especially around the surface and that the cave system was located within the range of the area measured. These observations allow us to conclude that with further study and investigation it is likely that a preferential flow pathway could be determined due to the fact that changes in the resistivity were so evident. The location of the cave also allows an indication as to where the readings are in contrast to the karst formations below which will later help the investigation.

Two possible water pathways are expected to be seen through the resistivity data. The first will be the water traveling down the slope of the hill along the surface and through the sediments (likely traveling to a valley). The second will be the water percolated down through the fissures into the karst formations below. The second pathway mentioned is expected to dominate.

An implication of such a conclusion is that recharge happens quickly in areas with high fracture content, even in areas of high elevation. A second implication is that pollution

has potential for being a problem in areas such as the one tested due to the possibility of direct entry of the pollutant into the aquifer through the fractures.

This study does not tell where the water goes after beginning the flow pathway (whether into the aquifer or along a different path) but further studies could be conducted to further pursue this line of research.

Acknowledgments

I would like to thank Marla Roberts, graduate student, at University of Texas San Antonio for helping me understand the project and allowing me to work with her. As well as her immense support.

I would also like to thank Dr. Alan Dutton, graduate professor, University of Texas San Antonio, for giving me a chance to work with him and for his constant offers for support.

Finally I would like to thank the MORE science program for giving me the funding and support to work on this project and for referring me to this line of study.

References

[1] Gregg Eckhardt, 1995 – 2006, "Edwards Aquifer Website," **www.edwardsaquifer.net**. Gregg Eckhardt.
[2] Jan M.H. Hendrickx and Markus Flury, **http://fermat.nap.edu/books/0309073022/html/149.html**, "Uniform and Preferential Flow Mechanisms in the Vadose Zone", Abstract.
[3] **John Pike**, 2000–2006, **http://www.globalsecurity.org/military/facility/camp-bullis.htm**, "Camp Bulllis," GlobalSecurity.
G Tyler Miller, Jr., 2005, Brooks / Cole Living in the Environment Fourteenth Edition, pp.305 – 345.

APPENDIX A

Figure 1a. The set up of the line once the conductive wires are set into place, in line with the electrodes. The meter and battery are located at the bottom center and right.

Figure 1b. Materials used: From top left to right are the meter, the conductive cables, the battery, the hammer and the connector cables.

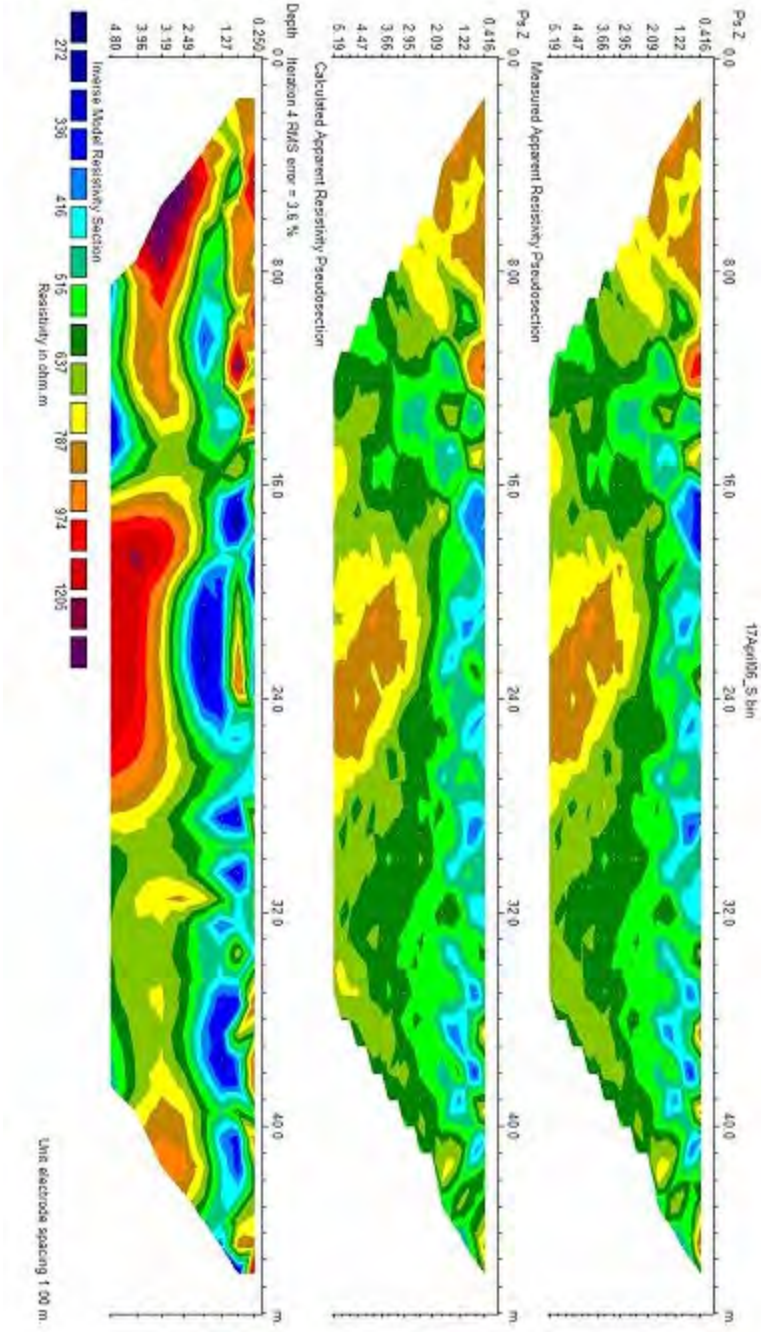

Figure 2a. Measured, Calculated and Inverse Resistivity Pseudo-sections for April 17th

APPENDIX A (continued)

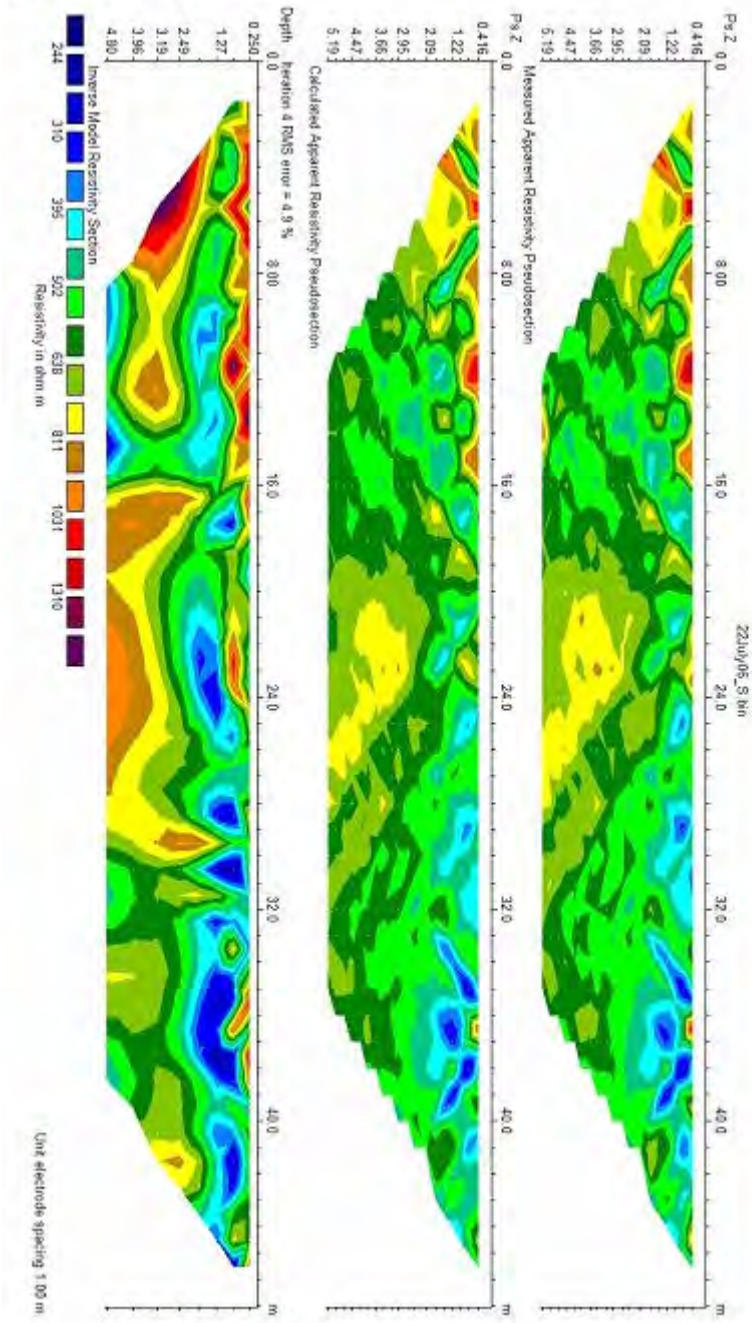

Figure 2b. Measured, Calculated and Inverse Resistivity Pseudo-sections for June 26th

APPENDIX A (continued)

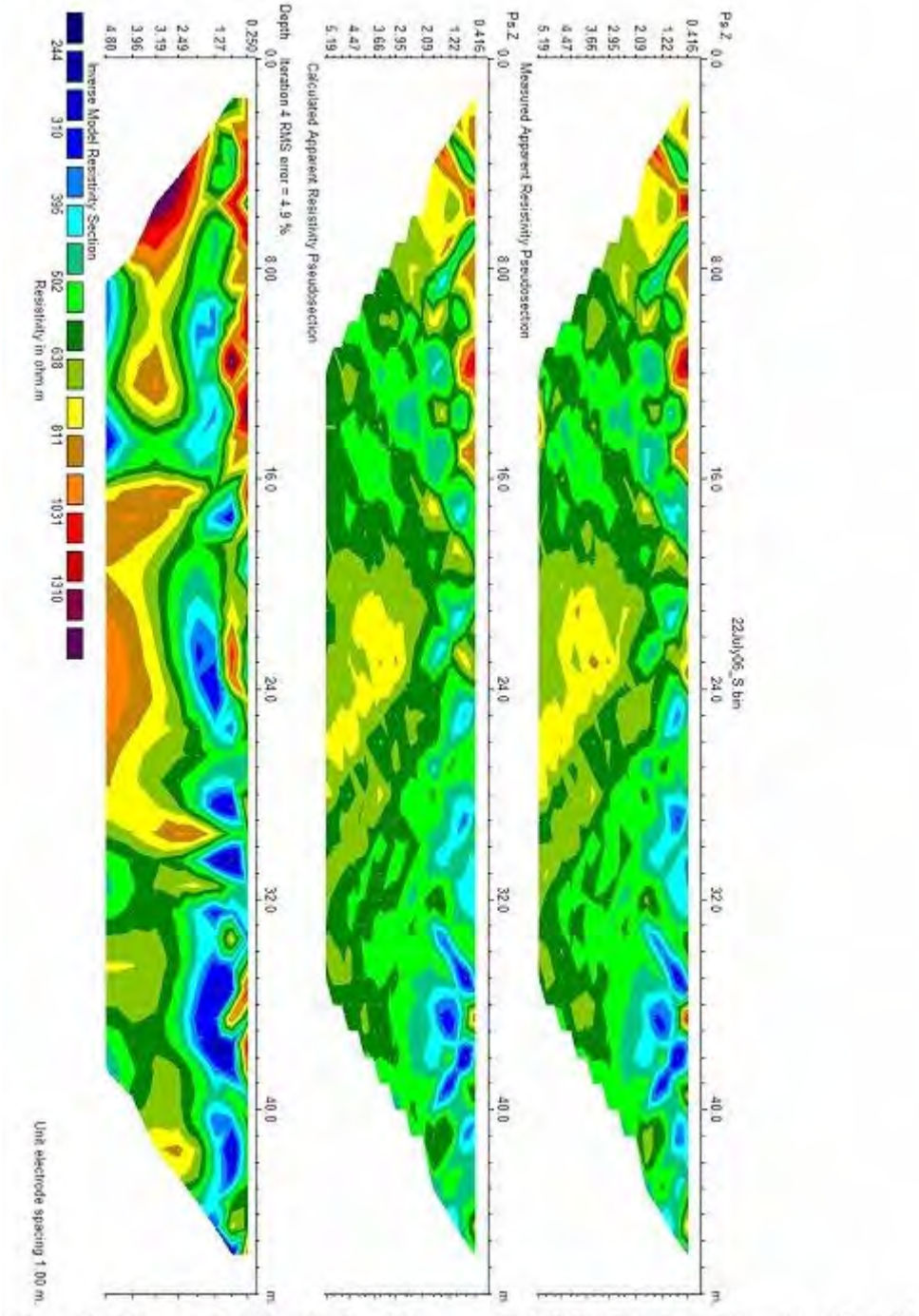

Figure 2c. Measured, Calculated and Inverse Resistivity Pseudo-sections for July 22nd

Utilizing the Soil Survey Geographic (SSURGO) Database for the Analysis of Soils in Bexar County, Texas

Undergraduate Student
Gabriela Sosa

Advisor
Oscar W. VanAuken
Department of Earth and Environmental Sciences
University of Texas at San Antonio

A preliminary study was conducted to determine the accuracy of the SSURGO Database in regard to soil samples that were collected from various locations in Bexar County, Texas. An analysis of those samples was then conducted; these procedures conducted included soil moisture content, particle size distribution and soil textures as well as soil pH and the amount of organic matter. In SSURGO it was indicted that the three sites selected were situated over different soil series. The SSURGO metadata provided soil characteristics for each of the series. The soil series that were analyzed in this study included the Frio soil series, Crawford soil series, as well as the Patrick soil series. Utilizing ArcMap software a map was created of several layers to produce a visual representation of the collection sites. Once the various analyses for each sample were completed the results showed that the classifications provided by SSURGO were accurate for each of the sites. The samples colleted from the area that pertained to the Frio soil series did indeed contain a significant amount of clay as it was stated. Through analysis in the laboratory it was demonstrated that the Crawford soil series area did have a more organic matter than the others which were deficient in respect to organic matter. The samples collected in the area designated Patrick soil series did meet the characteristics the metadata SSURGO provided. Further similar studies in different locations of Bexar County could strengthen the findings of this preliminary study.

Introduction:

A soil study of Bexar County, Texas was conducted at The University of Texas at San Antonio (UTSA) campus. The purpose of the preliminary study was to determine the accuracy of the SSURGO Database utilizing traditional field and laboratory surveying techniques. The study of soils is a fundamental yet often overlooked part of the study of our physical environment. Soil is the basic substrate for a majority of vegetation growth and is a major part of the water, carbon and nitrogen cycles. A wide range of academic

fields are interrelated with soil science, its importance and understanding is crucial. In just Bexar County there are 28 different soil series, soils that have profiles almost alike make up a distinct soil series. (USDA 1966) The locations that were surveyed were all supposed to be in different series. The main underling objective of this undergraduate study was to become acquainted with how to integrate traditional surveying techniques with global information systems mapping technologies.

Data and/or study area:

For this study all of the sites were to be located within boundaries of Bexar County. The three sampling sites were each selected for their vegetation as well as visually apparent differences in their soil characteristics. Utilizing the map Bexar County soil layer provided by NRCS, the different soils series were projected in ArcMap. The metadata collected from August 1995 to May 2006, for the Soil Survey Geographic (SSURGO) database for Bexar County, Texas was utilized for its detailed information. For background data on soils for Bexar County this study heavily relied on Bexar County Soil Manuscripts published originally by the Soil Conservation Service - United States Department of Agriculture in 1966.

Methods:

At each study site a total of five random sub samples were collected, each location was marked. A *Garmin12* global positioning systems (GPS) unit was used to mark each spatial location. For each sample of soil the only the top 15 cm of surface soil were collected using a hand shovel. The samples were each individually placed inside marked heavy duty plastic containers and were sealed. The given to each container was the same as the one given as its marked location on the GPS unit. An analysis of those samples was then conducted in the laboratory. The procedures conducted included soil moisture content, particle size distribution and soil textures as well as soil pH and the amount of organic matter analyses.

To perform find the moisture holding capacity of the soil, the samples collected were determined by weighing the wet or moist soil sample followed by drying the sample in an oven at 105^{o}C to for 24 hours to remove the water. At the completion of the 24 hours the samples were weighed, and then weighed once again in an hour to ensure the weight had stabilized. The data was recorded and the results were found for each sample utilizing

the gravimetric moisture content percentage formula. To determine the particle size distribution of each sample collected, the protocol was followed from the Bouyoucos Hydrometer method was performed. The hydrometer method was chosen to because it was the fastest to conduct of all methods, in this study a total 45 different samples were analyzed. (Milford 1991) The data was for each sample was recorded and the results were found for each sample calculating the percentage of clay, sand, and silt. Another method that was utilized to determine the particle size distribution of a soil sample was by conducting a ¨Texture by Feel" exercise, this means touching the soil to identify its profile. A step by step guide was followed to determine the soil texture. (NASA 2006) The guide was followed and each sample was tested, at the completion of the ¨Texture by Feel¨ exercise the results were recorded. Once the amount of sand silt and clay was known, the texture class name for each sample was given.

To compare the pH values found in the Bexar County Soil Manuscripts, a soil pH value for each of the samples was performed following the U.S.D.A. soil pH test guide. (USDA 2006) A gram of each sample was mixed with 1 mL of distilled water, the samples were thoroughly mixed. Each sample was allowed two minutes to settle. The pH meter was then inserted into the container containing the sample and the distilled water and the pH was recorded for each sample. To determine the total organic carbon in the soil the Walkley-Black procedure was used because it had minimal equipment needs. (University of Georgia 2006) The Walkley-Black procedure is a wet chemistry technique for determining the total organic carbon. This procedure requires the use of sulfuric acid; special care had to be taken when it was being conducted. The calculations performed at the end of the procedure provided the percentage of organic matter found in the each of the samples collected; all results were recorded and were later compared.

Results:

The moisture holding capacity of the soil three different sites were recorded once at the completion 24 hour and then an hour later. For each site five different readings were recorded. The results are provided in table 1, the percentage of moisture calculations were performed in the excel worksheet for each of the samples.

Table 1. The percentage of moisture content in each of the series collected in the different series is shown in table, Patrick Series (P1´s), Crawford Series (C1´s), and the Frio Series (F1´s).

Sample	Wet sample	after 24 hours	after 25 hours	Gravimetric Moisture Content %
P1-1	30	28.48	28.46	5.41
P2-1	30	28.96	28.95	3.63
P3-1	30	28.96	28.95	3.63
P4-1	30	28.62	28.62	4.82
P5-1	30	28.71	28.7	4.53
C1-1	30	27.37	27.37	9.61
C2-1	30	27.35	27.34	9.73
C3-1	30	27.21	27.19	10.33
C4-1	30	27.7	27.68	8.38
C5-1	30	27.64	27.64	8.54
F1-1	30	28.05	27.85	7.72
F2-1	30	28.62	28.58	4.97
F3-1	30	28.78	29.85	0.50
F4-1	30	28.4	28.4	5.63
F5-1	30	28.8	28.79	4.20

For the particle size distribution exercises there were two different methods that were attempted, one was the Bouyoucos Hydrometer method, for that the results are shown on table 2. The other method was the ¨Texture by Feel" exercise for this the results are shown on table 3.

Table 2. The percentage of particle size distribution utilizing the Bouyoucos Hydrometer method for each of the series collected in the different series is shown on the table, Patrick Series (P1´s), Crawford Series (C1´s), and the Frio Series (F1´s).

Sample	**% Sand**	**% Clay**	**% Silt**	**Soil Texture Class**
F1	56	5	39	Sandy loam
F2	28	66	6	Clay
F3	14	51	36	Clay
F4	15	50	35	Clay
F5	14	83	4	Clay
C1	27	7	67	Silt loam
C2	8	6	86	Silt
C3	22	14	64	Silt loam
C4	24	32	45	Clay loam
C5	7	7	87	Silt
P1	34	10	56	Silt loam
P2	11	10	79	Silt loam
P3	24	10	66	Silt loam
P4	36	7	57	Silt loam
P5	29	2	69	Silt loam

Table 3. The percentage of particle size distribution utilizing the ¨Texture by Feel" method for each of the series collected in the different series is shown on the table, Patrick Series (P1´s), Crawford Series (C1´s), and the Frio Series (F1´s).

Sample	Soil Texture Class
F1	Clay
F2	Clay
F3	Clay
F4	Clay
F5	Clay
C1	Silt loam
C2	Silt
C3	Silt loam
C4	Silt loam
C5	Silt
P1	Silt loam
P2	Silt loam
P3	Silt loam
P4	Silt loam
P5	Silt loam

The soil pH test was conducted for each of the samples; the results are on table 4. The different series were tested using a pH meter.

Table 4. The pH reading for each of the series collected in the different series is shown on the table, Patrick Series (P1´s), Crawford Series (C1´s), and the Frio Series (F1´s).

Sample	Soil pH
F1	7.94
F2	7.88
F3	7.90
F4	7.82
F5	8.03
C1	7.49
C2	7.47
C3	7.43
C4	7.41
C5	7.43
P1	7.50
P2	7.48
P3	7.43
P4	7.46
P5	7.44

By conducting the Walkley-Black procedure in the laboratory the total organic carbon in the soil was determined for each of the samples. The results for the procedure are found in table 5; it provides more detailed information on how the procedure was conducted.

Table 5. The percentage of total organic carbon content found in the soil in each of the series collected in the different series is shown in table, Patrick Series (P1´s), Crawford Series (C1´s), and the Frio Series (F1´s).

Sample Description	mL of Fe sample	mL of Blank	% of Organic Matter
Frio soil series			
F1-1	14.4	18.0	10
F1-2	13.0	17.9	9
F2-1	15.0	16.5	11
F2-2	15.5	17.9	11
F3-1	14.3	16.5	11
F3-2	14.9	17.9	10
F4-1	18.3	16.2	14
F4-2	16.0	17.9	11
F5-1	21.2	16.2	17
F5-2	15.1	17.9	11
Crawford soil series			
C1-1	14.1	18.0	10
C1-2	13.4	18.5	9
C2-1	19.0	18.0	13
C2-2	13.9	18.5	9
C3-1	16.3	18.0	11
C3-2	16.3	18.0	11
C4-1	15.3	18.5	10
C4-2	16.2	18.5	11
C5-1	15.9	16.2	12
C5-2	11.7	18.5	8
Patrick soil series			
P1-1	16.1	16.2	12
P1-2	14.2	17.9	10
P2-1	13.8	16.5	10
P2-2	15.1	17.9	11
P3-1	13.2	16.5	10
P3-2	17.1	17.9	12
P4-1	18.9	16.2	15
P4-2	13.9	18.5	9
P5-1	16.6	16.2	13
P5-2	14.4	17.9	10
Total # Samples = 30			

Conclusion / Discussion:

The purpose of the preliminary study was to determine the accuracy of the SSURGO Database utilizing traditional field and laboratory surveying techniques. The locations that were surveyed were found to be in different series, this was determined once the different results for the analysis were determined. The ArcMap with the soils of Bexar County as well as the points that were collected at the sites all showed to be in different

series. The samples collected from the area that pertained to the Frio soil series were found to contain a higher amount of clay content as it was stated in the Bexar County Soil Manuscripts. Through analysis in the laboratory, it was also demonstrated that the Frio soil series area contained more organic matter than the others analyzed which were deficient in carbon content. The GPS points taken next to Leon Creek were all found to be at the Frio soil series location. In the metadata it states that features in the soil map layer from SSURGO are large enough and contrasting enough to significantly influence use and management of soil. Through analysis in the laboratory, it was demonstrated that the Crawford soil series area did meet the pH levels provided in the Bexar County Soil Manuscripts. The samples collected in the area designated Patrick soil series did meet the particle size distribution characteristics the National Resource Conservation Service, of having a significant percentage of gravel in its upper layer. The main underling objective of this undergraduate study was to become acquainted with how to integrate traditional surveying techniques with global information systems mapping technologies. From all the filed and laboratory analyses conducted in this preliminary study it seems appropriate to state that the SSURGO Database for Bexar County, Texas is accurate, further similar studies in different locations of Bexar County could strengthen the findings of this study.

References:

[1] U.S. Department of Agriculture, Natural Resources Conservation Service, 2005. National Soil Survey Handbook, title 430-VI. [Online] Available: http://soils.usda.gov/technical/handbook/

[2] U.S. Department of Agriculture, Soil Conservation Service, 1966. Soil Survey of Bexar County, Texas

[3] Texture by Feel. NASA, 2006 [Online] Available: http://soil.gsfc.nasa.gov/tbf/tbfguide.htm

[4] University of Georgia. Methods for the analysis of Soil, Plant, Water, and Environmental Samples. 2006 [Online] Available: http://aesl.ces.uga.edu/protected/methods/details/stl-soil/12.html

[5] Milford, Murray H. Introduction to Soils and Soil Science, 14th Edition. Texas A&M University Press. 1991.

Acknowledgements:

I would like to thank the MORE Science administration for providing me with funding for my summer project. I also appreciate Dr. Van Auken's willingness to step in and provide me with an experience that will help prepare me for graduate study, as well as Dr. Janis Bush and graduate student Martha Ariza for their help in the field and laboratory.

Using OMEGA data to determine the optical depths of water vapor absorption bands in the Martian atmosphere

Undergraduate Student
Penelope Wagner

Advisors
Minqiang Zhu, Huade Guan and Hongjie Xie
Department of Earth and Environmental Sciences
University of Texas at San Antonio

This paper retrieved optical depths of four selected water vapor absorption bands at 1.126μm, 1.385μm, 1.871μm, and 2.566μm from the OMEGA/Mars Express hyperspectral imagery, based on a tau algorithm implemented using the Module Builder of Erdas Imagine. About 164 images covering latitudes 75ºN to 75ºS and spanning from solar longitude Ls=330 to Ls=118 were processed. The capability of those 4 bands in retrieving optical depths were compared and distribution maps of optical depth on the Latitude and Ls plane were created and compared as well. Our results show that all four bands are capable of retrieving optical depths of water vapor in the atmosphere, however, band 1.385μm and 2.566μm show the most consistent with previous instruments for seasonal distribution.

Introduction

Mars has an extremely thin and arid atmosphere. The Viking 1 measured surface pressure of Mars was at about 1% - 10% that of the earth varying with Martian seasons. Unlike Earths' atmosphere, that contains mostly nitrogen and oxygen, the composition of the Martian atmosphere on average is 95.3% CO_2, 2.7% N_2, 1.6% Ar, 0.13% O_2, 0.07% CO, 0.03% H_2O, with some insignificant amounts of Ne, Kr, and Xe (Carr, 1996). The primary sources of gas originate from volcanic eruptions. Although the atmosphere contains little water, it is always close to saturation (Carr, 1996, NASA sp. 408, 1976, and Garnitz, 1979). The amount of dust within the atmosphere varies from the optical depth of 0.3 – 0.6 (Carr, 1996) to 5 so it can be difficult to obtain clear data when

determining percentage of water and carbon dioxide. The optical depth, which is a measure of how opaque a medium when radiation passes through it, tends to be larger during dust storms therefore the higher the optical depth will create a lower ability to be seen (Garnitz, 1979).

The hydrological cycle on Mars is the most significant factor in determining surface and atmospheric interactions in the Martian climate. Past observations of what we know about Mars have been obtained by various instruments, of which we will compare our results. Initial information gathered about water vapor in the Martian atmosphere had been obtained from the Mars Atmospheric Water Detection (**MAWD**) experiments aboard the Viking 1 and 2 spacecraft (Fedorova et al., 2004) between 1977-1980. The Thermal Emission Spectrometer (**TES**) aboard the Mars Global Surveyor (MGS) also retrieved maps of water vapor distribution from March 1999 to March 2001 (Fedorova et al., 2004, and Smith, 2003). Latest information provided to understand the water cycle has been obtained through the use of the following Mars Express instruments: Visible and Infrared Mineralogical Mapping Spectrometer (**OMEGA),** Ultraviolet and Infrared Atmospheric Spectrometer **(SPICAM),** and Planetary Fourier Spectrometer **(PFS).** The purpose of these sensors is to collect mean data from the vertical profile of the Martian atmosphere at different latitudes each month (Melchiorri et al., 2006, Bertaux et al., 2005, and Fouchet, 2006].

The SPICAM instrument determines atmospheric composition by collecting data from sunlight absorbed by surrounding gases. Two components of this device are the use of an ultraviolet sensor (118 - 320 nm) to measure ozone and an infrared sensor (1 – 1.7 micron) to calculate water vapor. Measurements from this device using the 1.387 μm, 1.87 μm, and 2.566 μm bands (Bertaux et al., 2000) give the total amount of water vapor in atmospheric columns of 5 x 5 km^2 spatial resolutions. Past observations from MAWD showed that the major factors controlling water vapor distribution in the atmosphere are the amount of water ice concentrated at the northern pole caps, the transference of surface material, and air circulation (Fedorova et al., 2004). The PFS instrument measures the absorbed infrared radiation emitted by molecules in the atmosphere. Results for PFS relied on band 2.56 μm due to its higher absorption capacity for water instead of a mixture of trace gases. This data showed that the mean absorption of water vapor is

between 8 pr. µm – 15 pr. µm during the seasons Ls=330º and Ls=36º (Tschimmel et al., 2006).

Results from SPICAM and PFS clearly show a distinct pattern of increased water vapor in the North Pole originating from 90ºN and circulating to with increased rates in the southern winter season (Figures 1 and 2) (Tschimmel et al., 2006 and Bertaux et al., 2000). The outcome of data obtained from MAWD also shows the same seasonal distribution pattern of water vapor (Figure 3) (Fedorova, 2004). In all three graphs, data was not available for the winter seasons where albedo is significantly lower than in the summer months. Previous results from OMEGA used the 2.6 µm band because of it is most responsive to water and free of surface mineral elements (Melchiorri et al., 2006). The purpose of this paper is to retrieve the average optical depth of four selected water vapor absorption bands (1.126, 1.385, 1.871, 2.566 µm) within different latitudes on Mars from Ls 330° to Ls 120°.

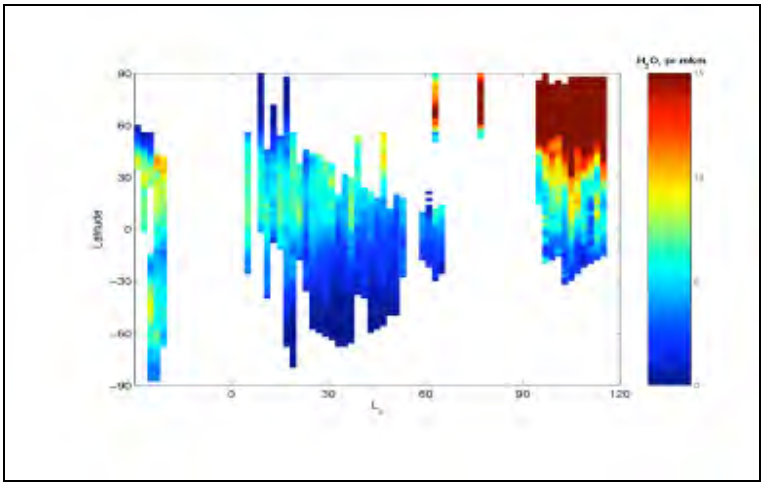

Figure 1. Seasonal distribution of water vapor (SPICAM) (Bertaux, 2000).

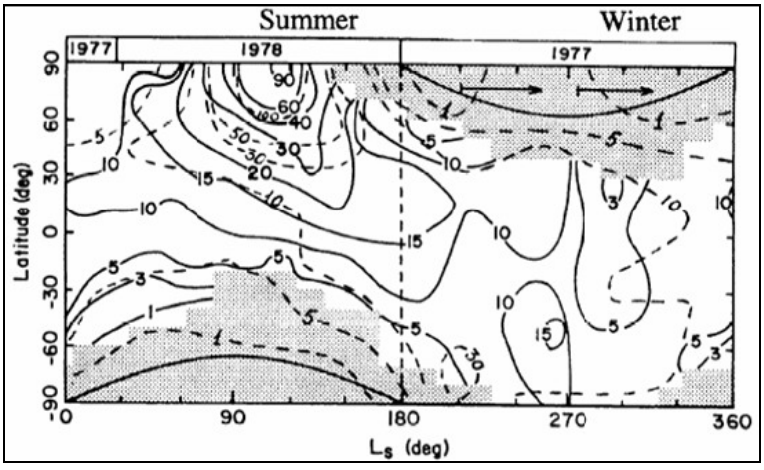

Figure 2. Seasonal distribution of water vapor (PFS) (Tschimmel et al., 2006)

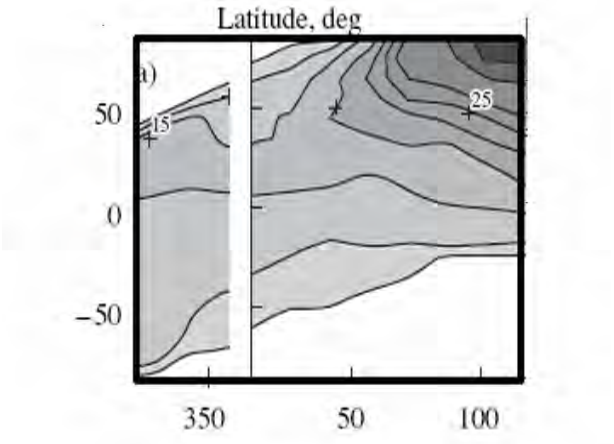

Figure 3. Seasonal distribution of water vapor (MAWD) (Fedorova et al. 2004)

Data

The OMEGA has spatial resolution of 300m-3km. It is able to determine the mineral composition of Martian surface and atmosphere from the visible and infrared light reflected from the planet's surface and in the wavelength range of 0.35-5.2 microns (Bibring et al., 2004). The OMEGA instrument absorbs light in 352 contiguous bands from 0.35 to 5.1 μm (Brown, 2006, Zhu et al., 2006, and Pelkey, 2005). OMEGA data were downloaded from ESA's Planetary Science Archive from January to November 2004 (http://www.rssd.esa.int/index.php?project=PSA). Data was retrieved through four bands at 1.126μm, 1.385μm, 1.871μm, and 2.566μm in order to conduct analysis comparable to that of SPICAM, MAWD, TES, and PFS. Each orbit for this span collected mean values to determine the vertical distribution of water vapor in the atmosphere. Averages given rely on the optical depth within various latitudes.

Methodology

Spatial distribution of optical depth was mapped using 164 data sets of OMEGA (Ls = 330° - Ls = 120° and latitude = -75° - +75°) from the Planetary Science Archive database. Initially, OMEGA data is given for specific latitude and solar longitude ranges. After determining the correct date and latitude, the information is extracted and formatted using an IDL program provided by ESA (Zhu et al., 2006) to create a tif. file. The tif. format allows the images to be read with geospatial imaging processing programs such as ERDAS and ENVI. The tif. image file and data is extrapolated from the IDL program and filtered through an algorithmic model using ERDAS. The model uses the tau (optical depth) logarithm to calculate the mean absorption for each band, using the

equation τ=Log (Rc/Rb) / 2 (Figure 4) (Zhu et al., 2006).Rb represents the reflectance at a water absorption band and Rc represents the reflectance of a closest band (to the water absorption band), completely free of water absorption. This value is calculated for each of the four selected bands and divided by 2 to factor in the relative reflectance of each band.

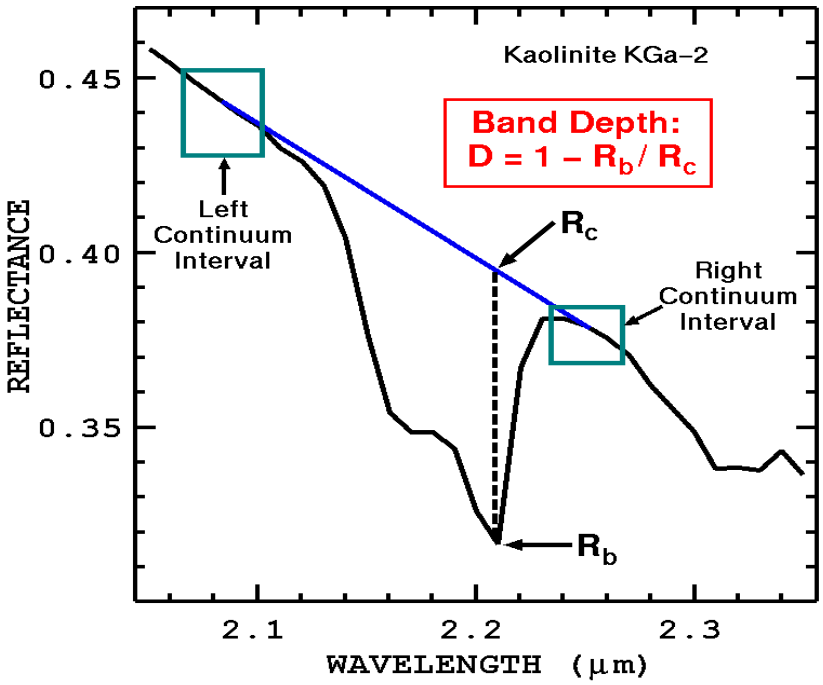

$$\tau_{1.126} = -\log\left(\frac{(I/F)_{1.1411}}{(I/F)_{1.126}}\right)$$

$$\tau_{1.385} = -\log\left(\frac{(I/F)_{1.3280}}{(I/F)_{1.3855}}\right)$$

$$\tau_{1.871} = -\log\left(\frac{(I/F)_{1.8568}}{(I/F)_{1.871}}\right)$$

$$\tau_{2.566} = -\log\left(\frac{(I/F)_{2.5402}}{(I/F)_{2.566}}\right)$$

Figure 4. Tau equation for water vapor absorption for each band

The mean averages are computed and stacked through this model to establish the relationship between optical depth and elevation for each band selected. It is expected that the optical depth of each absorption band will show higher values when pixels are at a lower elevation because the water vapor abundance between each column varies, in addition to the thickness above different pixels. To test this relationship, we used ORB501_4 because this image contains the data located over Olympus Mons, where the largest elevation difference occurs. Data for the majority of scenes calculated were separated into two to three parts using ENVI. Data sets that measured greater than a 15° range between the minimum and maximum latitude, were subset into increments of 10° so we can determine a mean optical depth for a smaller latitude range. ENVI allows the images to be easily manipulated to obtain statistical data of the mean optical depth for each of these subsets.

OMEGA scene ORB072_1 was chosen to represent this trend from 8.87° North to –32.06° South at Ls = 343° (end of winter in northern Hemisphere or end of summer in southern Hemisphere) because this area has the smallest topographic relief.

To further illustrate the spatial distribution of optical depth vs. latitude, 164 OMEGA scenes were plotted to create a columnar contour map using an Inverse Distance Weighted (IDW) method and Arc View that illustrates the mean optical depth of water vapor trends throughout specific seasons within specific latitudes. The optical depth differs with each band, therefore, specific data was omitted (Guan et al., 2006) to take into account location of concentration within surface materials in addition to the distribution of dust that may yield adverse results:

- .01 at 1.126μm
- .05 at 1.385μm
- .04 at 1.871μm
- .04 at 2.566μm

The major aspect that deters clear observation from the OMEGA instrument is potential surface materials, vertical vapor profile, and Martian pressure (Zhu et al., 2006 and Smith, 2003).

Results

All four absorption bands reflected that the water vapor near the North Pole increased in July at Ls 50°-100° during late spring, to mid summer (Ls 120°). Above 65°N data was unavailable until July, where an increase in data is given at 40°N and above. Between 340° - 0° during February and March (northern winter/southern summer) and 50°N - 90°N the data proved to be more problematic to obtain. Although each bands level of absorption reflects the optical depth, a clear trend occurs with all four bands that show a substantial decrease in water vapor from the North to the South latitudes.

High pixel elevation showed low optical depth for our results for ORB501_4 (Figure 5), therefore we determined that all of the four bands tested are adequate to be used to establish water vapor abundance. The bands with the greatest optical depth to the least are as follows; 1.871μm, 2.566μm, 1.385μm, and 1.126μm.

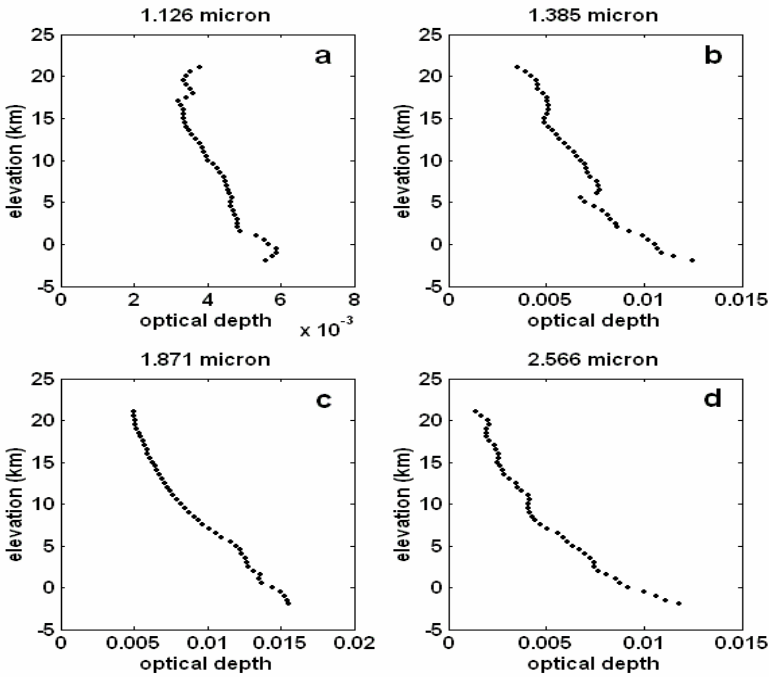

Figure 5. Each band 1.126 µm, 1.385µm, 1.871µm, and 2.566µm optical depth vs. elevation for ORB501_4(June 12, 2004, Ls=46)

The optical depth, when plotted against latitude-Ls for scene ORB072_1, shows a similar trend of water vapor abundance from the northern to the southern latitudes. Some elevated levels of optical depth at 25ºS are assumed to be caused by a reduction in surface albedo (Guan et al, 2006).

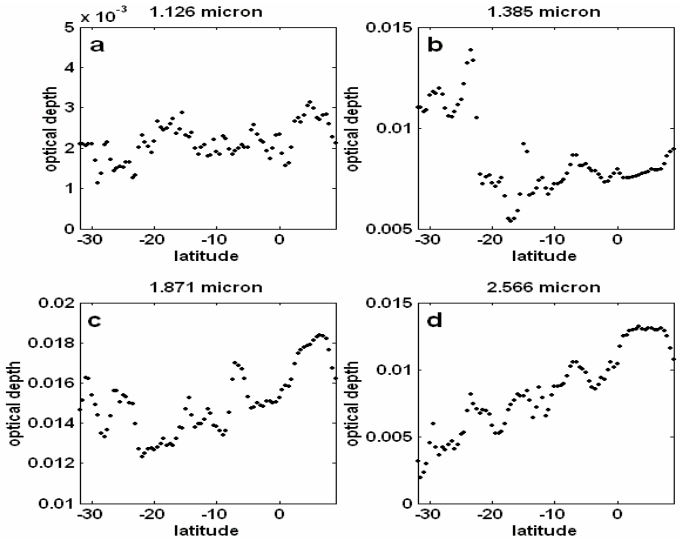

Figure 6. Each band 1.126 µm, 1.385µm, 1.871µm, and 2.566µm optical depth vs. latitude for ORB072_1(February1, 2004, Ls=343)

The optical depth for 164 images was plotted with results from OMEGA for each band with the TES vapor abundance. This was to determine the capability of the bands to produce spatial distribution of water vapor abundance (Figure 7). There are good

correlations with values of 0.61-0.80, in which all bands lie in the range except for 1.126 µm. Half data points were randomly selected by Dr. Guan and Dr. Zhu to establish a further linear regression with TES water vapor abundance and the OMEGA vapor abundance (Figure 8). Band 1.126µm performed similar to comparisons with the optical depth and TES water vapor abundance. This is assumed to be due to its' weak absorption strength. Band 1.871µm also showed values lower than the TES vapor abundance in these figures (Figure 8), suggesting this band will be weak in retrieving water vapor distribution on Mars.

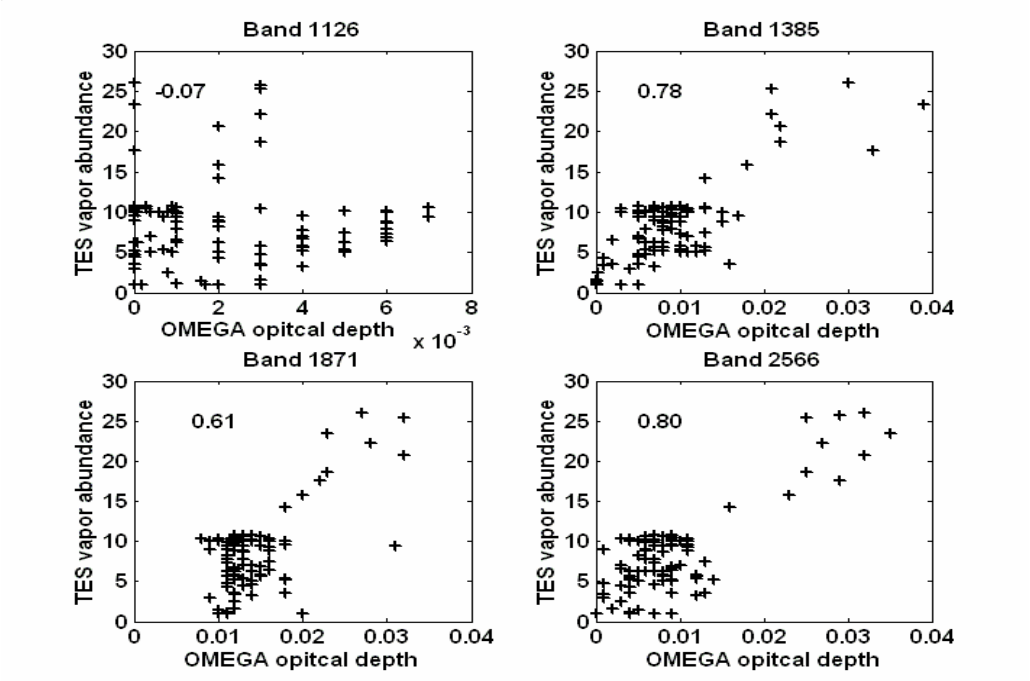

Figure 7. OMEGA optical depth for each band vs. TES vapor abundance

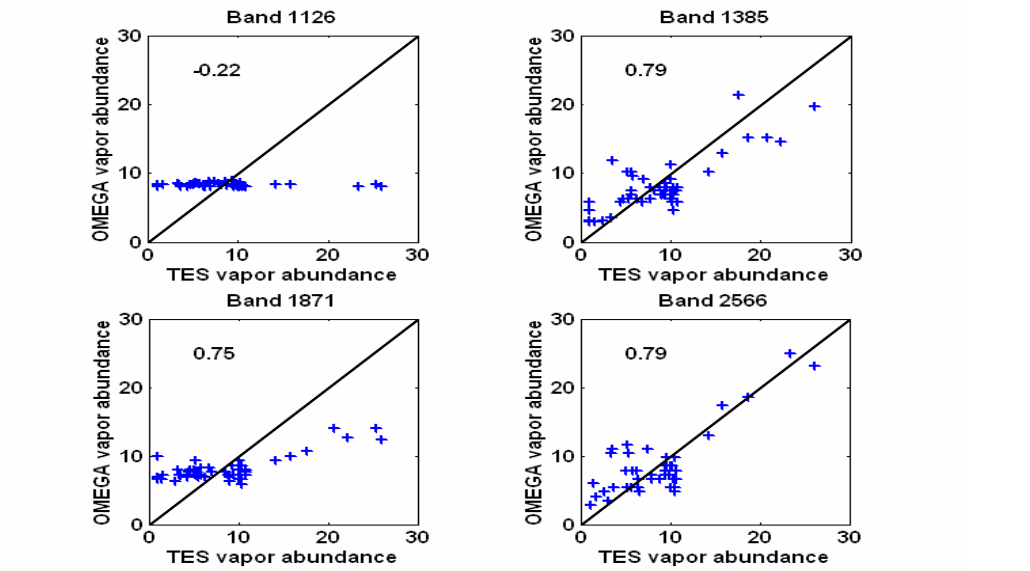

Figure 8. OMEGA vapor abundance for each band vs. TES vapor abundance

Results for the three consistent bands 1.126µm , 1.385µm , and 1.871µm of OMEGA water vapor abundance data were plotted against latitude-Ls using 164 data sets to show similar linear relationship with bands 1.385 µm 1.871 µm, and 2.566 µm(Figure 9).

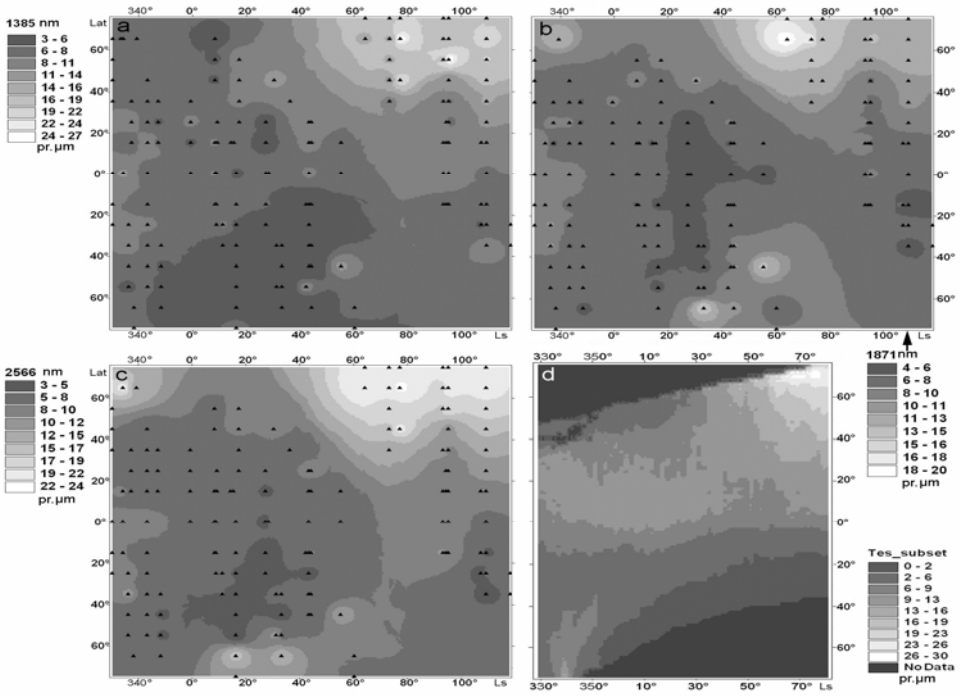

Figure 9. OMEGA vapor abundance vs. latitude-L*s*

All bands show the movement of decreasing water vapor from north to south latitudes presented by the optical depth of all for bands. Optical depth measurements rely on albedo levels so some high values for the 1.385µm and 1.871µm bands in the southern Hemisphere are potentially due to a reduction in albedo (Guan et al., 2006). The absorption band 1.385 µm provided similar data comparable to that of distribution of water vapor per Jakosky and Farmer, 1982 (Figure 3) (Fedorova et al., 2004). However, Band 1.871 µm and 2.566 µm show additional water vapor distribution at 40°S closer to the south pole at Ls 20° to 60°. Comparing results for each band on these spatial distribution contours illustrates the distribution of water vapor during the summer months which lie between Ls 90° and 180° in the North Pole and 290° and 360° in the South Pole.

Conclusion

Comparing this study to previous research by TES, SPICAM, MAWD, and PFS provides a similar linear correlation (Figure 1, 2, 3, and 5-9). Our data shows the three of the four bands 1.385 μm, 1.871 μm, and 2.56 μm show a continuous exchange of water vapor from the north polar caps to the southern pole caps (Figure 9) with some variations to each distribution curve. These patterns are potentially dependant upon aerosol concentration located near or in the surface water ice. Dust circulation or aerosol contaminants in the atmosphere can be an influential factor in creating insufficient data for specified latitude ranges similar to previous research (Fedorova et al., 2004).

Although bands 1.126μm, 1.385μm, 1.871μm, and 2.566μm were used, our results fared the best with band 1.385μm and 2.566μm. Our study tested the same bands used by previous instruments but not all have been tested with OMEGA. Additionally, clear data for band 1.126μm was problematic due to weak absorption levels (Figure 5 , 6, and 7). This band also can detect surrounding constituents in the atmosphere, which can obscure results (Tschimmel et al., 2006). Band 1.871μm produced lower values than expected.

Data was unavailable for the winter seasons of both poles with OMEGA similar to previous studies. Insufficient results were produced during the winter seasons, which we are to assume may be due to the fact that water vapor absorption and optical depth are a function of Martian seasons(Smith, 2006). All four bands showed sufficient capability to retrieve water vapor however, band 1.385μm and 2.566 μm demonstrated greater ability to test total water vapor abundance over 10 pr_μm than 1.871μm and 1.126μm. Water vapor is expected in these regions during the summer seasons where the water ice caps are melting and producing more water vapor in the atmosphere.

Acknowledgements

We want to thank the financial support from the MORE Science at UTSA project funded by Department of Education. Thanks also go to M. Smith for providing the TES data.

References:

Bertaux, Jean-loup et. al. *The study of the Martian atmosphere from top to bottom with SPICAM light on Mars Express*, Planetary and Space Science 48 (2000) 1303-1320.

Brown, A.J. (2006) LPS Abstract #1477

Carr, Michael H., *Water on Mars*, Oxford Univ. Press, 1996

Fedorova, A.A., A.V. Rodin, and I.V. Baklanova (2004b). MAWD Observations Revisited: Seasonal Behavior of Water Vapor in the Martian Atmosphere, Icarus, vol. 171, pp. 54–67.

Garnitz, Vivien, *Geology of the Planet Mars*, Dowden, Hutchinson, & Ross Inc., 1979.

http://pds-geosciences.wustl.edu/missions/mars_express/index.htm (nasa.gov) methods

http://pds-geosciences.wustl.edu/missions/mars_express/spicam.htm

http://www.esa.int/SPECIALS/Mars_Express/SEMUC75V9ED_0.html

http://www.esa.int/SPECIALS/Mars_Express/SEMYKEX5WRD_0.html

http://speclab.cr.usgs.gov/PAPERS/tetracorder/FIGURES/fig3.plot.tgif.gif

http://omega.ifsi.rm.cnr.it/

Maltagliati, L. D. Titov, H.U. Keller, M. Garcìa-Comas, *Water Vapor Retrieval in the Atmosphere of Mars: Results from the OMEGA experiment onboard Mars Express*

Melchiorri, R., et al., *A simulation of the OMEGA/Mars Express observations: Analysis of the atmosphere contribution*. (2006) Planetary Space and Science 54 p. 774-783.

Pelkey, S.M. et al (2005) LPS Abstract #1891

Tschimmel, M., Ignatiev, D.V. Titov, *Atmospheric water vapor from the PFS/Mars Express observations.*

Guan, H., Zhu, M., and Xie, H., Investigation of using OMEGA data to retrieve water vapor abundance in Martian atmosphere, 2006 (in preparation).

Smith, Michael D. TES Atmospheric temperature, aerosol optical depth, and water vapor observations 1999-2004, 2006.

Smith, Michael D. Interannual variability in TES atmospheric observations of Mars during 1999–2003, 2003.

Viking 1 – Early Results, NASA sp. 408, 1976